

STELLINGEN

behorende bij het proefschrift :

'Lumped pulses and discrete displacements'

van A.W.M. Kok

1. De introductie van continue snelheden en versnellingen in de Single Step algorithmen voor de numerieke integratie van structural dynamics problemen bemoeilijkt de fysische interpretatie van het numerieke model.
2. De gebruikelijke formulering van de stelling van Hamilton waarbij alleen naar potentiële en kinetische energie wordt gekeken is, fysisch gesproken, onvolledig; alleen als ook de begin- en eindcondities in de variatie-eis worden betrokken komt men tot een volledige beschrijving van het fysische probleem.
3. Numerieke instabiliteit is een divergerende respons die kan ontstaan als de numerieke integratiestap benaderingsgewijs samenvalt met de halve of de hele periode van een eigen-trilling.
4. De modellering van een dragende bodem door middel van een lineair-elastische bedding van Winkler-veren is een onnodige vereenvoudiging van de werkelijkheid; de bijdrage van gekoppelde veren is doorgaans verre van verwaarloosbaar terwijl het rekenproces er nauwelijks door wordt bemoeilijkt.
5. De onderstelling dat de Falling Weight Deflectometer test kan worden geïnterpreteerd door een statische analyse is in hoge mate onjuist voor wegconstructies met een stijve toplaag en een slappe bodem.
6. Hoogfrequente locale trillingen kunnen numeriek worden voorkomen door constructiedelen met grote locale stijfheid hetzij als star lichaam hetzij door middel van static condensation te modelleren.
7. Het vinden van een shear en membrane locking free zesknops schaalelement kan worden bereikt door het toevoegen van invariante orthogonale 'bubble' functies aan het verplaatsingsveld ten behoeve van afschuifspanningen en membraanspanningen.

8. De belangrijkste bijdrage van H.W. Loof aan het semi-Loof element is niet zozeer de introductie van de zogenaamde Loof-punten alswel de formulering van een consistente Kirchhoff schalentheorie die bruikbaar is voor de ontwikkeling van Kirchhoff schaalementen.

H.W. Loof, 'The Economical Computation of Stiffness Matrices of Large Structural Elements', Proc. Int. Symp. on the Use of Electronic Digital Computers in Structural Engineering. Newcastle, UK, 1966

B.M.Irons, 'The Semiloof Shell Element' in *Finite Elements for thin Shells and Curved Members*, John Wiley, London, 1976

M.A. Chrisfield, *Finite Elements and Solution Procedures for Structural Analysis*, Pineridge Press, Swansea, UK, 1986

9. Modelleren is een kunde die vroeger door langdurige ervaring werd opgebouwd, doch die tegenwoordig veel sneller kan worden ontwikkeld met geschikte computersimulaties.
10. Te weinig wetenschappers weten waar hun weten eindigt en hun geloven begint.
11. Vakliteratuur op het gebied van de numerieke mechanica is door toenemende specialisatie en excessieve kosten steeds moeilijker bereikbaar geworden.
12. De meest effectieve vorm van ontwikkelingshulp is het uitzenden van leraren en middelen ter opbouw van het lager en middelbaar beroeps-onderwijs in de hulpontvangende landen.
13. In Den Haag is de politiek er niet geloofwaardiger op geworden sinds men financieel wanbeheer in de gemeentepolitiek beloont met een zetel in de Tweede Kamer.
14. Als nieuwe generaties van bejaarden een beroep willen doen op de solidariteit van de werkende jongere generaties, is het goed te bedenken dat veel van de genoten welvaart werd verkregen door de kosten daarvan te verschuiven naar de toekomst.

LUMPED PULSES AND DISCRETE DISPLACEMENTS

A Physical Way to Understand

Numerical Dynamics

LUMPED PULSES AND DISCRETE DISPLACEMENTS

**A Physical Way to Understand
Numerical Dynamics**

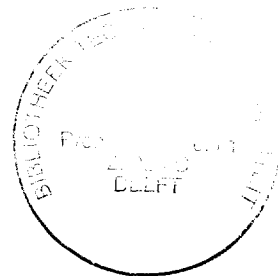
PROEFSCHRIFT

ter verkrijging van de graad van doctor aan de
Technische Universiteit Delft, op gezag van de
Rector Magnificus, prof. ir. K.F. Wakker,
in het openbaar te verdedigen ten overstaan van een
commissie aangewezen door het College van Dekanen,
op dinsdag 20 juni 1995 te 10.30 uur

door

Antonius Wilhelm Maria KOK

geboren te 's-Gravenhage
wiskundig ingenieur



Dit proefschrift is goedgekeurd door de promotor:
Prof. dr. ir. J. Blaauwendraad

Samenstelling van de promotiecommissie:

Rector Magnificus, voorzitter
Prof. dr. ir. J. Blaauwendraad, TU Delft, promotor
Prof. dr. ir. R. de Borst, TU Delft
Prof. dr. ir. C. Esveld, TU Delft
Prof. dr. ir. H.J. Grootenboer, TU Twente
Prof. dr. ir. A.A.A. Molenaar, TU Delft
dr. ir. E. Riks, TU Delft
Prof. dr. ir. P.A. Vermeer, TU Stuttgart, Duitsland

Published and distributed by:

Delft University Press
Stevinweg 1
2628 CN Delft
The Netherlands

Telephone +31 15 783254
Fax +31 15 781661

CIP-DATA KONINKLIJKE BIBLIOTHEEK, DEN HAAG

Kok, A.W.M.

Lumped Pulses and Discrete Displacements: A physical way to understand numerical dynamics
/ A.W.M. Kok. - Delft : Delft University Press. - Ill.

Thesis Delft University of Technology. With ref. - With summary in Dutch.

ISBN 90-407-1118-6

NUGI 841

Subject headings: nonlinear dynamics / pavement engineering / earthquake analysis.

Copyright © 1995 by A.W.M. Kok

All rights reserved.

No part of the material protected by this copyright notice may be reproduced or utilized in any form or by any means, electronic or mechanical, including photocopying, recording or by any information storage and retrieval system, without permission from the publisher: Delft University Press, Stevinweg 1, 2628 CN Delft, The Netherlands.

Printed in The Netherlands

ACKNOWLEDGEMENTS

The research has been carried out at the Department of Civil Engineering of Delft University of Technology.

First of all I would like to gratefully acknowledge my supervisor Professor J. Blaauwendraad for his encouragement and guidance during this study.

Furthermore I want to direct acknowledgements to my colleagues at the Faculty of Civil Engineering who helped me formulate and understand much of the technical and physical backgrounds of the investigated subjects. I am especially thankful to P. Vermeer and L.J.M. Houben who helped me understand the problems of soil and pavements.

I also want to acknowledge the Commission of the European Community that sponsored the research project for the investigation and better design of earthquake resistant adobe houses. In this research project I was invaluablely supported by the profs. C. Malpartido and G. Sovero of the Universidad Nacional de San Antonio Abad del Cusco in Peru.

I wish to thank my colleagues in the Structural Mechanics Group; since my occupation with this thesis left much work on their shoulders. The most substantial help came from our secretary Carla Roovers who took care of the typing and the layout of this thesis. Finally I want to thank my wife and children; too much spare time has gone to the development and elaboration of the work that has been put down in this thesis.

CONTENTS		page
1.	INTRODUCTION	
	1.1 Aims and goals	1
	1.2 Summary of methods	1
	1.3 Outline of the thesis	3
2.	INVENTORY OF DIRECT INTEGRATION METHODS	
	2.1 Central differences	5
	2.2 Houbolt's method	7
	2.3 Newmark's method	8
	2.4 Fourpoint models	9
	2.5 Evaluation	11
3.	CONSISTENT FINITE ELEMENT MODELS	
	3.1 Strong form	13
	3.2 The Galerkin weak form	17
	3.3 Nonconforming models	22
	3.4 Higher-order models	24
	3.5 Conservation of momentum	29
	3.6 Nonlinear dynamics	30
	3.7 Nonlinear SDOF systems	36
4.	NUMERICAL STABILITY, ROBUSTNESS AND ACCURACY	
	4.1 Introduction	41
	4.2 Direct approach for stability search	43
	4.3 Turning points of numerical stability	45
	4.4 Accuracy	48
	4.5 Artificial damping	51
	4.6 Summary of model characteristics	55
5.	BEAMS AND PLATES ON AN ELASTIC FOUNDATION	
	5.1 Introduction	57
	5.2 Numerical tools	60
	5.3 Beam structures	70
	5.4 Circular plates	84
	5.5 Numerical guidelines	91
6.	EARTHQUAKE LOADS AT ADOBE STRUCTURES	
	6.1 Introduction	97
	6.2 Constitutive equations of adobe	98
	6.3 Constitutions of adobe with one crack	101
	6.4 Constitutions of adobe with two cracks	104
	6.5 Bamboo properties	108
	6.6 Essential problems	110
	6.7 The numerical model	112
	6.8 Two adobe houses	114
7.	CONCLUSIONS AND RECOMMENDATIONS	129
	SUMMARY	131
	SAMENVATTING	133
	REFERENCES	137

Symbols

Scalars

A	cross section area of beam
E	Young's modulus
F	load
G	shear modulus
M	bending moment
P	pulse
R	residu Galerkin's variation
V	shear force
c	damping factor
k	spring stiffness
u, w	displacement
α^i	participation factor vibration mode
$\alpha(t)$	shape function with respect to time
β	Newmark's free parameter
γ	free parameter consistent models
Δt	time step
ϵ	strain
ϕ	rotation
κ	curvatures
λ	divergency factor, spectral radius
η	free parameter consistent model friction coefficient
ψ	transverse shear deformation
ρ	density
σ	stress
θ	free parameter collocation models parameter artificial damping
ζ_i	proportional damping
ω_i	eigenfrequency

Symbols

Vectors

a	accelerations
f	load vector
g	body loads
m	lumped pulses
p	distributed pulses
t_n	traction forces
u	displacements
v	velocities
ϵ	strains
ϕ	vibration mode
π	applied pulses
σ	stresses

Matrices

C	damping matrix
D	rigidity matrix
H	matrix relating pulses to displacements
K	stiffness matrix
M	mass matrix
N	interpolation matrix
R	density matrix

Operators

L	operator equilibrium conditions
-----	---------------------------------

1. INTRODUCTION

1.1 Aims and goals

The fast development of computers has had an overwhelming impact on the computation methods that serve structural engineers. Since the sixties the main development of numerical methods for structural analysis is found in the finite element method. First the developments were related to static and linear elastic problems, later, since the seventies, dynamics and nonlinear mechanics are more and more considered.

A development usually continues along a once taken track. For dynamics this track has been almost purely mathematical. In my opinion the relation between the physical and the numerical meaning of the used models was released too soon in the past. The result was a series of numerical tools that are hardly accessible for engineers.

The underlying investigation of the models for dynamic analysis goes back to the base of the finite element method. By a consequent and continuous comparison of physical and numerical models a much further reaching application and interpretation of these models will be possible. These aspects are the essentials of this research.

1.2 Summary of methods

In structural analysis dynamics may be considered from different points of view.

A suitable starting point is to first consider the loads, the basis of which we select the appropriate analysis method to solve the dynamic response.

Our first step is to subdivide loads into stochastic and deterministic loads. Deterministic loads are completely known and can be taken into account very accurately. Stochastic loads are based upon, sometimes very time-consuming, observations, which result into a probabilistic description of the load. Many loads such as dead weight, water pressure, mechanical vibrations etc. are almost deterministic. Other loads are evidently probabilistic, such as wave loads, traffic loads, wind loads etc. These loads require a stochastic approach. For our purposes we limit ourselves to deterministic loads.

The next step is to consider the nature of the loads.

We subdivide dynamic loads into transient loads and steady state loads. A steady state load is a periodically repeating load pattern, which causes a periodically repeating response of the structure. Usually an analysis will be based upon a Fourier series development to time of loading and response. Consideration of one single term of the Fourier series is called a harmonic analysis, the general case is called a steady state

analysis. A load that is not developed into a Fourier series is called a transient load; the corresponding analysis is called a transient analysis. By its nature a transient analysis always includes an initial value problem. A steady state analysis neglects the initial value problem because the contribution of the initial values always disappears, after some time, because of the structural damping.

The most well known methods for the computation of dynamic response are:

- The method of the characteristics. The most important advantage of the method of the characteristics is the capability to simulate discontinuities such as shock waves. The essential limitation is that only one-dimensional problems can be analyzed. Moreover, real shock waves are extremely rare.
- The direct integration methods. The direct integration methods immediately solve the response of a structure after a new time step. In some way the differential equations are discretized to geometry and time. The equations are solved step by step.
- Modal analysis. Modal analysis develops the response into a series of vibration modes. The essential limitation of modal analysis is its applicability for linear problems only.
- Laplace transformation etc. Sometimes it is possible to transform a problem into a shape that can easier be solved with analytical methods. In practice these transformation methods cannot be used for a general approach.

In the past decades the most used methods for structural analysis appear to be:

- The modal analysis for the solution of steady state and transient loadings on linear systems.
- Direct integration methods for the solution of nonlinear problems.

Because of the increasing demand for reliable computational models for nonlinear dynamics the *direct integration methods* will be investigated here.

Direct integration methods are usually subdivided into explicit and implicit methods. With an explicit method the d.o.f.s (degrees of freedom) at the next time point are uncoupled, which means that the integration process can be carried out very simply. Implicit methods formulate coupled d.o.f.s. at the next time point, which implies the solution of a coupled system of equations with every time step. Well known explicit methods are the central difference method and the Runge Kutta methods [24], [25], [13]. The main disadvantage of the explicit methods is the conditional stability; time steps have to be small.

Numerical stability is also a problem for implicit methods. However, many integration processes, have succeeded to overcome this problem.

A problem with many of the (implicit) direct integration methods concerns the damping.

An integration process that reaches far into the time domain should damp most of the initial disturbances; this physical requirement has to be simulated by a numerical process. Unfortunately many numerical processes neglect physical damping with increasing values for the integration steps. With large integration steps no damping is simulated. Another problem concerns the convergency of iteration processes with nonlinear systems. The introduction of sharp changes of the properties can be catastrophic for the numerical simulation process.

Direct integration models are checked on the following criteria:

- A. Consistency. The numerical model has to correspond with the physical model.
- B. Numerical stability. The process should not derail with large time steps or sudden and sharp changes of the properties.
- C. Robustness. Initial disturbances have to damp even with large time steps.
- D. Accuracy. Accuracy is the rate of convergence to the exact solution.

1.3 Outline of the thesis

Chapter 2 summarizes the most widely used direct integration methods. Some attention will be paid to numerical stability and artificial and physical damping. Based on this inventory we note several shortcomings of the existing models and the presentation of these models.

In chapter 3 the equations of motion and the boundary conditions are formulated. Galerkin's variational condition is applied to the equations of motion and the boundary conditions at a domain finite with respect to time and geometry. Models with low and higher order accuracy with respect to time are developed. The resulting equations, which relate lumped pulses to discrete displacements, show a perfect correspondence with the wellknown stiffness matrix methods that relate lumped forces to discrete displacements. Nonlinear applications are anticipated and demonstrated with the help of some SDOF systems.

Chapter 4 pays attention to numerical stability, artificial damping and accuracy. A high accuracy model with unlimited numerical stability is proposed. Optimal artificial damping is related to the free model parameter. An evaluation of the investigated models concludes this chapter.

In chapter 5 these models are applied to beams and plates on an elastic foundation. The most important model parameters for pavement structures, subjected to a FWD load and a moving load, are investigated. Some nonlinear properties are considered. The investigated parameters are the mass and the damping of the subgrade, and the shear

stiffness of the base and the subgrade. The investigation compares the results of a dynamic analysis with the results of a static analysis of the peak load values. Conclusions are drawn with respect to the relevance of the investigated parameters.

In chapter 6 these methods are applied, taking into account the nonlinear constitutive equations of adobe and the nonlinear bamboo adobe interface condition, to investigate the response of adobe houses to a medium size earthquake load. The earthquake load is applied to a one-storey and a two-storey structure. Based on this analysis conclusions are drawn on the safety of these houses with respect to earthquake loads.

Chapter 7 summarizes the most important results, the limitations and the recommendations for further research.

2. INVENTORY OF DIRECT INTEGRATION METHODS

2.1 Central differences

One of the most commonly used discretisation methods is the method of the central differences.

Introducing

- K stiffness matrix
- C damping matrix
- M mass matrix
- u_n discrete displacements at $t = n \Delta t$
- v_n discrete velocities at $t = n \Delta t$
- a_n discrete accelerations at $t = n \Delta t$
- f_n load vector at $t = n \Delta t$

the equations of motion are given by

$$K u_n + C v_n + M a_n = f_n \quad (2.1)$$

and discretized following

$$\begin{aligned} v_n &= \frac{1}{2} \Delta t (u_{n+1} - u_{n-1}) \\ a_n &= \frac{1}{\Delta t^2} (u_{n+1} - 2u_n + u_{n-1}) \end{aligned} \quad (2.2)$$

The truncation error is $O[\Delta t^2]$, thus convergency is guaranteed.

Numerical stability is the limiting factor of this method. Numerical instability is the phenomenon of the exponential growth of some contributions to the numerical solution. The numerical stability is investigated by the development of an error $e(t)$ into a series of vibration modes ϕ_i which are defined by the eigenvalue problem

$$K \phi_i = \omega_i^2 M \phi_i$$

The error $e(t)$ is given by the series development

$$e(t) = \sum_i \alpha^i(t) \phi_i \quad (2.3)$$

Application of the orthogonality conditions

$$\begin{aligned} \phi_i^T M \phi_j & \begin{cases} = 0 & i \neq j \\ = 1 & i = j \end{cases} \\ \phi_i^T K \phi_j & \begin{cases} = 0 & i \neq j \\ = \omega_i^2 & i = j \end{cases} \\ \phi_i^T C \phi_j & \begin{cases} = 0 & i \neq j \\ = 2\zeta\omega_i & i = j \end{cases} \end{aligned} \quad (2.4)$$

yields the uncoupled equations of motion

$$\omega_i^2 \alpha_n + \frac{1}{\Delta t} \zeta_i \omega_i (\alpha_{n+1} - \alpha_{n-1}) + \frac{1}{\Delta t^2} (\alpha_{n+1} - 2\alpha_n + \alpha_{n-1}) = 0 \quad (2.5)$$

To solve (2.4) we substitute

$$\alpha_n = \lambda_i^n$$

which results into the characteristic equation

$$(1 + \zeta_i \omega_i \Delta t) \lambda_i^2 + (\omega_i^2 \Delta t^2 - 2) \lambda_i + (1 - \zeta_i \omega_i \Delta t) = 0 \quad (2.6)$$

The process is numerically stable if the amplification factor (spectral radius) $|\lambda_i|_{\max} \leq 1$.

From (2.6) we obtain

$$\lambda_i = \frac{1 - \frac{1}{2} \omega_i^2 \Delta t^2 \pm \sqrt{(1 - \frac{1}{2} \omega_i^2 \Delta t^2)^2 - (1 - \zeta_i^2 \omega_i^2 \Delta t^2)}}{1 + \zeta_i \omega_i \Delta t} \quad (2.7)$$

The relation between the amplification factor $|\lambda_i|$ and the radians per time step, $\omega_i \Delta t$, is shown in figure 2.1.

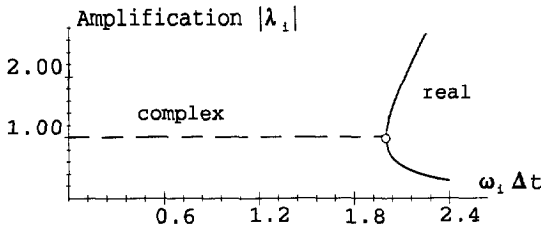


Figure 2.1 - Central differences

It appears that undamped systems ($\zeta_i = 0$) are numerically stable if $\omega_i \Delta t \leq 2$ for every ω_i . For each ω_i in this interval $|\lambda_i|$ will be exactly 1. With lumped mass matrix M , and diagonal damping matrix C , the procedure of (2.2) shows a very simple explicit computation scheme.

The central difference method is quite often used in nonlinear analyses, in which a short response time suffices. For a short time the disadvantage of many small time steps is balanced by the simplicity of an explicit method.

2.2 Houbolt's method

Houbolt [2] proposed a backward difference scheme of $O[\Delta t^2]$ accuracy. The following finite difference formulae

$$a_n = \frac{1}{\Delta t^2} (2u_n - 5u_{n-1} + 4u_{n-2} - u_{n-3}) \quad (2.8)$$

$$v_n = \frac{1}{6\Delta t} (11u_n - 18u_{n-1} + 9u_{n-2} - 2u_{n-3})$$

are substituted into the equations of motion

$$K u_n + C v_n + M a_n = f_n$$

Consistency and convergency are guaranteed. The process is unconditionally, numerically stable. For large values of $\omega_i \Delta t$ the spectral radius converges to zero.

Even if no physical damping is modelled the procedure shows considerable numerical or artificial damping for large values of $\omega_i \Delta t$. This is what we want. A disadvantage is that Houbolt's method requires special start procedures; the first two time steps can not be elaborated following (2.8).

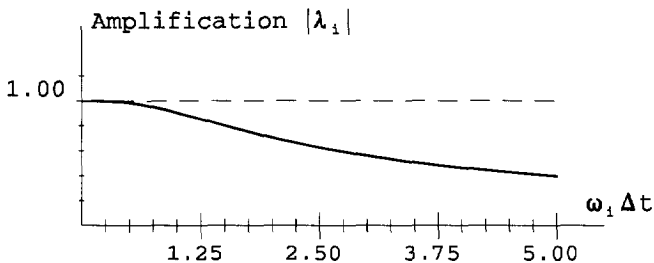


Figure 2.2 - Houbolt's method

2.3 Newmark's method

Perhaps the most widely used method is Newmark's method [1]. Starting points for this method are the displacements u_n , velocities v_n and accelerations a_n at time $t = n \Delta t$. Using the free parameters β and γ , the displacements u_{n+1} and the velocities v_{n+1} are estimated by

$$u_{n+1} = u_n + \Delta t v_n + \frac{1}{2} \Delta t^2 \{(1 - 2\beta)a_n + 2\beta a_{n+1}\} \quad (2.9)$$

$$v_{n+1} = v_n + \Delta t \{(1 - \gamma)a_n + \gamma a_{n+1}\}$$

These assumptions are substituted into the equations of motion at $t = (n+1) \Delta t$

$$\mathbf{K} u_{n+1} + \mathbf{C} v_{n+1} + \mathbf{M} a_{n+1} = f_{n+1}$$

from which the accelerations a_{n+1} are solved. Backsubstitution into (2.9) solves u_{n+1} and velocities v_{n+1} .

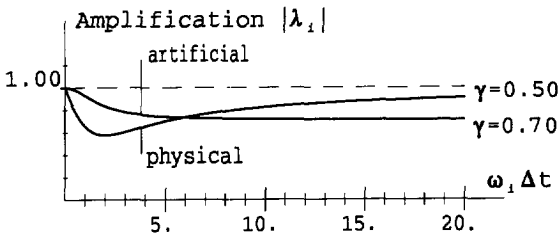


Figure 2.3 - Newmark's method

Another elaboration yields the threepoint finite difference formula

$$\begin{aligned} & \{M + \gamma \Delta t C + \beta \Delta t^2 K\} u_{n+1} + \\ & + \{-2M + (1 - 2\gamma) \Delta t C + (\frac{1}{2} - 2\beta + \gamma) \Delta t^2 K\} u_n + \\ & + \{M + (\gamma - 1) \Delta t C + (\frac{1}{2} + \beta - \gamma) \Delta t^2 K\} u_{n-1} = \Delta t^2 f_n \end{aligned} \quad (2.10)$$

Investigation of the spectral radius with the method applied in section 2.1, shows that unconditional numerical stability is guaranteed if $2\beta \geq \gamma \geq 1/2$. Artificial damping occurs if $\gamma > 1/2$. Taking the value $\beta = 1/4$ and $\gamma = 1/2$ gives us the classical trapezoidal rule. The value $\beta = 1/12$ and $\gamma = 1/2$ gives us the so-called Fox Goodwin rule (the royal road),

a model with $O[\Delta t^3]$ accuracy for undamped systems.

For large values of $\omega \Delta t$, both the Newmark method and the other direct integration methods neglect physical damping. Artificial damping -see section 4.5- has to be introduced to provide the models with the,also numerical, required damping properties. As mentioned above, the use of $\gamma > 1/2$ introduces the necessary damping to the Newmark models.

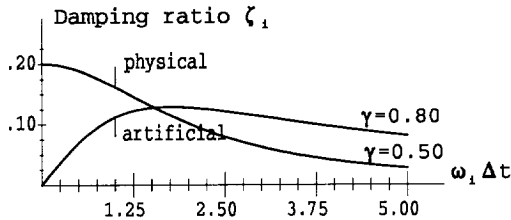


Figure 2.4 - Newmark's method

2.4 Fourpoint models

The Newmark model may be considered as a generalisation of the threepoint models. Zienkiewicz proposes a generalisation of the fourpoint models [37] of which the Wilson θ and the Hughes α -method are the most well known.

The collocation models, among which the Wilson θ method, consider the equations of motion at a time τ .

$$\tau = t + \theta \Delta t$$

with a free parameter θ

$$\mathbf{K} \mathbf{u}_\tau + \mathbf{C} \mathbf{v}_\tau + \mathbf{M} \mathbf{a}_\tau = \mathbf{f}_\tau \quad (2.11)$$

In the collocation model we substitute

$$\begin{aligned} \mathbf{u}_\tau &= \mathbf{u}_n + \theta \Delta t \mathbf{v}_n + \frac{1}{2} (\theta \Delta t)^2 \{(1 - 2\beta) \mathbf{a}_n + 2\beta \mathbf{a}_\tau\} \\ \mathbf{v}_\tau &= \mathbf{v}_n + \theta \Delta t \{(1 - \gamma) \mathbf{a}_n + \gamma \mathbf{a}_\tau\} \\ \mathbf{a}_\tau &= (1 - \theta) \mathbf{a}_n + \theta \mathbf{a}_{n+1} \end{aligned} \quad (2.12)$$

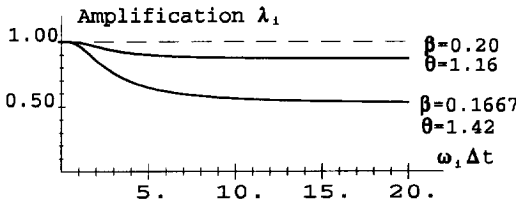


Figure 2.5 - Collocation models

By substitution of $\beta = 1/6$ we obtain the Wilson θ method [3], by substitution of $\theta = 1$ we obtain Newmark's method. Unconditional numerical stability is possible with a suitable choice of β and θ , artificial damping occurs with $\gamma > 1/2$.

The α -method [4] of Hughes/Hilber/Taylor formulates the equations of motion at $\tau = t_n + \theta\Delta t$ by

$$(1 - \theta)Ku_n + \theta Ku_{n+1} + (1 - \theta)Cv_n + \theta Cv_{n+1} + Ma_{n+1} = f_\tau \tag{2.13}$$

where u_{n+1} and v_{n+1} are taken following Newmark's assumptions

$$u_{n+1} = u_n + \Delta t v_n + \frac{1}{2} \Delta t^2 \{(1 - 2\beta) a_n + 2\beta a_{n+1}\}$$

$$v_{n+1} = v_n + \Delta t \{(1 - \gamma) a_n + \gamma a_{n+1}\}$$

To maintain the accuracy $O[\Delta t^2]$ we take $\gamma = 1/2$.

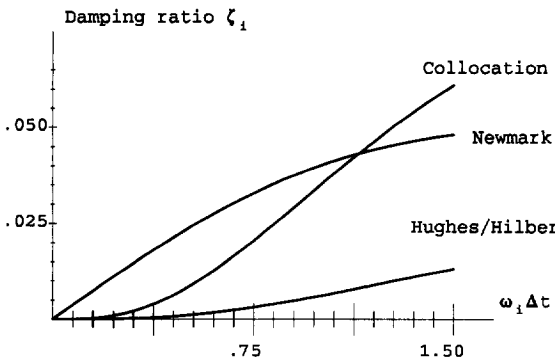


Figure 2.6 - Artificial damping

Both the α -method and the collocation methods can be rewritten as fourpoint finite difference formulae.

For small values of Δt the artificial damping of the low frequencies is very low compared with the high frequencies, see fig. 2.6.

2.5 Evaluation

Reconsidering our starting point we notice that many applications of the direct integration methods should be of a nonlinear nature. It is remarkable that the scarce literature available on this subject seldom shows parallels with the abundant literature available on nonlinear statics. Usually the nonlinear dynamic models are more problem oriented and thus, not very generally applicable.

A quite often discussed criterion in literature is the 'selfstarting' capability. On the base of initial values the direct integration process generates the new initial values for the next integration step. Commonly used are the displacements, velocities and accelerations at each time point between two adjacent time intervals. This choice, however, assumes continuity of velocities and accelerations. From a physical point of view there is no need for these assumptions, since a pulse load destroys the continuity of the velocities and a step load destroys the continuity of the accelerations. A priori conditions to these quantities do not contribute to a general applicability of the methods.

In general there is a consensus on the use of Linear Multistep Methods (LMS models). These models compute only one series of new displacements at a new time point per integration step. Higher-order models, which include more than one new time point per integration step, are not considered. The characteristic problem is the need for unconditional numerical stability with large time steps while especially the higher frequency modes should damp very fast. These properties can not be realized by physical damping; the solution is found in artificial damping.

Another confusing factor lies in the usual approach to first discretize the structure to geometry with the finite element method and to subsequently discretize the problem to time with one of these integration models. In this way discretisation is carried out in two steps. From many points of view it is preferable to perform both discretizations in one single step.

It can be concluded that there is a need for a generally applicable consistent model, which allows for discontinuities in velocities and accelerations, which does not block the search for higher-order models, and in which the discretizations to geometry and time are done in one single step. This new model is presented and discussed in the chapters 3 and 4.

3. CONSISTENT FINITE ELEMENT MODELS

3.1 Strong form

The mathematical description of the physical behaviour of a structure is always obtained by imposing conditions on the basic physical components. In structural mechanics the components of the physical behaviour are usually the forces and the deformations. Equilibrium conditions describe the force relations, kinematic conditions describe the deformations and constitutive conditions give the relations between forces and deformations. Similar components and relations are applicable to all kinds of mechanics problems, e.g. the physical components of the heat problem are heat flow and temperature, the components of electricity are currents and potentials, etc. The relations between these components are usually given by the differential equations and the boundary conditions.

A typical aspect of the finite element method (f.e.m.) is that we consider the mechanical properties within a finite domain. For a consequent approach it is necessary that we scrutinously formulate the differential equations and the boundary conditions per domain. When we want to introduce time dependent problems, we have to describe the dynamics properties within a finite domain with respect to geometry and with respect to time. The introduction of time dependency in structural mechanics requires some generalizations.

To begin with, a finite element consideration assumes a domain limited by a geometry V^e and a time interval Δt^e . Within this domain we have to formulate the conditions. Secondly the mechanical quantities have to be generalized. The generalization with respect to time introduces pulses in addition to the forces and adds velocities to the kinematic conditions. Instead of the equilibrium conditions for forces we require a pulse balance formulated by the equations of motion. In the static case these equations will degenerate into the equilibrium conditions. The constitutive equations have to include relations between the pulses and the velocities, whereas the stress/strain relations can be time dependent.

Finally, the boundary conditions have to include conditions with respect to the impulse balance at the beginning and at the end of a time interval.

Based on the physical law of conservation of momentum the equations of motion are formulated

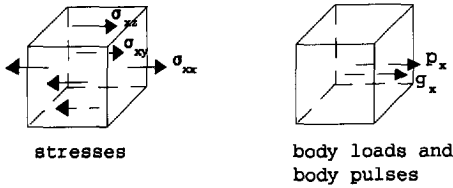
$$L \sigma + g = \dot{p} \quad (3.1)$$

in which

L - differential operator, describing the equilibrium conditions

- σ - stress vector
 p - body pulse vector
 g - body load factor

The dot means differentiation with respect to time.



Condition (3.1) has to be met within the geometrical domain (the 'element') V^e and the time domain Δt^e .

Figure 3.1 - Stresses, loads and pulses

Kinematic conditions, related to strains and velocities, are given by

$$\left. \begin{aligned} \boldsymbol{\varepsilon}^e &= L^* \boldsymbol{u}_c^e \\ \boldsymbol{v}^e &= \dot{\boldsymbol{u}}_c^e \end{aligned} \right\} \in V^e, \Delta t^e \quad (3.2)$$

in which

- L^* - differential operator, here the selfadjoint of L
 $\boldsymbol{\varepsilon}$ - strain vector
 \boldsymbol{v} - velocities
 \boldsymbol{u}_c - displacements

The underlying meaning of (3.2) is that strains and velocities exist everywhere.

The constitutive conditions relate the stresses and the pulses to the strains and the velocities. We require

$$\left. \begin{aligned} \boldsymbol{\sigma}^e &= \boldsymbol{D}^e \boldsymbol{\varepsilon}^e \\ \boldsymbol{p}^e &= \boldsymbol{R}^e \boldsymbol{v}^e \end{aligned} \right\} \in V^e, \Delta t^e \quad (3.3)$$

in which

- \boldsymbol{D}^e - rigidity matrix
 \boldsymbol{R}^e - density matrix

For isotropic linear elastic materials we use Young's modulus E and Poisson's ratio ν to define rigidity matrix \boldsymbol{D} . In a nonlinear analysis we can replace (3.3) by more complex constitutive conditions. In these paragraphs we limit ourselves to the linear case.

If desired we can also associate σ to the strain velocities by

$$\dot{\sigma}^e = D_1^e \dot{\varepsilon}^e + D_2^e \dot{\varepsilon}^e \quad (3.3a)$$

which is a way to introduce damping properties.

The density matrix R is given by the density ρ ; usually the relation between pulses and velocities is linear.

The boundary conditions have to be formulated per element, limited by geometry and time. We will confine ourselves to time independent geometrical boundaries and geometrically independent time boundaries.

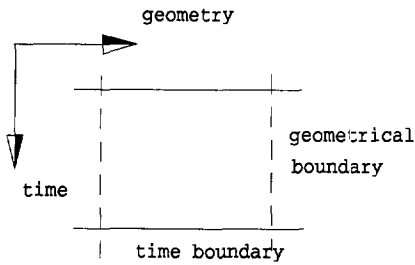


Figure 3.2 - Element with respect to geometry and time

At the geometrical boundaries equilibrium is required following the condition that

$$\sigma_n^e = t_n^e \quad \in A^e, \Delta t^e \quad (3.4a)$$

which implies that the resulting boundary stresses σ_n^e are equal to the applied boundary loads (tractions) t_n^e .

The kinematic conditions at the geometrical boundaries require

$$u_n^e = u_n^s \quad \in A^e, \Delta t^e \quad (3.5a)$$

which means that the element displacements u_n^e have to be compatible with the boundary or sectional displacements u_n^s

At the time boundaries satisfaction of the law of conservation of momentum is required, which implies that

$$p^e = \pi^e \in V^e \quad (3.4b)$$

in which π^e is the pulse distribution of element V^e at the beginning or at the end of time interval Δt^e .

The kinematic conditions require compatibility of the displacements with respect to time (no dislocations). We require

$$u^e = u^t \in V^e \quad (3.5b)$$

in which u^t are the displacements of element V^e at the beginning or the end of time interval Δt^e .

The assembly of the elements about time and geometry results into the formulation of the conditions for the entire structure over the entire time period.

During the assembly the law of conservation of momentum has to be satisfied, which requires

$$\pi^{e-} + \pi^t = \pi^{e+} \in V^e \quad (3.6a)$$

in which π^{e-} are the resulting pulses just before, and π^{e+} the applied pulses just after the time boundary. The vector π^t is the known applied pulse load at the time boundary.

The compatibility of displacements requires

$$u^t = u_0 \in V^e \quad (3.7a)$$

in which u_0 are the known displacements at the beginning of the analysis.

At the geometrical boundaries we require equilibrium following

$$\Sigma t_n^e = t_n^s \in A_t, A_s, \Delta t^e \quad (3.6b)$$

in which t_n^s is known at sections A_s and boundary A_t .

The kinematic boundary conditions are given by

$$u_n^s = \bar{\bar{u}}_n \in A_u, \Delta t^e \quad (3.7b)$$

in which $\bar{\bar{u}}_n$ are prescribed displacements at boundary A_u .

Satisfaction of the conditions (3.1) until (3.7) leads to the exact solution of the dynamics problem.

3.2 The Galerkin weak form

Very few dynamics problems are solved exactly. Especially the solution of 2D and 3D problems requires approximation methods to obtain results. A most successful method is the Galerkin-Bubnov variational method. Applying Galerkin's method to the dynamics problem as formulated in (3.1) until (3.5) per element the following is required

$$\begin{aligned}
 R^e = & \int_{V^e} \int_{\Delta t^e} \delta \tilde{\mathbf{u}}_c^e{}^T (L \tilde{\boldsymbol{\sigma}}^e - \tilde{\mathbf{p}}^e + \mathbf{g}^e) dV dt \\
 & + \oint_{A^e} \int_{\Delta t^e} \delta \tilde{\mathbf{u}}_c^e{}^T (\mathbf{t}_n^e - \tilde{\boldsymbol{\sigma}}_n^e) dA dt + \int_{V^e} \delta \tilde{\mathbf{u}}_c^e{}^T (-\boldsymbol{\pi}^e + \mathbf{p}^e) dV \Big|_{t^e=0}^{t^e=1} = 0
 \end{aligned} \tag{3.8}$$

which should hold for every kinematically admissible variation $\delta \mathbf{u}_c^e$ of the continuous displacement field $\tilde{\mathbf{u}}_c^e(x, y, z, t)$.

We will elaborate this condition. As a consequence of Green's lemma we can rewrite (3.8) as

$$\begin{aligned}
 R^e = & \int_{V^e} \int_{\Delta t^e} (-\delta \tilde{\boldsymbol{\epsilon}}^e{}^T \boldsymbol{\sigma}^e + \delta \tilde{\mathbf{v}}^e{}^T \tilde{\mathbf{p}} + \delta \tilde{\mathbf{u}}_c^e{}^T \mathbf{g}^e) dV dt \\
 & + \oint_{A^e} \int_{\Delta t^e} \delta \tilde{\mathbf{u}}_n^e{}^T \mathbf{t}_n^e dA dt - \int_{V^e} \delta \tilde{\mathbf{u}}_c^e{}^T \boldsymbol{\pi}^e dV \Big|_{t^e=0}^{t^e=1} = 0
 \end{aligned} \tag{3.9}$$

Dropping the time boundary term we easily recognize Hamilton's variational principle.

Based upon (3.9) we can develop our finite element models. The basic choice is to take the approximations of the displacements that satisfy the kinematic conditions. The simplest way is to define a time interval Δt^e , with initial displacements \mathbf{u}_0^e and final displacements \mathbf{u}_1^e , and to approximate the displacements in between in a linear way following

$$\mathbf{u}^e(t) = \alpha_0(t) \mathbf{u}_0^e + \alpha_1(t) \mathbf{u}_1^e \tag{3.10}$$

with

$$\alpha_0(t) = \frac{1}{2} - \frac{t}{\Delta t}$$

$$\alpha_1(t) = \frac{1}{2} + \frac{t}{\Delta t}$$

The time interval is illustrated in fig. 3.3. A *conforming* displacement field in the time domain is achieved in this way.

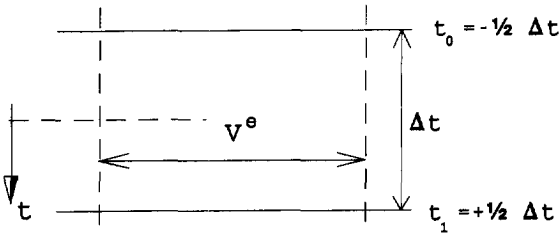


Figure 3.3 - Time interval Δt

Within the elements, between the geometrical boundaries, we take the classical shape functions following

$$\tilde{\mathbf{u}}_c^e(x,y,z,t) = \mathbf{N}^e(x,y,z) \mathbf{u}^e(t) \quad (3.11)$$

with the time dependent nodal displacements $\mathbf{u}^e(t)$.

Substitution of (3.10) and (3.11) into variational condition (3.9) yields a condition that is formulated with the use of the well known stiffness matrix \mathbf{K}^e and mass matrix \mathbf{M}^e and consistent pulse vector \mathbf{m}^e . The use of constitutive equation (3.3a) introduces a damping matrix \mathbf{C}^e .

We obtain

$$\mathbf{R}^e = -\delta \mathbf{u}_0^e{}^T \mathbf{H}_{00}^e \mathbf{u}_0^e - \delta \mathbf{u}_0^e{}^T \mathbf{H}_{01}^e \mathbf{u}_1^e - \delta \mathbf{u}_1^e{}^T \mathbf{H}_{10}^e \mathbf{u}_0^e$$

$$- \delta \mathbf{u}_1^e{}^T \mathbf{H}_{11}^e \mathbf{u}_1^e + \delta \mathbf{u}_0^e{}^T \mathbf{m}_0^{e+} + \delta \mathbf{u}_1^e{}^T \mathbf{m}_1^{e-} = 0 \quad (3.12)$$

in which

$$\begin{aligned}
 H_{00}^e &= \frac{1}{3} \Delta t K^e - \frac{1}{2} C^e - \frac{1}{\Delta t} M^e \\
 H_{01}^e &= \frac{1}{6} \Delta t K^e + \frac{1}{2} C^e + \frac{1}{\Delta t} M^e \\
 H_{10}^e &= \frac{1}{3} \Delta t K^e - \frac{1}{2} C^e + \frac{1}{\Delta t} M^e \\
 H_{11}^e &= \frac{1}{3} \Delta t K^e + \frac{1}{2} C^e - \frac{1}{\Delta t} M^e
 \end{aligned} \tag{3.13}$$

and

$$K^e = \int_{V^e} \mathbf{B}^{eT} D_1 \mathbf{B}^e dV \quad \text{stiffness matrix}$$

$$C^e = \int_{V^e} \mathbf{B}^{eT} D_2 \mathbf{B}^e dV \quad \text{damping matrix}$$

$$M^e = \int_{V^e} \mathbf{N}^{eT} \mathbf{R} \mathbf{N}^e dV \quad \text{mass matrix}$$

in which \mathbf{B}^e is the strain displacement matrix, relating the strains to the nodal displacements.

The vector \mathbf{m}^e is called the consistent pulse vector, given by

$$\begin{bmatrix} \mathbf{m}_0^{e+} \\ \mathbf{m}_1^{e-} \end{bmatrix} = \int_{\Delta t} \int_{V^e} \mathbf{N}^{eT} \mathbf{g}^e dV dt + \int_{\Delta t} \oint_{A^e} \mathbf{N}_n^{eT} \mathbf{t}_n^e dA dt + \int_{V^e} \mathbf{N}^{eT} \begin{bmatrix} +\pi_0^e \\ -\pi_1^e \end{bmatrix} dV \tag{3.14}$$

Since $R^e = 0$ for every kinematically admissible variation $\delta \mathbf{u}^e$ it should hold that

$$H_{00}^e \mathbf{u}_0^e + H_{01}^e \mathbf{u}_1^e = \mathbf{m}_0^{e+}$$

$$H_{10}^e \mathbf{u}_0^e + H_{11}^e \mathbf{u}_1^e = \mathbf{m}_1^{e-}$$

For all elements together we have to comply with

$$H_{00} u_0 + H_{01} u_1 = m_0^+ \quad (3.15)$$

$$H_{10} u_0 + H_{11} u_1 = m_1^-$$

The equations (3.15) can be interpreted as the relation between the discrete displacements u_0 and u_1 at the time points $t = t_0$ and $t = t_1$ and the equivalent pulse loads at the same time points. In these equations the initial displacements u_0 and pulses m_0^+ are known whereas the displacements u_1 and pulses m_1^- are not known.

From (3.15) we can solve the equations in more than one way. The first way is to solve u_1 from (3.15) following

$$u_1 = H_{01}^{-1} (m_0^+ - H_{00} u_0)$$

and subsequently

$$m_1^- = H_{10} u_0 + H_{11} u_1 \quad (3.16)$$

Together with the applied pulse load m_1^f at $t = t_1$ this consistent vector yields the initial pulses m_1^+ for the next time interval

$$m_1^+ + m_1^- = m_1^f$$

Another way is to apply condition (3.6a) at the assembly of R^e over two successive time intervals. Assuming the next time interval given by $[t_1, t_2]$ and displacements u_1 and u_2 , we obtain the conditions

$$H_{00} u_0 + H_{01} u_1 = m_0^+$$

$$H_{10} u_0 + (H_{11} + H_{00}) u_1 + H_{01} u_2 = m_1^- + m_1^+ = m_1^f \quad (3.17)$$

$$H_{10} u_1 + H_{11} u_2 = m_2^-$$

Example

We will demonstrate this f.e.m. model by a single degree of freedom (SDOF) system, subjected to a pulse load $P = 1$.

The equations of motions are given by

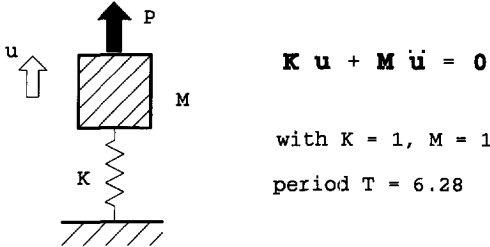


Figure 3.4 - SDOF system with pulse load

The chosen time step is $\Delta t = 0.5$. Pulses and displacements are computed following (3.15). The results are shown in table 3.1 and in figure 3.5.

Time	Displacement	Pulse	
		actual	increments
.000	.000	1.000	
.500	.480	.880	-.120
1.000	.845	.549	-.331
1.500	1.007	.086	-.463
2.000	.927	-.398	-.484
2.500	.625	-.786	-.388
3.000	.173	-.985	-.200
3.500	-.321	-.948	.037
4.000	-.737	-.684	.265
4.500	-.977	-.255	.429
5.000	-.982	.235	.490
5.500	-.752	.668	.434
6.000	-.341	.941	.273
6.500	.152	.989	.047
7.000	.608	.799	-.190
7.500	.919	.417	-.382
8.000	1.008	-.065	-.482
8.500	.856	-.531	-.466
9.000	.499	-.870	-.339
9.500	.021	-1.000	-.130
10.000	-.461	-.890	.110

Table 3.1

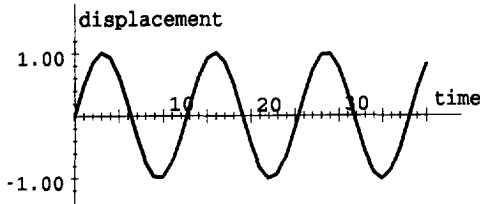


Figure 3.5 - Response of a SDOF system under pulse load

3.3 Nonconforming models

The conforming finite element model as described in the previous section is not applicable for reasons of accuracy and numerical stability, as will be discussed in chapter 4. However, a modification may solve many shortcomings. The restriction to conforming displacement fields is quite often too rigid. For convergency purposes it is sufficient to approach the stresses and strains in such a way that, after integration about time an accuracy $[\Delta t]$ is maintained.

Instead of (3.10) we choose

$$u^*(t) = \frac{1}{2}(u_0 + u_1) + \eta \frac{t}{\Delta t}(u_1 - u_0) \quad (3.18)$$

with a free parameter η .

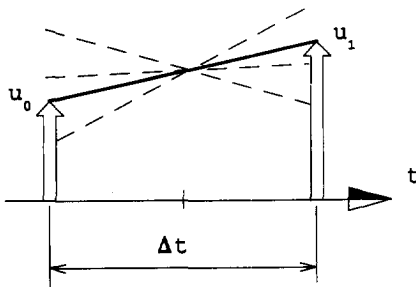


Figure 3.6 - Nonconforming displacements

The choice of (3.18) guarantees an $O[\Delta t]$ accuracy for the contributions of σ and ϵ . Substitution of (3.18) into variational condition (3.9) yields the matrices H_{ij} , with

$$\begin{aligned} H_{00} &= \left(\frac{1}{4} + \frac{1}{12} \gamma\right) \Delta t K - \frac{1}{2} C - \frac{1}{\Delta t} M \\ H_{01} &= \left(\frac{1}{4} - \frac{1}{12} \gamma\right) \Delta t K + \frac{1}{2} C + \frac{1}{\Delta t} M \\ H_{10} &= \left(\frac{1}{4} - \frac{1}{12} \gamma\right) \Delta t K - \frac{1}{2} C + \frac{1}{\Delta t} M \\ H_{11} &= \left(\frac{1}{4} + \frac{1}{12} \gamma\right) \Delta t K + \frac{1}{2} C - \frac{1}{\Delta t} M \end{aligned} \quad (3.19)$$

and $\gamma = \eta^2$.

The parameter γ differs from Newmark's γ .

Substitution of (3.19) into (3.17) leads to the Newmark finite difference formula of (2.10) in which Newmarks $\gamma = \frac{1}{2}$ and $\beta = \frac{1}{4} - \frac{1}{12} \eta^2$.

As mentioned in section 2.3 several well known models are found for different values of γ . Chapter 4 will show how parameter γ can be used to control numerical stability and accuracy.

The SDOF of figure 3.4 is used to demonstrate the effect of different values of γ . It turns out that values $\gamma > 2$ reduce the periods whereas the amplitudes are not visibly affected. Results with $\Delta t = 1$ are shown in figures 3.7 and 3.8.

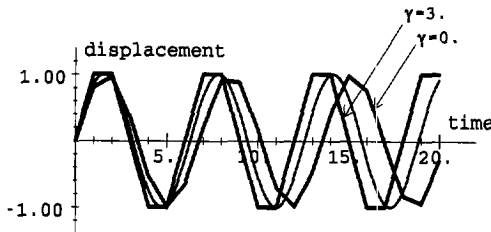


Figure 3.7 - Linear nonconforming models

Extreme accuracy is obtained for $\gamma = 2$. This model appears to be the royal road (the Goodwin-Fox model), see section 2.3. Note the time scale in figure 3.8. The use of $\Delta t = 1$ still leads to very accurate results after 15 periods.

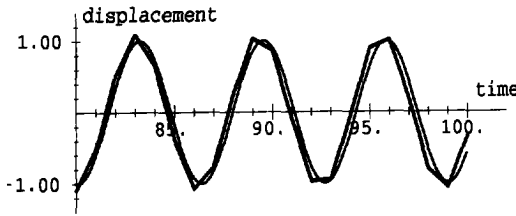


Figure 3.8 - The royal road, $\gamma = 2$

3.4 Higher-order models

The models discussed in section 3.3 are all based on a linear approximation with respect to time. These models possess $O[\Delta t]$ accuracy with respect to time. In order to obtain $O[\Delta t^2]$ accuracy we have to apply higher-order approximations with respect to time. For this purpose we introduce per time interval Δt^e a midtime discrete value per degree of freedom (d.o.f).

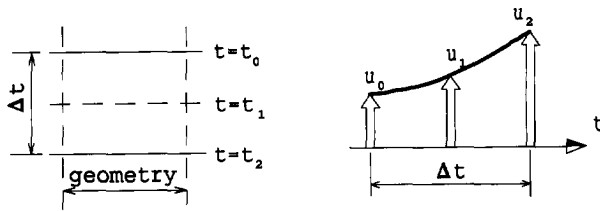


Figure 3.9 - Discrete values with respect to time

Dropping superscript e we describe the displacement field by

$$u(t) = \alpha_0(t) u_0 + \alpha_1(t) u_1 + \alpha_2(t) u_2$$

with

$$\alpha_0(t) = -\frac{t}{\Delta t} \left(1 - 2 \frac{t}{\Delta t} \right)$$

$$\alpha_1(t) = 1 - 4 \frac{t^2}{\Delta t^2}$$

$$\alpha_2(t) = \frac{t}{\Delta t} \left(1 + 2 \frac{t}{\Delta t} \right)$$

(3.20)

Substitution into the variational condition (3.9) yields the matrices H_{ij} following

$$\begin{aligned}
 H_{00} &= \frac{2}{15} \Delta t K - \frac{1}{2} C - \frac{7}{3\Delta t} M \\
 H_{01} &= \frac{1}{15} \Delta t K + \frac{2}{3} C + \frac{8}{3\Delta t} M \\
 H_{02} &= \frac{1}{30} \Delta t K - \frac{1}{6} C - \frac{1}{3\Delta t} M \\
 H_{10} &= \frac{1}{15} \Delta t K - \frac{2}{3} C + \frac{8}{3\Delta t} M \\
 H_{11} &= \frac{8}{15} \Delta t K - \frac{16}{3\Delta t} M \\
 H_{12} &= \frac{1}{15} \Delta t K + \frac{2}{3} C + \frac{8}{3\Delta t} M \\
 H_{20} &= \frac{1}{30} \Delta t K + \frac{1}{6} C - \frac{1}{3\Delta t} M \\
 H_{21} &= \frac{1}{15} \Delta t K - \frac{2}{3} C + \frac{8}{3\Delta t} M \\
 H_{22} &= \frac{2}{15} \Delta t K + \frac{1}{2} C - \frac{7}{3\Delta t} M
 \end{aligned} \tag{3.21}$$

and the equivalent pulse loads m_0^+ , m_1 and m_2^- .

The resulting equations are

$$\begin{aligned}
 H_{00} u_0 + H_{01} u_1 + H_{02} u_2 &= m_0^+ \\
 H_{10} u_0 + H_{11} u_1 + H_{12} u_2 &= m_1 \\
 H_{20} u_0 + H_{21} u_1 + H_{22} u_2 &= m_2^-
 \end{aligned} \tag{3.22}$$

Here the initial displacements u_0 and the pulse vectors m_0^+ and m_1 are known, whereas displacements u_1 and u_2 and pulse vector m_2^- are unknown.

Again we can follow two paths to solve these equations. One way is to assemble the time steps and to apply the pulse condition (3.6a). The resulting equations are formulated in u_i only.

The second way is to first solve the displacements u_1 and u_2 from (3.23) by

$$H_{01} u_1 + H_{02} u_2 = m_0^+ - H_{00} u_0 \quad (3.23)$$

$$H_{11} u_1 + H_{12} u_2 = m_1 - H_{10} u_0$$

and to compute the pulse vector by backsubstitution

$$m_2^- = H_{20} u_0 + H_{21} u_1 + H_{22} u_2 \quad (3.24)$$

With m_2^- and applied pulse load m_2^f we have the initial pulses for the next time interval.

The results of such an analysis with $\Delta t = 2.00$ for the SDOF system of figure 3.4 are shown in table 3.2 and figure 3.10.

Note that Δt is about one third of the natural period T .

Time	Displacement	Pulse	
		actual	increment
0.00	0.000	1.000	
1.00	0.825		
2.00	0.900	-0.400	-1.400
3.00	0.165		
4.00	-0.720	-0.680	-0.280
5.00	-0.957		
6.00	-0.324	0.944	1.624
7.00	0.601		
8.00	0.979	-0.075	-1.019
9.00	0.477		
10.00	-0.459	-0.884	-0.809

Table 3.2

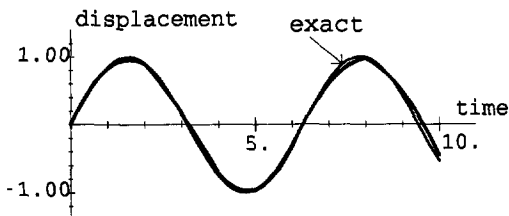


Figure 3.10 - Results for quadratic conforming model

It is possible to develop higher-order models with cubic approximations [11] or higher-order approximations with respect to time. The higher the polynomial degree, the more discrete values we have to solve within one time step. Assuming we approach the time dependency with a polynomial of the degree n, we have in correspondence with (3.22) to solve the system of equations

$$\begin{aligned}
 H_{00}u_0 + H_{01}u_1 + \dots + H_{0n}u_n &= m_0^+ \\
 H_{10}u_0 + H_{11}u_1 + \dots + H_{1n}u_n &= m_1 \\
 \vdots & \\
 H_{n0}u_0 + H_{n1}u_1 + \dots + H_{nn}u_n &= m_n^-
 \end{aligned}
 \tag{3.25}$$

The matrices H_{ij} are found by elaboration of the variational condition (3.9) using n-th degree polynomials with respect to time. Because no realistic application of the higher-order models are known we will not elaborate them. We continue with the quadratic models.

Just like the linear model in section 3.3, the quadratic models can be modified without loss of accuracy. To describe stresses and strains instead of (3.21) we use

$$u^*(t) = \frac{1}{6}u_0 + \frac{2}{3}u_1 + \frac{1}{6}u_2 + \frac{t}{\Delta t}(u_2 - u_0) - 2\eta\left(\frac{1}{12} - \frac{t^2}{\Delta t^2}\right)(u_0 - 2u_1 + u_2)
 \tag{3.26}$$

The description can be interpreted as a series development to Legendre polynomials with a free parameter η for the second Legendre polynomial.

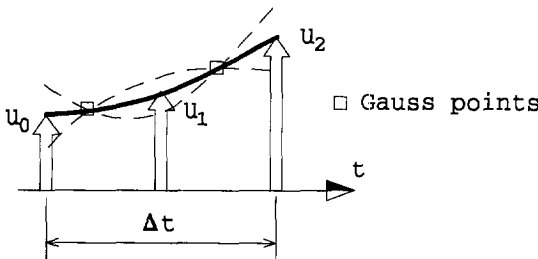


Figure 3.11 - Free contribution of the second Legendre polynomial

Substitution of (3.26) in variational condition (3.9) yields the matrices H_{ij} , with $\gamma = \eta^2$

$$\begin{aligned}
 H_{00} &= \Delta t \left(\frac{1}{9} + \frac{1}{45} \gamma \right) K - \frac{1}{2} C - \frac{7}{3 \Delta t} M \\
 H_{01} &= \Delta t \left(\frac{1}{9} - \frac{2}{45} \gamma \right) K + \frac{2}{3} C + \frac{8}{3 \Delta t} M \\
 H_{02} &= \Delta t \left(-\frac{1}{18} + \frac{1}{45} \gamma \right) K - \frac{1}{6} C - \frac{1}{3 \Delta t} M \\
 H_{10} &= \Delta t \left(\frac{1}{9} - \frac{2}{45} \gamma \right) K - \frac{2}{3} C + \frac{8}{3 \Delta t} M \\
 H_{11} &= \Delta t \left(\frac{4}{9} + \frac{4}{45} \gamma \right) K - \frac{16}{3 \Delta t} M \\
 H_{12} &= \Delta t \left(\frac{1}{9} - \frac{2}{45} \gamma \right) K + \frac{2}{3} C + \frac{8}{3 \Delta t} M \\
 H_{20} &= \Delta t \left(-\frac{1}{18} + \frac{1}{45} \gamma \right) K + \frac{1}{6} C - \frac{1}{3 \Delta t} M \\
 H_{21} &= \Delta t \left(\frac{1}{9} - \frac{2}{45} \gamma \right) K - \frac{2}{3} C + \frac{8}{3 \Delta t} M \\
 H_{22} &= \Delta t \left(\frac{1}{9} + \frac{1}{45} \gamma \right) K + \frac{1}{2} C - \frac{7}{3 \Delta t} M
 \end{aligned} \tag{3.27}$$

The SDOF system in figure 3.4 is analyzed with quadratic models using time step $\Delta t = 2$ and $\gamma = 0$ and $\gamma = 2$. The results are shown in the figures 3.12 and 3.13.

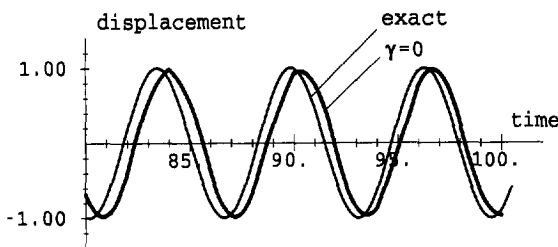


Figure 3.12 - Quadratic model, $\gamma = 0$

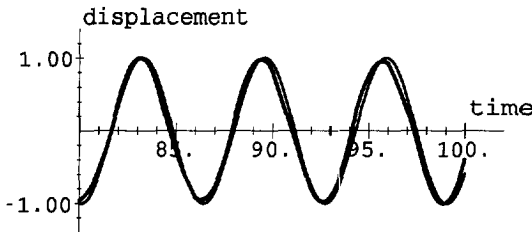


Figure 3.13 - Quadratic model, $\gamma = 2$

The results in figure 3.12 are evidently better than in the linear models of section 3.3 - see figure 3.7 - although not as accurate as the Goodwin-Fox model in figure 3.8. On the other hand the model with $\gamma = 2$ again shows an extreme accuracy, which indicates an even higher accuracy than the Goodwin-Fox model. Again, the nature of the response is a small increment of the periods for $\gamma > 2$ and shows a decrement for $\gamma < 2$. The amplitude appears to be unaffected.

3.5 Conservation of momentum

For elements exactly satisfying the rigid body motion it is possible to formulate the following lemma:

The resulting pulses vanish per element and per time step .

The consequence of this lemma is very useful. It means that in a transient analysis, based on the models of the previous sections, the pulses resulting from applied loads, stresses and body pulses exactly satisfy the law of conservation of momentum. *This conclusion is completely parallel to the static analysis in which the resulting forces of applied loads and stresses exactly satisfy the equilibrium conditions .* This property gives us a criterion to check numerical loss of accuracy (e.g. caused by ill conditioning). The proof of this criterion is as follows: For every variation $\delta \hat{u}_c^e$ we have satisfied the variational condition

$$R^e = - \int_{V^e} \int_{\Delta t^e} \left(\delta \bar{\mathbf{e}}^e \cdot \bar{\boldsymbol{\sigma}} - \delta \bar{\mathbf{v}}^e \cdot \bar{\mathbf{p}}^e \right) dV dt + \delta \hat{u}_0^e \cdot \mathbf{m}_0^{e+} + \delta \hat{u}_n^e \cdot \mathbf{m}_n^{e-} = 0$$

When we subsequently consider the virtual rigid body motions and the virtual dislocation $\delta \hat{u}^e$ with the virtual strains $\delta \hat{\epsilon}^e = 0$ and the velocities $\delta \hat{v}^e = 0$ then R^e satisfies for every rigid body motion $\delta \hat{u}^e$

$$R^e = \delta \hat{u}^e T \left(\hat{m}_0^+ + \hat{m}_n^- \right) = 0 \quad (3.28)$$

Here $\hat{m}_0^+ + \hat{m}_n^-$ are the resulting pulses at $t = t_0$ and $t = t_1$.

Hence the resulting pulses vanish.

3.6 Nonlinear dynamics

The most relevant applications of a direct integration method are found in nonlinear dynamics. The Galerkin variational method, as outlined before, can be applied to nonlinear problems as well. The use of the linear constitutive models of (3.3) and the linear kinematic conditions of (3.2) never essentially limits the elaboration of variational condition (3.9). We can formulate and apply nonlinear kinematic conditions by the finite increments

$$\Delta \epsilon = \Delta \epsilon(u, \Delta u) \quad (3.29)$$

$$\Delta v = \Delta v(\Delta u)$$

with strain increment $\Delta \epsilon$, velocity increment Δv and displacement increment Δu .

Nonlinear constitutive equations are taken into account by

$$\Delta \sigma = \Delta \alpha(\alpha, \Delta \epsilon) \quad (3.30)$$

$$\Delta p = \Delta p(\Delta v)$$

Nonlinear stress/strain relations are taken into account, pulse velocity relations are assumed to be linear. It is even possible to introduce nonlinear damping by nonlinear constitutive equations that are dependent on the strain velocities

$$\Delta \sigma = \Delta \sigma(\alpha, p, \Delta \epsilon, \Delta \dot{\epsilon}) \quad (3.30a)$$

We start an iteration process by application of the full load during time step Δt . In (3.9) we substitute the linearized equations and obtain the conditions to calculate an estimate of the displacements u_1 and, in the quadratic model, also u_2 .

Using the nonlinear kinematic conditions (3.29) and the nonlinear constitutive equations (3.30), and confining ourselves to the linear model, we recalculate the consistent initial pulses m_0^+ and final pulses m_1^- following

$$\delta u_0^T m_0^+ + \delta u_1^T m_1^- = \int_{\Delta t V} (\delta \bar{\epsilon}^T \bar{\sigma} - \delta v^T \bar{p}) dV dt \quad (3.31)$$

It is very likely that the new m_0^+ differs from the initial pulses so that a correction is necessary.

The residu between the applied initial pulse and the computed initial pulse following (3.31) is applied again as initial pulse of this time interval. The increments of the displacements are calculated, the same steps corresponding to a nonlinear static analysis are executed.

The following iteration procedure is performed for the linear model.

For the numerical elaborations we assume

$$\bar{u}(t) = u_0 + \Delta \bar{u}(t)$$

with $\Delta u = 0$ at $t = t_0$

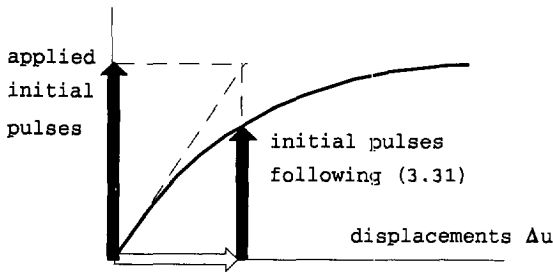


Figure 3.14 - Calculation of consistent pulses in a nonlinear analysis

Now velocities, stresses and pulses are found by

$$\bar{\sigma}(t) = \bar{\sigma}_0 + \Delta \bar{\sigma}(t)$$

$$\bar{v}(t) = \Delta \bar{v}(t)$$

$$\bar{p}(t) = \Delta \bar{p}(t)$$

Substitution in the variational conditions yields

$$\begin{aligned}
 R^e = & \int \int (-\delta \tilde{\mathbf{e}}^T \Delta \tilde{\boldsymbol{\sigma}} + \delta \tilde{\mathbf{v}}^T \Delta \tilde{\boldsymbol{p}}) dV dt + \int \int (-\delta \tilde{\mathbf{e}}^T \tilde{\boldsymbol{\sigma}}_0 + \delta \tilde{\mathbf{u}}_c^T \mathbf{g}) dV dt \\
 & + \oint \int -\delta \tilde{\mathbf{u}}_n^T \mathbf{t}_n dA dt - \int_V \delta \tilde{\mathbf{u}}_c^T \boldsymbol{\pi} dV \Big|_{t=t_0}^{t=t_1} = 0
 \end{aligned} \tag{3.32}$$

Based upon these starting points the following procedure has been developed.

1. Set up the matrix \mathbf{H}_{0I}
2. Decompose matrix \mathbf{H}_{0I}
3. Compute an estimate of increments of the displacements

$$\Delta \mathbf{u}_1 = \mathbf{H}_{0I}^{-1} \Delta \mathbf{m}_0$$

with the start values $\Delta \mathbf{u}_0 = 0$.

4. Compute strain and velocity increments at the integration points

$$\Delta \boldsymbol{\varepsilon} = \Delta \boldsymbol{\varepsilon}(\mathbf{u}, \Delta \mathbf{u})$$

$$\Delta \mathbf{v} = \Delta \mathbf{v}(\Delta \mathbf{u})$$

5. Compute stress and pulse increments

$$\Delta \boldsymbol{\sigma} = \Delta \boldsymbol{\sigma}(\boldsymbol{\alpha} \boldsymbol{p}, \Delta \boldsymbol{\varepsilon}, \Delta \dot{\boldsymbol{\varepsilon}})$$

$$\Delta \boldsymbol{p} = \Delta \boldsymbol{p}(\Delta \mathbf{v})$$

6. Compute the consistent pulse vectors \mathbf{m}_0^+ en \mathbf{m}_1^-

$$\delta \mathbf{u}_0^T \mathbf{m}_0^+ + \delta \mathbf{u}_1^T \mathbf{m}_1^- = \int \int_{\Delta t V} (\delta \tilde{\mathbf{e}}^T \tilde{\boldsymbol{\sigma}} - \delta \tilde{\mathbf{v}}^T \tilde{\boldsymbol{p}}) dV dt$$

7. Compute the residual initial pulses. Repeat the analysis with the residual initial pulses until sufficient accuracy has been achieved.

In general it will be sufficient to compute the results for the linear model at only one integration point, the midtime point of interval Δt . For quadratic models with $\gamma = 0$ it will be sufficient to compute the results at the two Gauss points of time interval Δt .

With reference to the variational condition of (3.31) we take the convergence criterion

$$\Delta H = |\Delta u_0 m_0^+ + \Delta u_1 m_1^-| < \text{tolerance factor} * |H_{ref}|$$

in which H_{ref} is the first value of ΔH in the iteration procedure. This criterion is very similar to the energy criterion for static problems.

The iteration procedure as outlined previously is not unambiguous for $\gamma \neq 0$. The computation of the equivalent pulse vectors in step 6 can be carried out in more than one way. The simplest procedure is to take a linear distribution of $\Delta \sigma(t)$ with respect to time, assuming

$$\Delta \sigma(t) = \left(\frac{1}{2} - \eta \frac{t}{\Delta t}\right) \Delta \sigma_0 + \left(\frac{1}{2} + \eta \frac{t}{\Delta t}\right) \Delta \sigma_1 \quad (3.33)$$

and for the strains

$$\Delta \epsilon(t) = \left(\frac{1}{2} - \eta \frac{t}{\Delta t}\right) \Delta \epsilon_0 + \left(\frac{1}{2} + \eta \frac{t}{\Delta t}\right) \Delta \epsilon_1$$

Elaboration of yields the (tangent) matrices H_{ij} following ($\gamma = \eta^2$):

$$H_{00} = \left(\frac{1}{4} + \frac{1}{12} \gamma\right) \Delta t K_0 - \left(\frac{1}{4} + \frac{1}{12} \gamma\right) C_0 - \left(\frac{1}{4} - \frac{1}{12} \gamma\right) C_1 - \frac{1}{\Delta t} M$$

$$H_{01} = \left(\frac{1}{4} - \frac{1}{12} \gamma\right) \Delta t K_1 + \left(\frac{1}{4} + \frac{1}{12} \gamma\right) C_0 + \left(\frac{1}{4} - \frac{1}{12} \gamma\right) C_1 + \frac{1}{\Delta t} M$$

$$H_{10} = \left(\frac{1}{4} - \frac{1}{12} \gamma\right) \Delta t K_0 - \left(\frac{1}{4} - \frac{1}{12} \gamma\right) C_0 - \left(\frac{1}{4} + \frac{1}{12} \gamma\right) C_1 + \frac{1}{\Delta t} M$$

$$H_{11} = \left(\frac{1}{4} + \frac{1}{12} \gamma\right) \Delta t K_1 + \left(\frac{1}{4} - \frac{1}{12} \gamma\right) C_0 + \left(\frac{1}{4} + \frac{1}{12} \gamma\right) C_1 - \frac{1}{\Delta t} M$$

in which K_0 and C_0 the tangent stiffness and damping matrices at $t = t_0$ and K_1 and C_1 are the tangent and stiffness damping matrices at $t = t_1$. It should be noted that even for undamped structures matrix H is no longer symmetric because $K_1 \neq K_0$.

Instead of (3.33) we can assume that $\sigma(t)$ follows the strains following

$$\Delta \sigma(t) = D(t) \Delta \epsilon(t) \quad (3.35)$$

in which

$$D(t) = \left(\frac{1}{2} - \eta \frac{t}{\Delta t}\right) D_0 + \left(\frac{1}{2} + \eta \frac{t}{\Delta t}\right) D_1$$

Now the stresses $\Delta \sigma(t)$ follow a quadratic distribution with respect to time.

Substitution into a variational condition of the undamped system yields the matrices H_{ij} :

$$H_{00} = \Delta t \left(\frac{1}{8} + \frac{1}{24} \eta^2 \right) (\mathbf{K}_0 + \mathbf{K}_1) - \frac{\Delta t}{12} \eta^2 (\mathbf{K}_1 - \mathbf{K}_0) - \frac{1}{\Delta t} \mathbf{M}$$

$$H_{01} = \Delta t \left(\frac{1}{8} - \frac{1}{24} \eta^2 \right) (\mathbf{K}_0 + \mathbf{K}_1) + \frac{1}{\Delta t} \mathbf{M}$$

$$H_{10} = H_{01}$$

$$H_{11} = \Delta t \left(\frac{1}{8} + \frac{1}{24} \eta^2 \right) (\mathbf{K}_0 + \mathbf{K}_1) + \frac{\Delta t}{12} \eta^2 (\mathbf{K}_1 - \mathbf{K}_0) - \frac{1}{\Delta t} \mathbf{M}$$

This time matrix H is symmetric for undamped structures.

The iteration procedure also has to be considered for the quadratic models. In fact only one quadratic model is interesting, namely the value $\gamma = 0$; since all other models are only conditionally numerically stable and therefore not feasible. For this model we again consider the options of (3.33) and (3.35).

The first option assumes, with $\gamma = 0$

$$\Delta \mathbf{e} = \frac{1}{6} \Delta \mathbf{e}_0 + \frac{2}{3} \Delta \mathbf{e}_1 + \frac{1}{6} \Delta \mathbf{e}_2 + \frac{t}{\Delta t} (\Delta \mathbf{e}_2 - \Delta \mathbf{e}_0) \quad (3.36)$$

$$\Delta \sigma = \frac{1}{6} \Delta \sigma_0 + \frac{2}{3} \Delta \sigma_1 + \frac{1}{6} \Delta \sigma_2 + \frac{t}{\Delta t} (\Delta \sigma_2 - \Delta \sigma_0)$$

in which

$$\Delta \sigma_0 = \mathbf{D}_0 \Delta \mathbf{e}_0$$

$$\Delta \sigma_1 = \mathbf{D}_1 \Delta \mathbf{e}_1$$

$$\Delta \sigma_2 = \mathbf{D}_2 \Delta \mathbf{e}_2$$

Substitution into the variational condition (3.31) yields to H the contribution H_k

$$H_k = \Delta t \begin{bmatrix} \frac{1}{9} \mathbf{K}_0 & \frac{1}{9} \mathbf{K}_1 & -\frac{1}{18} \mathbf{K}_2 \\ \frac{1}{9} \mathbf{K}_0 & \frac{4}{9} \mathbf{K}_1 & \frac{1}{9} \mathbf{K}_2 \\ -\frac{1}{18} \mathbf{K}_0 & \frac{1}{9} \mathbf{K}_1 & \frac{1}{9} \mathbf{K}_2 \end{bmatrix}$$

It turns out that matrix H_k is no longer symmetric.

In correspondence with (3.35) the second option assumes

$$\Delta\sigma(t) = \mathbf{D}(t) \Delta\mathbf{e}(t) \quad (3.38)$$

in which

$$\mathbf{D}(t) = \mathbf{D}_I + \frac{t}{\Delta t} \mathbf{D}_{II} - \eta^2 \left(\frac{1}{12} - \frac{t^2}{\Delta t^2} \right) \mathbf{D}_{III}$$

$$\mathbf{D}_I = \frac{1}{6} \mathbf{D}_0 + \frac{2}{3} \mathbf{D}_1 + \frac{1}{6} \mathbf{D}_2$$

$$\mathbf{D}_{II} = \mathbf{D}_2 - \mathbf{D}_0$$

$$\mathbf{D}_{III} = \mathbf{D}_0 - 2\mathbf{D}_1 + \mathbf{D}_2$$

Taking $\eta^2 = 0$ and substitution into the variational condition (3.31) yields the following contribution of the stiffness matrices to \mathbf{H}

$$\mathbf{H}_k = \Delta t \begin{bmatrix} \frac{1}{9} \mathbf{K}_I - \frac{1}{36} \mathbf{K}_{II} & \frac{1}{9} \mathbf{K}_I - \frac{1}{18} \mathbf{K}_{II} & -\frac{1}{18} \mathbf{K}_I \\ \frac{1}{9} \mathbf{K}_I - \frac{1}{18} \mathbf{K}_{II} & \frac{4}{9} \mathbf{K}_I & \frac{1}{9} \mathbf{K}_I + \frac{1}{18} \mathbf{K}_{II} \\ -\frac{1}{18} \mathbf{K}_I & \frac{1}{9} \mathbf{K}_I + \frac{1}{18} \mathbf{K}_{II} & \frac{1}{9} \mathbf{K}_I + \frac{1}{36} \mathbf{K}_{II} \end{bmatrix}$$

in which

$$\mathbf{K}_I = \frac{1}{6} \mathbf{K}_0 + \frac{2}{3} \mathbf{K}_1 + \frac{1}{6} \mathbf{K}_2$$

$$\mathbf{K}_{II} = \mathbf{K}_2 - \mathbf{K}_0$$

Now the matrix \mathbf{H}_k is symmetric.

Summarizing the two options:

- Option 1 Stresses $\Delta\sigma$ follow the same interpolation rules as $\Delta\mathbf{e}$. Matrix \mathbf{H}_k is not symmetric.
- Option 2 Strains $\Delta\mathbf{e}$ and rigidity \mathbf{D} follow the same interpolation rules. Stresses $\Delta\sigma$ are always obtained via the constitutive equations.
Matrix \mathbf{H}_k is symmetric.

Based on physical considerations matrix \mathbf{H}_k has to be symmetric, which implies that option 1 has to be rejected.

Utilization in the TILLY program

The linear model has been implemented in the TILLY program of the Structural Mechanics Group of the Faculty of Civil Engineering. This program is a general-purpose package for nonlinear dynamic structural problems [52] based on the Discrete Element Method (DEM) .

3.7 Nonlinear SDOF systems

Example 1

The procedure as outlined in section 3.6 is applied to the structure in figure 3.15.

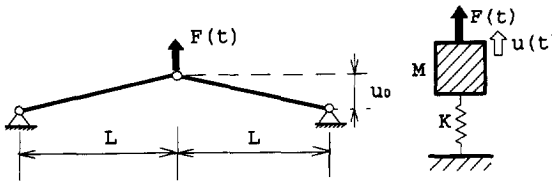


Figure 3.15 - Geometrical nonlinear system

The structure is modelled to a SDOF system with nonlinear spring properties.

The axial stiffness of the two bars is EA , the axial strain ϵ and the normal force N .

Assuming initial displacement u_0 and small strains we use the nonlinear kinematic relation

$$\epsilon = \frac{u_0 u + \frac{1}{2} u^2}{L^2}$$

and the linear constitutive equation

$$N = EA \epsilon$$

The resulting force F is now given by

$$F \approx \frac{EA}{L^3} (2u_0^2 u + 3u_0 u^2 + u^3) \quad (3.40)$$

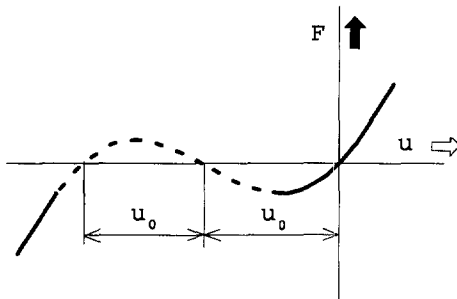


Figure 3.16 - Force/displacements diagram

For small strain increments we obtain

$$\Delta F = K_t \Delta u$$

with

$$K_t = \frac{EA}{L^3} (2u_0^2 + 6u_0u + 3u^2) \tag{3.41}$$

The example of figure 3.15 is elaborated with the iteration procedure of (3.33) and (3.35) and the values $EA = 100$, $M = 1$, $u_0 = 0.50$, $L = 5.00$, $\Delta t = 0.5$ and subjected to a pulse load $P = -0.50$. For model parameter $\gamma = 0$ the results are shown in fig. 3.17.

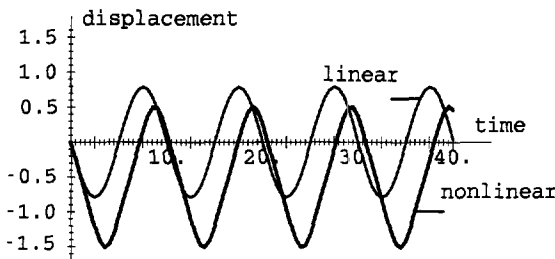


Figure 3.17 - A nonlinear SDOF system

For reasons of comparison also the linear solution, based on small displacements of u , is shown.

Example 2

The second example concerns an SDOF system with physically nonlinear properties. The spring is assumed to follow an ideal plastic force displacement relation

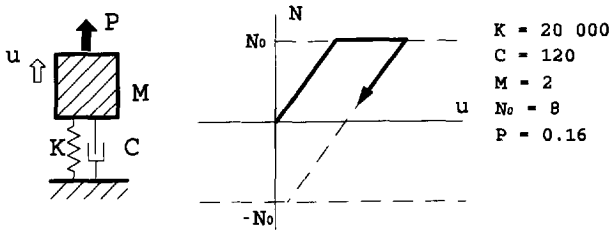


Figure 3.18 -A physically nonlinear SDOF system

The system is subjected to a pulse load $P = 0.16$. The iteration procedure has to be started at the time interval where the plastic zone is entered. Taking $\Delta t = 0.00025$ this will be the third time step, which is the only time step in which such a situation arises, see figure 3.19.

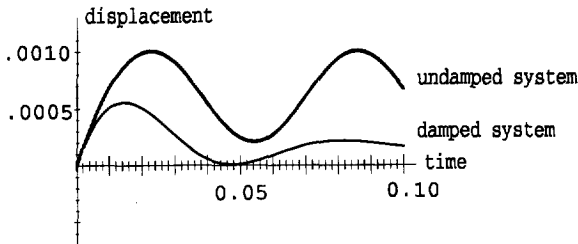


Figure 3.19 - Plastic nonlinear SDOF system

During the analysis a second source of numerical instability became evident. Even for $\gamma \leq 0$ small values of the integration time step Δt have to be used in order to ensure numerical stability. It turns out that the iteration procedure can provoke numerical instability. Usually the iteration procedure derails with strong variations of the stiffness during one time step [11]. In those cases a (automatic) reduction of the time steps has to be considered.

The procedure followed here assumes a constant stiffness that is determined by the quotient of the total force increment and the displacement increment over the time step Δt , see figure 3.20 .

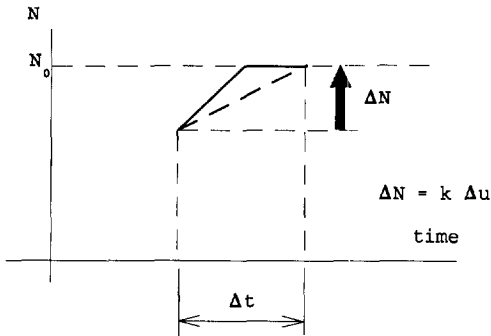


Figure 3.20 - Constant spring stiffness during a time step

Example 3

Another SDOF system is subjected to a cyclic load $F(t) = 30 \sin 20 \pi t$. Here we use the material constants $K = 20\,000$, $C = 0$, $M = 2$, $N_0 = 30$.

The nonlinear response for the spring is shown in figure 3.21.

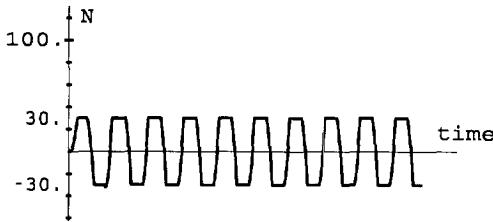


Figure 3.21 - Response to a cyclic load of a nonlinear SDOF system

For both loads the accuracy of both the linear and the quadratic model is very high; differences are not very well recognizable in the pictures and no attempt has been made to show them.

The quadratic model appeared to be very sensible to the choice of time step Δt ; too large values cause divergency of the iteration processes. More sophisticated iteration procedures will certainly improve the results. Given the accuracy of the results, this example does not invite to search for more improvements.

4. NUMERICAL STABILITY, ROBUSTNESS AND ACCURACY

4.1 Introduction

As was pointed out in chapter 1 and 2, *numerical stability*, *robustness* and *accuracy* are the main problems of a direct integration process. Numerical instability is the phenomenon of a derailment of the integration process by exponential growth of initially small errors. Inaccuracy results from round off errors, truncation errors are errors caused by discretization to time and geometry. Convergency to the exact solution is a problem of accuracy, derailment is a question of numerical stability.

The figures 4.1 and 4.2 show some manifestations of numerical instability of the SDOF system.

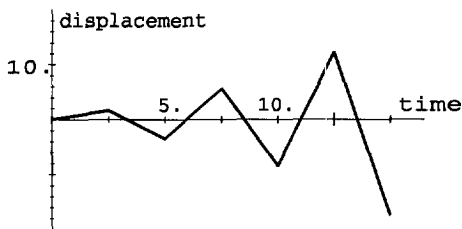


Figure 4.1 - Unstable linear model

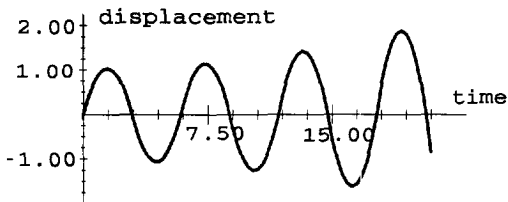


Figure 4.2 - Unstable quadratic model

The usual approach is to develop an error $\Delta u_i = e_i$ for $t = i \Delta t$ into a series of vibration modes ϕ_k following

$$e = \sum_k \alpha^k \phi_k \quad (4.1)$$

with participation factors α^k .

We consider the development of e as a result of an initial displacement error Δu_0 and an initial pulse load error Δm_0^+ . No other loads are applied.

Substitution of (4.1) into the equations (3.25) and application of the orthogonality relations

$$\begin{aligned} \Phi_k^T K \Phi_m & \begin{cases} = 0 & k \neq m \\ = \omega_k^2 & k = m \end{cases} \\ \Phi_k^T C \Phi_m & \begin{cases} = 0 & k \neq m \\ = 2\zeta_k \omega_k & k = m \end{cases} \\ \Phi_k^T M \Phi_m & \begin{cases} = 0 & k \neq m \\ = 1 & k = m \end{cases} \end{aligned} \quad (4.2)$$

yields, for each vibration mode, the equations of motion

$$h_{ij} \alpha_j \begin{cases} = \mu_0^+ & i = 0 \\ = 0 & i = 1, 2, \dots, n-1 \\ = \mu_n^- & i = n \end{cases} \quad (4.3)$$

with

$$h_{ij} = \Phi_k^T H_{ij} \Phi_k$$

$$\mu_0^+ = \Phi_k^T m_0^+ \quad k = 1, 2, \dots, n-1$$

$$\mu_n^- = \Phi_k^T m_n^-$$

and in which

$$\left. \begin{array}{l} i = 0, 1 \\ j = 0, 1 \end{array} \right\} \text{linear model}$$

$$\left. \begin{array}{l} i = 0, 1, 2 \\ j = 0, 1, 2 \end{array} \right\} \text{quadratic model}$$

For each mode Φ_k we investigate the development of participation factor α_i^k .

4.2 Direct approach for stability search

The direct approach is to solve α from the assembly of (4.3) over two time steps, given by

$$\begin{aligned}
 h_{00}\alpha_0 + h_{01}\alpha_1 + \dots + h_{0n}\alpha_n &= \mu_0^+ \\
 h_{10}\alpha_0 + h_{11}\alpha_1 + \dots + h_{1n}\alpha_n &= 0 \\
 &\vdots \\
 h_{n0}\alpha_0 + h_{n1}\alpha_1 + \dots + (h_{nn} + h_{00})\alpha_n + h_{01}\alpha_{n+1} + \dots + h_{0n}\alpha_{2n} &= 0 \\
 &\quad h_{10}\alpha_n \quad + h_{11}\alpha_{n+1} + \dots + h_{1n}\alpha_{2n} = 0 \\
 &\quad \vdots \\
 &\quad h_{n0}\alpha_n \quad + h_{n1}\alpha_{n+1} + \dots + (h_{nn} + h_{00})\alpha_{2n} + \dots
 \end{aligned} \tag{4.4}$$

The general equation is

$$A_0 \alpha_{i-1} + A_1 \alpha_i + A_2 \alpha_{i+1} = 0 \tag{4.5}$$

with α for three successive time steps and

$$\begin{aligned}
 A_0 &= \begin{bmatrix} 0 & \dots & h_{n0} \\ \vdots & & \\ 0 & \dots & 0 \end{bmatrix} \\
 A_1 &= \begin{bmatrix} h_{n1} & h_{n2} & \dots & (h_{nn} + h_{00}) \\ 0 & \dots & 0 & h_{10} \\ \vdots & & & \\ 0 & \dots & & h_{n-10} \end{bmatrix} \\
 A_2 &= \begin{bmatrix} h_{01} & h_{02} & \dots & h_{0n} \\ h_{11} & h_{12} & \dots & h_{1n} \\ \vdots & & & \\ h_{n-11} & \dots & & h_{n-1n} \end{bmatrix}
 \end{aligned}$$

For the solution of (4.5) we substitute

$$\alpha_i = \lambda^i \alpha_0$$

with which (4.5) can be written as

$$\lambda^{i-1} (A_0 + \lambda A_1 + \lambda^2 A_2) \alpha_0 = 0$$

Nontrivial solutions are found if

$$\det(A_0 + \lambda A_1 + \lambda^2 A_2) = 0 \tag{4.6}$$

The solution of (4.6) yields the eigenvalues λ . If $|\lambda|_{\max} > 1$ the error α_0 will diverge, if $|\lambda|_{\max} \leq 1$ the error will be kept stable. Our problem is to fix the limits between which numerical stability is guaranteed.

When ignoring the damping matrix C , the matrix $[h_{ij}]$ defined by (4.3) will be symmetric. As a consequence determinant (4.6) can be written as

$$\det = \lambda^p (1 - 2\lambda\eta + \lambda^2) = 0 \tag{4.7}$$

in which η depends on the chosen model.

The solution of (4.7) shows complex roots with $|\lambda| = 1$ if $|\eta| \leq 1$. The roots are real with $|\lambda|_{\max} > 1$ if $|\eta| > 1$.

Numerical stability is ensured if $|\eta| \leq 1$. We will elaborate this condition per model.

The *linear model* yields for the characteristic equation (4.7)

$$h_{10} + \lambda(h_{00} + h_{11}) + \lambda^2 h_{01} = 0 \tag{4.8}$$

with

$$h_{00} = h_{11} = \left(\frac{1}{4} + \frac{1}{12}\gamma\right)\omega^2 \Delta t - \frac{1}{\Delta t}$$

$$h_{01} = h_{11} = \left(\frac{1}{4} - \frac{1}{12}\gamma\right)\omega^2 \Delta t + \frac{1}{\Delta t}$$

Solution of (4.8) shows that the eigenvalues λ are complex and $|\lambda| = 1$ if

$$\gamma \omega^2 \Delta t^2 \leq 12 \tag{4.9}$$

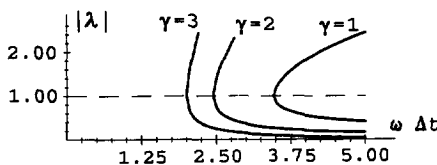


Figure 4.3 visualizes the domain of $\omega \Delta t$ in which linear models are stable for different values of γ . Taking $\gamma \leq 0$ these models are always numerically stable.

Figure 4.3 - Conditionally stable linear models

The *quadratic* models require following (4.6)

$$\lambda^2 \det \begin{bmatrix} h_{20} + \lambda(h_{00} + h_{22}) + \lambda^2 h_{02} & h_{21} + \lambda h_{01} \\ h_{10} + \lambda h_{12} & h_{11} \end{bmatrix} = 0 \quad (4.10)$$

or, applying the symmetry of h_{ij}

$$(1 + \lambda^2)(h_{02}h_{11} - h_{01}h_{12}) + \lambda(h_{11}h_{00} + h_{11}h_{22} - h_{01}^2 - h_{12}^2) = 0 \quad (4.11)$$

with

$$h_{00} = \left(\frac{1}{9} + \frac{1}{45}\gamma\right)\omega^2\Delta t - \frac{7}{3\Delta t}$$

$$h_{01} = h_{10} = h_{12} = h_{21} = \left(\frac{1}{9} - \frac{2}{45}\gamma\right)\omega^2\Delta t + \frac{8}{3\Delta t}$$

$$h_{02} = h_{20} = \left(-\frac{1}{18} + \frac{1}{45}\gamma\right)\omega^2\Delta t - \frac{1}{3\Delta t}$$

$$h_{11} = \left(\frac{4}{9} + \frac{4}{45}\gamma\right)\omega^2\Delta t - \frac{16}{3\Delta t}$$

Again λ can be solved from (4.11), see fig. 4.4.

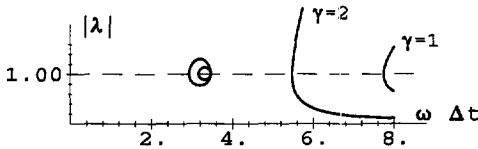


Figure 4.4 - Conditionally stable quadratic models

4.3 Turning points of numerical stability

The roots of (4.7) give us the amplification factor λ of an error y_0 in the equations of motion. Divergency arises if the roots are real with $|\lambda|_{\max} > 1$, convergency is ensured if the roots are complex with $|\lambda| = 1$ and the turning point is the point where these domains meet. This procedure is very straight forward and useful. A closer examination of the turning points, however, generates some interesting results and interpretations.

The turning point is the point with two identical roots with $\lambda^2 = 1$, thus at the turning point $\lambda = +1$ or $\lambda = -1$. Because of the symmetry of the mechanical properties (no damping)

and the numerical model, the solution $e(t)$ and also the participation factor $\alpha(t)$ are either symmetric or antisymmetric.

Assume $\alpha = c'\alpha' + c''\alpha''$ where α' is given by

$$h_{ij}\alpha_j' = \begin{cases} = 0 & i \neq n \\ = \mu_n' & i = n \end{cases} \quad (4.12a)$$

with $\alpha_0' = 1$ and $\mu_0' = 0$

and in which α'' is given by

$$h_{ij}\alpha_j'' = \begin{cases} = 1 & i = 0 \\ = 0 & i \neq 0, i \neq n \\ = \mu_n'' & i = n \end{cases} \quad (4.12b)$$

with $\alpha_0'' = 0$ and $\mu_0'' = 1$.

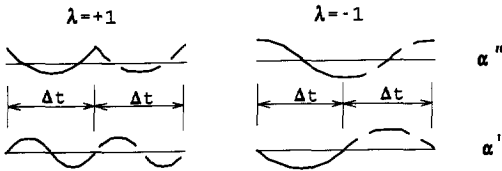


Figure 4.5 - Participation gactor $\alpha(t)$ at the turning points

The participation factors α' and α'' , which yield the turning points, have to satisfy the symmetry conditions, see Fig. 4.5 .

$$\begin{aligned} \alpha_0' &= 1 & \alpha_n' &= 1 & \text{symmetric, } \lambda &= 1 \\ \alpha_0' &= 1 & \alpha_n' &= -1 & \text{antisymmetric, } \lambda &= -1 \\ \text{and} & & & & & (4.13) \\ \alpha_0'' &= 0 & \alpha_n'' &= 0 & \text{symmetric, } \lambda &= -1 \\ \alpha_0'' &= 0 & \alpha_n'' &= 0 & \text{antisymmetric, } \lambda &= 1 \end{aligned}$$

Application of (4.13) to the equation of motion of (4.12) results into the (eigenvalue) problem

$$\begin{aligned} h_{ij}\alpha_j' &= 0 & \text{for } i, j &= 0, 1, 2, \dots, n & \text{with } \alpha_0' &= 1 \\ h_{ij}\alpha_j'' &= 0 & \text{for } i, j &= 1, 2, \dots, n-1 & \text{with } \mu_0'' &= 1 \end{aligned}$$

with nontrivial solutions for $\omega\Delta t$.

After multiplication with Δt and substitution of $\tau = \omega \Delta t$ application of (4.14) to the *linear models* of (3.19) yields .

$$\det \begin{bmatrix} \left(\frac{1}{4} + \frac{1}{12} \gamma\right) \tau^2 - 1 & \left(\frac{1}{4} - \frac{1}{12} \gamma\right) \tau^2 + 1 \\ \left(\frac{1}{4} - \frac{1}{12} \gamma\right) \tau^2 + 1 & \left(\frac{1}{4} + \frac{1}{12} \gamma\right) \tau^2 - 1 \end{bmatrix} = 0 \quad (4.15)$$

with solution $\omega^2 \Delta t^2 = 0$ for the symmetric function and $\gamma \omega^2 \Delta t^2 = 12$ for the antisymmetric function.

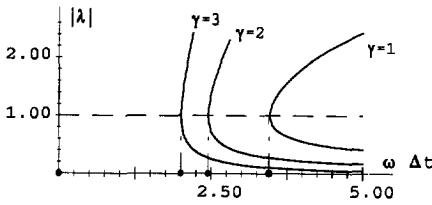


Figure 4.6 - Linear model: turning points

As shown in (4.9) we obtain unconditional numerical stability for $\gamma \leq 0$.

Application of (4.14) to the *quadratic models* of (3.27) yields the conditions

$$\det \begin{bmatrix} \left(\frac{1}{9} + \frac{1}{45} \gamma\right) \tau^2 - \frac{7}{3} & \left(\frac{1}{9} - \frac{2}{45} \gamma\right) \tau^2 + \frac{8}{3} & \left(-\frac{1}{18} + \frac{1}{45} \gamma\right) \tau^2 - \frac{1}{3} \\ \left(\frac{1}{9} - \frac{2}{45} \gamma\right) \tau^2 + \frac{8}{3} & \left(\frac{4}{9} + \frac{4}{45} \gamma\right) \tau^2 - \frac{16}{3} & \left(\frac{1}{9} - \frac{1}{45} \gamma\right) \tau^2 + \frac{8}{3} \\ \left(-\frac{1}{18} + \frac{1}{45} \gamma\right) \tau^2 - \frac{1}{3} & \left(\frac{1}{9} - \frac{1}{45} \gamma\right) \tau^2 + \frac{8}{3} & \left(\frac{1}{9} + \frac{1}{45} \gamma\right) \tau^2 - \frac{7}{3} \end{bmatrix} = 0 \quad (4.16a)$$

and

$$\det \left[\left(\frac{4}{9} + \frac{4}{45} \gamma\right) \tau^2 - \frac{16}{3} \right] = 0 \quad (4.16b)$$

From (4.16a) we obtain the antisymmetric solutions

$$\gamma \omega^2 \Delta t^2 = 60 \quad \text{and} \quad \omega^2 \Delta t^2 = 12 \quad (4.17)$$

and the symmetric solution $\omega^2 \Delta t^2 = 0$.

From (4.16b) we obtain the symmetric solution

$$\omega^2 \Delta t^2 = \frac{60}{\gamma + 5} \quad (4.18)$$

The lucky coincidence that occurs here is that two domains of conditional numerical stability vanish with the identical value of $\gamma = 0$.

For $\gamma = 0$ we obtain unconditional numerical stability.

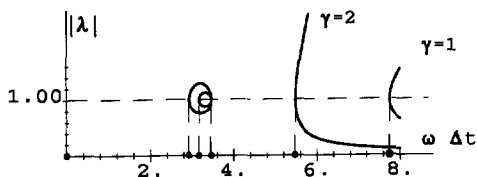


Figure 4.7 - Quadratic model: turning points

At the interval $\Delta t = [-\frac{1}{2}\Delta t, \frac{1}{2}\Delta t]$ exact solutions of the participation factors α' and α'' , defined by (4.12), have to satisfy the differential equation

$$\omega^2 \alpha + \ddot{\alpha} = 0 \quad (4.19)$$

with the initial conditions

$$\alpha'_0 = 1$$

$$\dot{\alpha}'_0 = 0$$

and

$$\alpha''_0 = 0$$

$$\dot{\alpha}''_0 = 1$$

The solution of (4.19) is given by

$$\alpha'(t) = \cos \omega(t + \frac{1}{2}\Delta t) \quad (4.20a)$$

and

$$\alpha''(t) = \frac{1}{\omega} \sin \omega(t + \frac{1}{2}\Delta t) \quad (4.20b)$$

A solution $\alpha'(t)$ and $\alpha''(t)$ exists for every $\omega\Delta t = n\pi$. This exercise shows that the turning points of (4.15) and (4.16) are approximations of the periods $\omega\Delta t = n\pi$.

Numerical stability may be considered as an overshoot caused by time steps that are larger than the (approximated) time between two nodes of a vibration mode.

4.4 Accuracy

The accuracy of a model is responsible for the convergency to the exact solution. Usually the accuracy order is related to the truncation error of the approximation polynomials

with respect to time. In this way we obtain linear models with an $O[\Delta t]$ accuracy and quadratic models with an $O[\Delta t^2]$ accuracy. For our models we can use an appropriate choice of γ to optimize the accuracy. To elaborate this process we need a reference criterion; we will use the so-called 'action', given by the product of pulses and displacements.

Per vibration mode we investigate the resulting action

$$\text{action} = \alpha_0 \mu_0 + \alpha_n \mu_n \quad (4.21)$$

Substitution of

$$\alpha = c' \alpha' + c'' \alpha''$$

$$\mu = c' \mu' + c'' \mu''$$

in which α' and α'' are defined in (4.12), yields

$$\text{action} = [c' c''] \begin{bmatrix} \alpha_n' \mu_n' & \alpha_n' \mu_n'' + 1 \\ \alpha_n'' \mu_n' & \alpha_n'' \mu_n'' \end{bmatrix} \begin{bmatrix} c' \\ c'' \end{bmatrix} \quad (4.22)$$

or

$$\text{action} = c^T A c$$

We take $\det(A)$ as a reference value, with

$$\det(A) = -\alpha_n'' \mu_n' \quad (4.23)$$

The solution of the differential equation following (4.19) gives us the reference value

$$\alpha_n'' \mu_n' = \sin^2 \omega \left(t + \frac{1}{2} \Delta t \right)$$

For $t = 0$ we apply a series development to $\omega \Delta t$

$$\alpha_n'' \mu_n' \approx \tau^2 \left\{ 1 - \frac{1}{3} \tau^2 + \frac{2}{45} \tau^4 - \dots \right\} \quad (4.24)$$

with $\tau = \omega \Delta t$.

Solving the linear model following (4.12) we obtain

$$\alpha_n'' = \frac{\Delta t}{1 + \left(\frac{1}{4} - \frac{1}{12} \gamma \right) \tau^2} \quad (4.25)$$

$$\mu_n' = \frac{\tau^2}{\Delta t} \frac{1 - \frac{1}{12} \gamma \tau^2}{1 + \left(\frac{1}{4} - \frac{1}{12} \gamma \right) \tau^2}$$

A series development of the action increment shows

$$\alpha_n'' \mu_n' \approx \tau^2 \left\{ 1 - \left(\frac{1}{2} - \frac{1}{12} \gamma \right) \tau^2 + \dots \right\}$$

The best approximation of the exact solution (4.24) is found by taking $\gamma = 2$. This model, the Goodwin-Fox model or the royal road, possesses $O[\Delta t^3]$ accuracy.

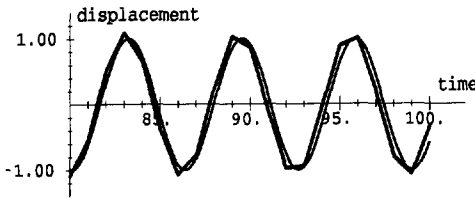


Figure 4.8 - The royal road

The quadratic model, again to be solved following (4.12), yields

$$\alpha_n'' = -\Delta t \frac{1 - \tau^2 \left(\frac{1}{12} + \frac{1}{60} \gamma \right)}{1 + \tau^2 \left(\frac{1}{12} - \frac{1}{60} \gamma \right) + \tau^4 \left(\frac{1}{144} - \frac{1}{360} \gamma \right)} \quad (4.26)$$

$$\mu_n' = \frac{\tau^2}{\Delta t} \frac{\left(1 - \frac{1}{12} \tau^2 \right) \left(1 - \frac{1}{60} \gamma \tau^2 \right)}{1 + \tau^2 \left(\frac{1}{12} - \frac{1}{60} \gamma \right) + \tau^4 \left(\frac{1}{144} - \frac{1}{360} \gamma \right)}$$

A series development of the action increment shows

$$\alpha_n'' \mu_n' \approx \tau^2 \left\{ 1 - \frac{1}{3} \tau^2 + \left(\frac{1}{24} + \frac{1}{720} \gamma \right) \tau^4 + \dots \right\}$$

with a best choice of $\gamma = 2$. This model possesses $O[\Delta t^4]$ accuracy.

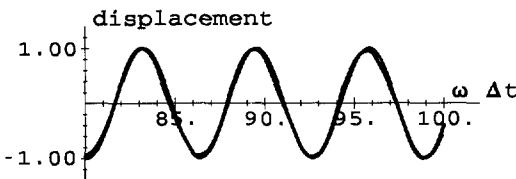


Figure 4.9 - Quadratic model: $\gamma = 2$

4.5 Artificial damping

The classic models, such as the Newmark- β method, suppress physical damping with growing Δt . Investigation of the spectral radius of unconditional numerical stable processes with nonzero physical damping shows that $|\lambda| \rightarrow 1$ for $\omega\Delta t \rightarrow \infty$.

The effect of physical damping, especially of the high frequency modes, is neglectable. Consequently disturbances caused by high frequency modes can be a source of inaccuracies. This behaviour can easily be predicted by a consideration of the discretization of the uncoupled equations of motion in which

$$\omega_k^2 \alpha^k + 2\zeta_k \omega_k \dot{\alpha}^k + \ddot{\alpha}^k = 0 \quad (4.27)$$

is modelled by, dropping super and subscript k,

$$\sum_i (a_i \omega^2 \alpha_i + 2\zeta \omega \frac{b_i}{\Delta t} \alpha_i + \frac{c_i}{\Delta t^2} \alpha_i) = 0 \quad (4.28)$$

The parameters a_i , b_i and c_i are dependent on the chosen model and are independent of time parameter $\omega\Delta t$. With an increase of values of $\omega\Delta t$ the contributions of damping and inertia terms vanish, thus damping and inertia properties are ignored for large values of $\omega\Delta t$.

In order to maintain damping properties for large values of $\omega\Delta t$ we introduce artificial (numerical) damping, which is proportional to the stiffness matrix \mathbf{K} . For small time steps the contribution has to be neglectable, for large time steps the contribution has to be linearly dependent on $\omega\Delta t$. We examine the effect for linear models and quadratic models.

Linear models

We introduce damping of the stresses by a contribution of the strain velocities to the constitutive equations following (see 3.3a)

$$\boldsymbol{\sigma} = \mathbf{D} \boldsymbol{\varepsilon} + \theta \Delta t \mathbf{D} \dot{\boldsymbol{\varepsilon}} \quad (4.29)$$

Since the damping matrix is proportional to the stiffness matrix, the damping of the high frequencies is much larger than the damping of the low frequencies.

For damping ratio ζ_k we obtain

$$\zeta_k = \frac{1}{2} \theta \Delta t \omega_k$$

which implies strong damping for large values of Δt and ω_k , see fig. 4.11.

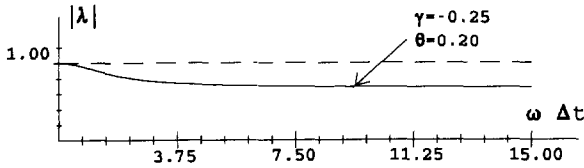


Figure 4.10 - Spectral radius with artificial damping

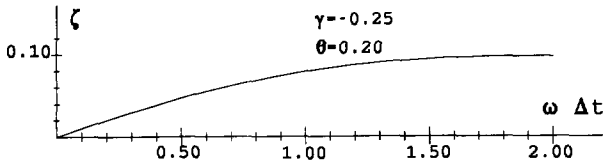


Figure 4.11 - Damping ratio with artificial damping

Investigation of the spectral radius λ of the linear model for large values of $\omega \Delta t$ shows that numerical stability is ensured if $\gamma < 0$.

Complex roots are found if

$$\frac{1}{3}\gamma + \theta^2 \leq 0 \quad (4.30)$$

with

$$|\lambda| = \sqrt{\frac{1 - \frac{1}{3}\gamma - 2\theta}{1 - \frac{1}{3}\gamma + 2\theta}} \quad (4.31)$$

Extreme values are obtained for $\theta^2 = -\frac{1}{3}\gamma$ with

$$|\lambda| = \frac{1 - \theta}{1 + \theta} \quad (4.32)$$

In figure 4.12 the spectral radius is shown as a function of θ according to (4.31) and figure 4.13 shows the extreme spectral radius as a function of γ .

It should be noted that for $\gamma = -3$ and $\theta = 1$ the artificial damping is very strong.

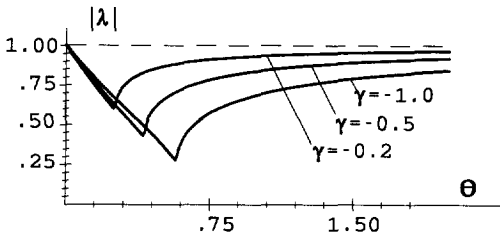


Figure 4.12 - Limit spectral radius

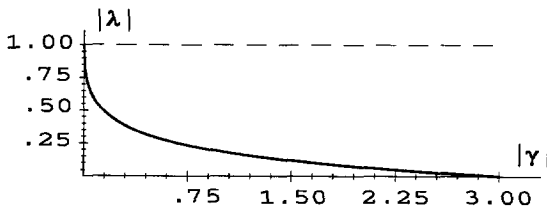
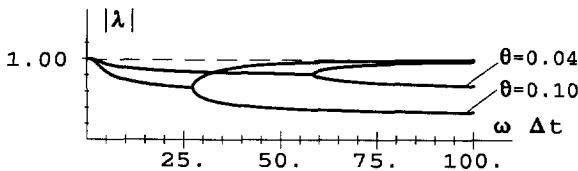


Figure 4.13 - Limit spectral radius

Quadratic models

An investigation of the quadratic models shows that we obtain real amplification factors $|\lambda|_{\max} \rightarrow 1$ for $\omega \Delta t \rightarrow \infty$. Figure 4.14 shows the spectral radius for some values of θ . The conclusion has to be that quadratic models are unable to model adequate numerical damping with the simple assumptions of (4.29).

Figure 4.14 - Spectral radius with $\gamma = 0$ and artificial damping

Artificial damping based on the damping of stresses is not very fruitful for the generation of a robust quadratic model.

Another approach is the generation of artificial damping of the pulses. For this purpose we add a contribution of the strain velocities and accelerations to the constitutive equations following

$$\begin{aligned} \sigma &= D \epsilon + \theta \Delta t D \dot{\epsilon} \\ p &= R v + \psi_1 \Delta t^2 D \dot{\epsilon} + \psi_2 \Delta t^3 D \ddot{\epsilon} \end{aligned} \tag{4.33}$$

with arbitrary numbers θ , ψ_1 and ψ_2 .

Elaboration of Galerkin's variational condition (3.8) yields the extra contribution

$$\Delta G = \int \{ \psi_1 \Delta t^2 \delta v^T K v + \psi_2 \Delta t^3 \delta v^T K \dot{v} + \theta \Delta t \delta v^T K v \} dt \tag{4.34}$$

and additional terms $c_{ij}K$ to H in which

$$[c_{ij}] = \Delta t \begin{bmatrix} (-\frac{1}{2}\theta - \frac{7}{3}\psi_1 - 4\psi_2) & (\frac{2}{3}\theta + \frac{8}{3}\psi_1 + 8\psi_2) & (-\frac{1}{6}\theta - \frac{1}{3}\psi_1 - 4\psi_2) \\ (-\frac{2}{3}\theta + \frac{8}{3}\psi_1) & -\frac{16}{3}\psi_1 & (\frac{2}{3}\theta + \frac{8}{3}\psi_1) \\ (\frac{1}{6}\theta - \frac{1}{3}\psi_1 - 4\psi_2) & (-\frac{2}{3}\theta + \frac{8}{3}\psi_1 - 8\psi_2) & (\frac{1}{2}\theta - \frac{7}{3}\psi_1 + 4\psi_2) \end{bmatrix}$$

An investigation of the spectral radius of the quadratic model following (4.10) shows:

- a. *Damping by stresses*: we take $\gamma = 0, \psi_2 = 0$.
Numerical stability and artificial damping are guaranteed with $\theta > 0, \psi_1 > 0$, see Fig. 4.15.
- b. *Damping by pulses*: we take $\gamma = 0, \theta = 0$.
Numerical stability and artificial damping are guaranteed with $\psi_1 > 0, \psi_2 > 0$, see Fig. 4.15.

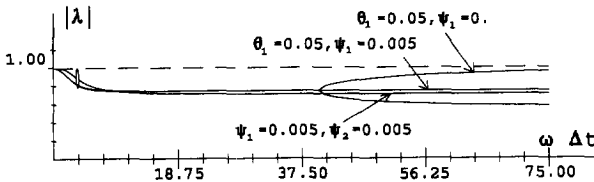


Figure 4.15 - Spectral radius of quadratic models

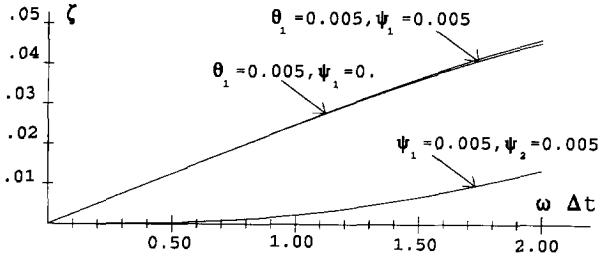


Figure 4.16 - Proportional damping for small time steps

Since damping by stresses implies an accuracy of $O[\Delta t]$ and damping by pulses implies an accuracy of $O[\Delta t^2]$ - see (4.33) -, damping by pulses should be preferred. Fig. 4.16 shows the development of the damping ratio ζ as a function of time step Δt .

An approximation of the complex spectral radius for large values of $\omega \Delta t$ is now given by

$$\lambda^2 \approx \frac{1 + 12\psi_1 + 144\psi_1^2 - 72\psi_2}{1 + 12\psi_1 + 144\psi_1^2 + 72\psi_2} \quad (4.35)$$

Summarizing: A robust second order model is obtained with $\gamma = 0$, $\theta = 0$, $\psi_1 > 0$ and $\psi_2 > 0$.

4.6 Summary of model characteristics

Based upon our investigation of numerical stability, accuracy and robustness the model characteristics can be summarized as follows

Linear models

$\gamma < 0$ Unconditional numerical stability. Accuracy $O[\Delta t]$.

Implicit. Optimal artificial damping ($C^* = \theta \Delta t \mathbf{K}$) with $\theta = \sqrt{-\frac{1}{3}\gamma}$.

The model shows good properties during nonlinear iteration procedures. The model is very robust and is recommended for linear and nonlinear transient analysis with long response times.

- $\gamma = 0$ Unconditional numerical stability. Accuracy $O[\Delta t]$.
Implicit. Artificial damping is suppressed for large values of Δt . The model shows good properties during nonlinear iteration procedures. The model misses the robustness of the models with $\gamma < 0$. Suitable for smooth processes.
- $\gamma = 2$ Conditional numerical stability. If no damping is involved, the accuracy is $O[\Delta t^3]$.
Implicit. Good properties during nonlinear iteration. The model is recommended for undamped systems with a short response time.
- $\gamma = 3$ Conditional numerical stability. Accuracy $O[\Delta t]$.
Explicit if damping and mass properties are modelled by lumped matrices (in literature: central differences). Good properties during nonlinear iteration. The explicit model is recommended for transient analyses with a short response time. Because of the explicit procedure a lot more time steps can be considered than in an implicit procedure. For this reason $\gamma = 3$ is quite often preferred with respect to the implicit models.

Quadratic models

- $\gamma = 0$ Unconditional numerical stability. Accuracy $O[\Delta t^2]$.
Implicit. Artificial damping has to be introduced by damping of the pulses, using $\psi_1 > 0$, $\psi_2 > 0$. The model is expected to be robust and recommended for linear and nonlinear transient analyses with long response times.
- $\gamma = 2$ Conditional numerical stability. Accuracy $O[\Delta t^4]$ if no damping is involved.
Implicit. The model is feasible for analyses with a short response time.

All these models can be mixed very smoothly. The transition between two models for two adjacent time intervals is fully fixed by the displacement vector and the pulse vector at the intersection between two time intervals. It should be noted that conditional numerical stability is never in accordance with robustness. Only unconditional numerical stability may contribute to a robust model.

5. BEAMS AND PLATES ON AN ELASTIC FOUNDATION

5.1 Introduction

A subject that still requires much research into and validation of model parameters is the beam or plate on an elastic foundation. Quite often the beam on an elastic foundation represents a pavement structure or a railway structure and a foundation.

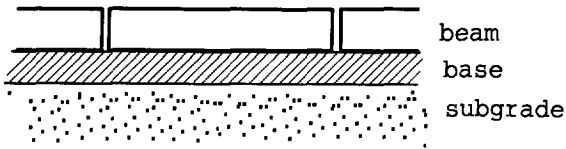


Figure 5.1 - Beam on an elastic foundation

Usually the beam is modelled by a slender beam and sometimes by a Timoshenko beam, which takes into account the shear deformation. The elastic foundation is usually modelled by a Winkler foundation, which implies uncoupled linear elastic springs. The common reference model is the elastic half space (the Boussinesq solution), in which it is understood that neither the Winkler model nor the elastic half space corresponds perfectly with the real (in situ) situation.

To find a compromise between these models, the so called Pasternak model (or the equivalent Vlassov model) has been introduced. This model takes into account the shear deformation of the foundation. Such a model is called a *two parameter model* because of the axial spring parameter of the Winkler subgrade modulus and the shear parameter to model the shear deformation.

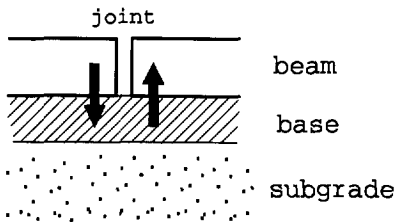


Figure 5.2 - A joint

The Pasternak foundation model of subgrade and base obtains much of the shear stiffness from the base. The base cannot contribute very much to bending stresses since it cracks easily. The contribution of the base to the shear forces, however, can be

considerable and is probably larger than the subgrade contribution. Especially under an undoweled joint it is the basement that enables a transfer of forces between two adjacent plates.

The study of the behaviour of the joints necessitates a consideration of the base. A second complicating factor is the nonlinear nature of the subgrade material. In pavement engineering it is practice to introduce the so-called "resilient modulus", which specifies a load history dependent relation between loads and deformations. Depending on the number of applied load cycles - and load amplitude - a permanent deformation develops. After many cycles an almost static situation arises which can be characterized by a linear stress/strain relation, see fig. 5.3.

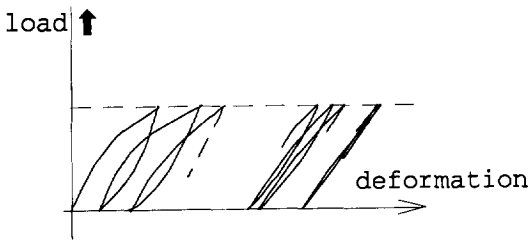


Figure 5.3 - Resilient modulus

In our examples we assume a constant "resilient modulus" or constant material properties.

Because the stress amplitude in the subgrade under the edges is higher than the stress amplitude at the centre of a plate, also the resilient modulus is much higher. Under the edges the resilient modulus may be far higher than the resilient modulus under the plate centre.

A well known nonlinear problem is the so-called "slope instability". The source of this phenomenon is the development of a yield zone, such as "slip circles" in which the subgrade stresses have reached the yield stress. If the yield zone takes the shape of an unstable structure, collapse follows.

Yielding is also a relevant phenomenon for the description of permanent deformation of the foundation of the plate or beam. Usually these phenomena are strictly local. However, the consequence of permanent deformations near the joints of concrete plates is one of the major drawbacks of concrete pavements.

Some nonlinear properties of granular structures can be perfectly described by a simple "no-tension" model. Granular structures obtain their stiffness from the contact surfaces between the grains. Only pressure can be transferred in this way; no tension is possible.

This property is only relevant for layers near the surface; at some depth the compression stresses of the dead weight are much larger than any stress generated by surface loads.

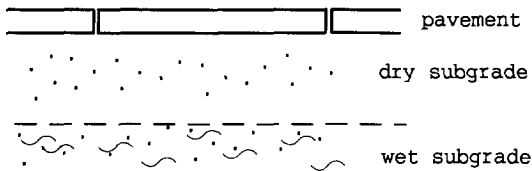


Figure 5.4 - Groundwater

Groundwater is another complicating factor. The presence of groundwater changes the stiffness properties entirely. Suction is closely related to fully saturated soil. Where the stiffness of fully saturated soil reduces, unsaturated soil very often shows a considerable increase in stiffness [38]. Summarizing it should be possible to anticipate on a strong variation of stiffness properties depending on many different parameters.

Quite often the nature of the applied load is dynamical. This implies the introduction of inertial forces and damping forces and thus an idealization of mass and damping properties. The modelling of the mass properties is quite easy, the modelling of the damping properties is less self-evident. Nevertheless we will assume anyhow that damping is linearly dependent on the velocities.

In our model we neglect the effects of long time static phenomena, such as consolidation, and limit ourselves to dynamic loads such as traffic loads and pulse like test loads. Some attention is paid to temperature loads which are neither typical static nor typical dynamic loads. The most important feature of temperature loads is that gaps may develop between top layer and base. For static loads these effects appear to be quite considerable [39].

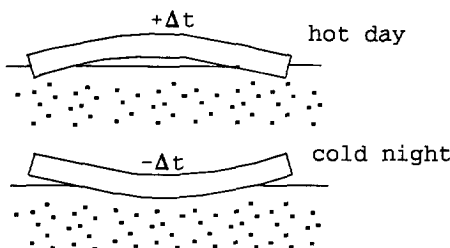


Figure 5.5 - Gap development under temperature loads

Another time dependent phenomenon is the way in which the subgrade reacts to a time dependent load. Static load are supported by reaction forces resulting from the elastic bed. An elastic bed using the Winkler's subgrade modulus and, if desired, a Pasternak parameter models the static response. With very short time loads we may assume that the subgrade does not reflect any stress wave; stress waves simply travel to infinity! It may be expected that the results of a stress analysis which takes into account these boundary conditions, will be quite different from an analysis on the basis of a simple Winkler or Pasternak foundation.

It is our objective to idealize a pavement structure, as shown in figure 5.6, by a model with a minimum of parameters in such a way that the results are applicable for pavement engineering purposes.

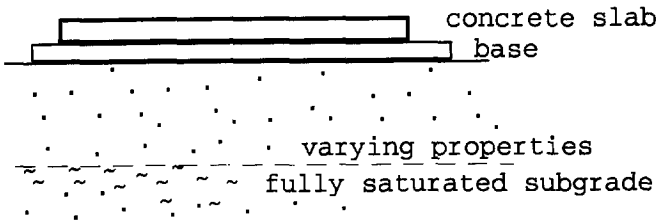


Figure 5.6 - The pavement problem

5.2 Numerical tools

The beam

On behalf of the modelling of a beam on an elastic foundation a series of numerical tools has been developed. To model the concrete or asphalt top-layer we use beam elements that take into account the bending stiffness and shear deformation (the Timoshenko beam).

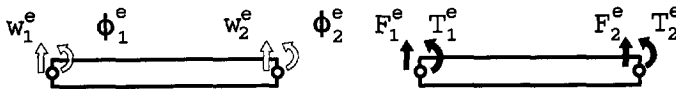


Figure 5.7 - Nodal displacements and nodal forces of a beam element

The nodal displacements are put into a displacement vector u^e following

$$u^e{}^T = [w_1^e \quad \phi_1^e \quad w_2^e \quad \phi_2^e]$$

with translations w_i^e and rotations ϕ_i^e .

The nodal forces are put into the load vector f^e following

$$f^e{}^T = [F_1^e \quad T_1^e \quad F_2^e \quad T_2^e]$$

with translational forces F_i^e and torques T_i^e .

Based upon the usual concepts of the finite element method we obtain a stiffness matrix K^e following [22]

$$K_{\text{beam}}^e = \begin{bmatrix} \frac{\lambda}{a} & \frac{1}{2}\lambda & -\frac{\lambda}{a} & \frac{1}{2}\lambda \\ \frac{1}{2}\lambda & p & -\frac{1}{2}\lambda & -q \\ -\frac{\lambda}{a} & -\frac{1}{2}\lambda & \frac{\lambda}{a} & -\frac{1}{2}\lambda \\ \frac{1}{2}\lambda & -q & -\frac{1}{2}\lambda & p \end{bmatrix} \quad (5.1)$$

with

$$\frac{1}{\lambda} = \frac{a^2}{12EI} + \frac{1}{GA_y}$$

a = length beam element

A_y = cross section area shear forces

I = moment of inertia

E = Young's modulus

G = shear modulus

$$p = \frac{EI}{a} + \frac{1}{4} \lambda a$$

$$q = \frac{EI}{a} - \frac{1}{4} \lambda a$$

The inertia properties are modelled by translational inertia and rotational inertia, which results in a mass matrix M^e [22] :

$$M_{\text{beam}}^e = \frac{\rho A a}{(1 + \phi)^2} \begin{bmatrix} f_1 & f_3 & f_4 & f_5 \\ f_3 & f_2 & f_5 & f_6 \\ f_4 & f_5 & f_1 & f_3 \\ f_5 & f_6 & f_3 & f_2 \end{bmatrix} \quad (5.2)$$

with

$$\rho = \text{density}$$

$$A = \text{cross section area}$$

$$\phi = \frac{12EI}{GA a^2}$$

and

$$f_1 = \frac{13}{35} + \frac{7}{10}\phi + \frac{1}{3}\phi^2 + \frac{6}{5}R$$

$$f_2 = a^2 \left(\frac{1}{105} + \frac{1}{60}\phi + \frac{1}{120}\phi^2 + R \left(\frac{2}{15} + \frac{1}{6}\phi + \frac{1}{3}\phi^2 \right) \right)$$

$$f_3 = a \left(\frac{11}{210} + \frac{11}{120}\phi + \frac{1}{24}\phi^2 + R \left(\frac{1}{10} - \frac{1}{2}\phi \right) \right)$$

$$f_4 = \frac{9}{70} + \frac{3}{10}\phi^2 - \frac{6}{5}R$$

$$f_5 = a \left(\frac{13}{420} + \frac{3}{40}\phi + \frac{1}{24}\phi^2 - R \left(\frac{1}{10} - \frac{1}{2}\phi \right) \right)$$

$$f_6 = a^2 \left(\frac{1}{140} + \frac{1}{60}\phi + \frac{1}{120}\phi^2 + R \left(\frac{1}{30} + \frac{1}{6}\phi - \frac{1}{6}\phi^2 \right) \right)$$

$$R = \frac{I}{A a^2}$$

The base

The contribution of the base to the stiffness properties is given by

$$V = GA^* \psi$$

in which the shear deformation ψ is given by

$$\psi = w_{,x}$$

in which dw/dx is denoted by $w_{,x}$ and x is the coordinate along the base.

The representative shear stiffness GA^* may also include a contribution of the soil to the shear forces.

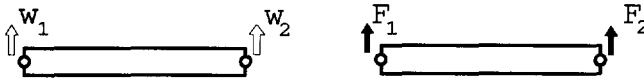


Figure 5.8 - Nodal displacements and nodal forces of a base element

From these shear properties we obtain a contribution to the stiffness matrix given by

$$K_{base} = \begin{bmatrix} k_b & -k_b \\ -k_b & k_b \end{bmatrix} \tag{5.3}$$

with

$$k_b = \frac{GA^*}{a}$$

In our analyses we model the limited shear capacity of the base by an ideal elasto-plastic material model. We assume that

$$\begin{aligned} dV &= GA^* d\psi & \text{if } -F_0 < V < F_0 \\ dV &= 0 & \text{if } V = \pm F_0 \end{aligned} \tag{5.4}$$

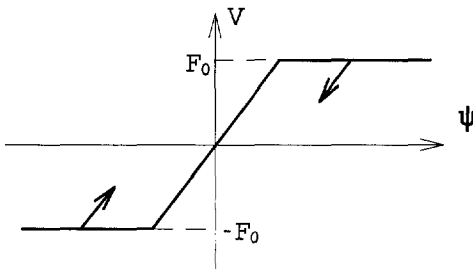


Figure 5.9 - Ideal elasto-plastic material model for shear forces in the base

Subgrade

The contribution of the subgrade is modelled by distributed Winkler springs. Shear stiffness, if any, has been introduced to the base element.

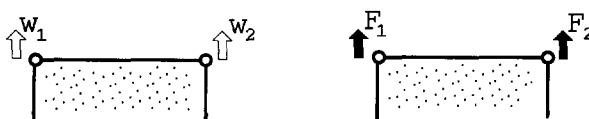


Figure 5.10 - Nodal displacements and nodal forces of a subgrade element

Both the base element and the subgrade element are not perfectly compatible with the beam element. The accuracy, however, is hardly affected by this incompatibility.

The Winkler springs yield the stiffness matrix contribution

$$K_{\text{soil}} = \begin{bmatrix} \frac{1}{3}ka & \frac{1}{6}ka \\ \frac{1}{6}ka & \frac{1}{3}ka \end{bmatrix} \quad (5.5)$$

with k = Winkler subgrade modulus.

Base and subgrade together are called a Pasternak foundation.

The contribution to the consistent mass matrix is given by

$$M_{\text{soil}} = \begin{bmatrix} \frac{1}{3}ma & \frac{1}{6}ma \\ \frac{1}{6}ma & \frac{1}{3}ma \end{bmatrix} \quad (5.6)$$

in which m = the specific mass per unit length of the foundation.

It is typical for concrete pavement structures that the layers are *unbonded* which means that interaction of shear forces between toplayer and foundation is impossible. As a consequence the connection between the beam and the base can be released; this is called "gapping". Especially with temperature loads this phenomenon can easily occur. Interaction between beam and base is impossible when an interface node has been released.

In the statical case the gapping criterion is represented by the condition that no tension forces between beam and base are possible. The dynamical case requires that "tension" pulses between beam and base are impossible.

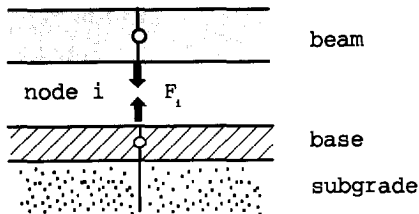


Figure 5.11 - Gapping between beam and base. No tension forces between beam and base. Node i has to be released.

Lumped springs

Additional stiffness of the foundation is modelled by lumped springs . One contribution can be made by a higher resilient modulus at the beginning and the end of the beam, another source can be the shear stiffness of the semi-infinite elastic foundation next to the start and end of the beam.

To model the shear stiffness of the semi-infinite elastic foundation, the relation between force F and displacement w - see figure 5.12 - has to be found. This relation is given by the differential equation

$$GA^* w_{,xx} + k w = 0 \tag{5.7}$$

and the boundary condition at $x = 0$:

$$GA^* w_{,x} = -F$$

in which GA^* represents the shear stiffness of the soil only.

At $x = 0$ we get the solution

$$F = K_p w_0$$

in which

$$K_p = \sqrt{kGA^*}$$

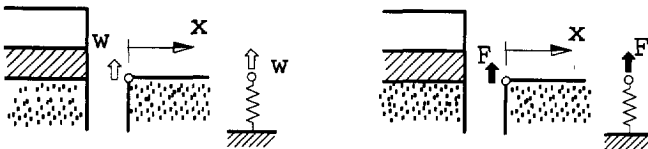


Figure 5.12 - Lumped spring at the end of the beam

With small values of K_p the contribution of the semi infinite Pasternak foundation is neglected.

Silent boundary

The function of a silent bed or a silent boundary is to model the surroundings of the f.e.m. model in such a way that all stress waves arriving at the boundary will pass into the surroundings [42]. The ideal silent boundary does not reflect any stress wave contribution.

To model the soil by a silent boundary we consider an infinite column - see figure 5.13 - with Young's modulus E and density ρ . This column is loaded by an incoming normal

stress wave, which applies a constant load F during a time interval Δt .

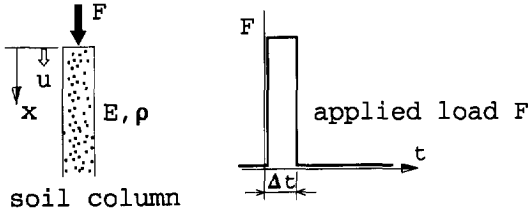


Figure 5.13 - A silent boundary model

The equation of motion of the column is given by

$$E u_{,xx} - \rho u_{,tt} = 0$$

The solution at $x = 0$ is given by

$$u_0(t) = \begin{cases} 0 & t < 0 \\ \frac{F}{\sqrt{E\rho}} t & 0 < t < \Delta t \\ \frac{F}{\sqrt{E\rho}} \Delta t & t > \Delta t \end{cases} \quad (5.8)$$

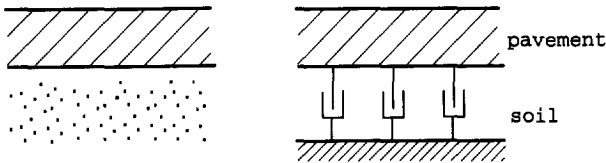


Figure 5.14 - Modelling of a silent bed by dampers

From this result we may conclude that

$$F = \sqrt{E\rho} \dot{u}_0 \quad 0 < t < \Delta t \quad (5.9)$$

It turns out that the silent boundary condition can be modelled by visco-elastic dampers with a *damping factor* c

$$c = \sqrt{E\rho}$$

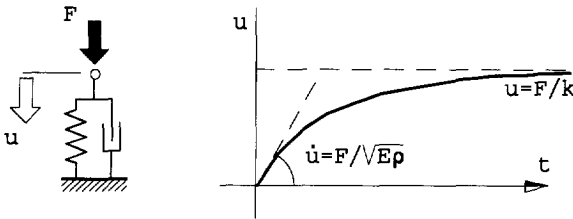


Figure 5.15 - Response to a step load F

It is more realistic to model the elastic foundation by a combined Winkler spring bed and a silent bed, see figure 5.15. By such a combination the dynamic loads are primarily carried by the dampers and the static loads are carried by the elastic springs. The shear wave propagation in the shear layer can be modelled in a similar way.

The equation of motion is given by

$$GA u_{,xx} - \rho A u_{,tt} = 0 \tag{5.10}$$

which results into a visco-elastic damper with a *damping factor* c_s

$$c_s = \sqrt{G\rho} A$$

The bending behaviour of the beam will yield a rotational damper with a *damping factor*

$$c_\phi = \sqrt{E\rho} I$$

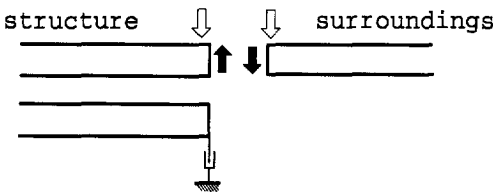


Figure 5.16 - Silent boundary at the end of a beams

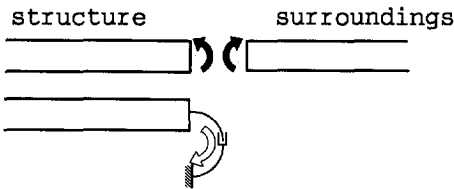


Figure 5.17 - Silent boundary at the end of a beams

It should be noted that this model is oversimplified. A better model of the beam border requires coupling of transversal and rotational d.o.f.s.; such a model, however, has not been elaborated here.

Joints

Two adjacent beams are separated from each other by a joint. In order to provide some transverse shear stiffness, dowels are applied between two beams.

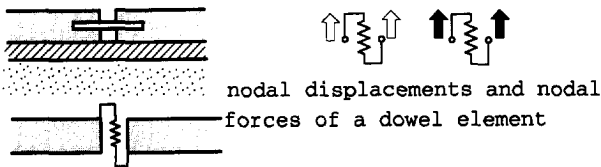


Figure 5.18 - Dowel spring model

The dowel stiffness matrix is given by

$$K_{dow} = \begin{bmatrix} k_d & -k_d \\ -k_d & k_d \end{bmatrix} \quad (5.11)$$

The stiffness k_d of the dowels is a number that is dependent on the joint width, the dowel diameter and Young's modulus of steel and concrete [43].

Even without dowels some shear forces can be transferred by a joint since the base and the subgrade will provide some shear stiffness. This stiffness, however, is limited because of the limited shear strength of the foundation.

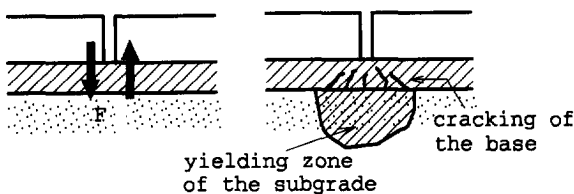


Figure 5.19 - Yielding of the base

To simplify this problem we model the joint behaviour by a dry friction component.

We assume

$$\begin{aligned} \Delta u &= 0 & \text{if } |F| < F_0 \\ k_{joint} &= 0 & \text{if } |F| = F_0 \end{aligned} \quad (5.12)$$

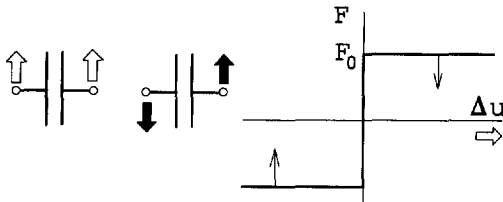


Figure 5.20 - A dry friction element

After failure of the joint the dowel element can become active and show a kind of hardening of the joint, see figure 5.21.

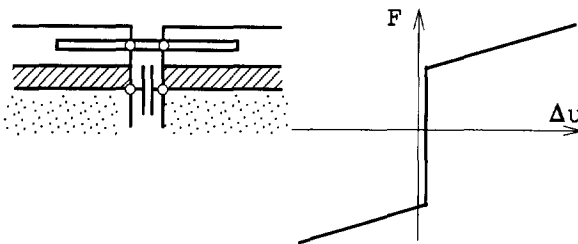


Figure 5.21 - A joint with a dowel

Because dry friction elements are irreversible, permanent deformations can be the result of an analysis. In the static case we check the interaction forces of the dry friction element with the yield criterion. In the dynamic case we check the resulting interaction pulses at the beginning of each time interval Δt with the corresponding yield criterion.

$$|p_0| < F_0 \Delta t \quad \text{no yielding} \quad (5.13)$$

If this criterion is satisfied no yielding occurs.

5.3 Beam structures

Example 1 : Pulse load at a simply supported beam

To test the direct integration methods of chapter 3 we apply these methods to a concrete beam with the parameters

$$E = 3 \cdot 10^7 \text{ kN/m}^2$$

$$\nu = 0$$

$$\rho = 2000 \text{ kg/m}^3$$

$$cte = 10^{-5} \text{ coefficient of thermal expansion}$$

and the dimensions

$$h = 0.20 \text{ m}$$

$$b = 1.00 \text{ m}$$

$$L = 4.00 \text{ m}$$

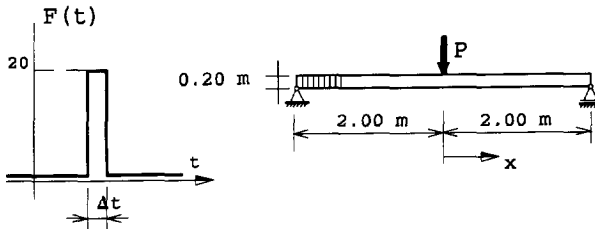


Figure 5.22 - Pulse load on a beam

The structure is loaded by a force $F = 20 \text{ kN}$ during a period of $\Delta t = 0.005$ second. This load corresponds with a pulse load $P = F \Delta t = 0.1 \text{ kNs}$. The beam, which is simply supported, is subdivided into 40 elements of 0.1 m each. Because of the short waves we expect notable contributions of shear deformation and rotational inertia. For this reason we apply a stiffness matrix \mathbf{K} , which takes into account the shear deformation, and a consistent mass matrix \mathbf{M} , which takes into account the rotational inertia [22].

The subject of our interest is the response of the lower frequency modes. To take some damping into account we apply some structural damping by means of the Rayleigh damping matrix

$$\mathbf{C} = p \mathbf{K} \quad (5.14)$$

in which p is taken in such a way that the low frequencies are slightly damped and the high frequencies are strong damped. In this example we take $p = 0.000025$ which corresponds to a damping of 0.2% of the lowest frequency.

In order to obtain accurate results we run the integration process with very small time steps

$t = 0.$	(0.00001)	0.0010
$t = 0.0010$	(0.00002)	0.0040
$t = 0.0040$	(0.00005)	0.0100
$t = 0.0100$	(0.00020)	0.0400
$t = 0.0400$	(0.00050)	0.1000

which makes a total of 640 integration steps. Because we apply a large number of time steps we introduce some artificial damping by taking $\gamma = -0.1$ and $\theta^2 = 1/30$. The results are called "exact".

With both the linear model and the quadratic model, using the parameter $\gamma = 0$, the same problem is run with $\Delta t^* = 10 \Delta t$, thus with 64 integration steps. The displacements of the centre of the beam are shown in figure 5.23

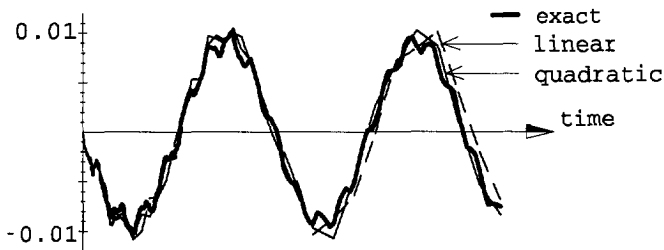


Figure 5.23 - Displacements at $x = 0.00$

As expected the quadratic model shows more accurate results than the linear model. Neither the linear nor the quadratic model show any trace of numerical instability, overshooting or evident loss of accuracy.

Example 2 : Silent boundaries

To test the silent boundary we apply a pulse load P at the left hand side of a horizontal bar. The right hand side is modelled either as a free edge, a supported edge or a silent edge, as shown in fig. 5.24.

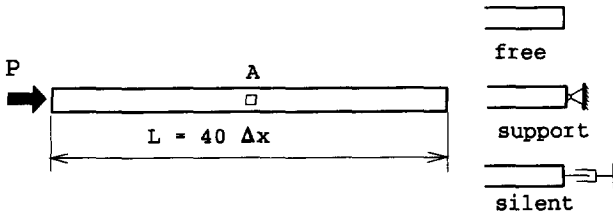
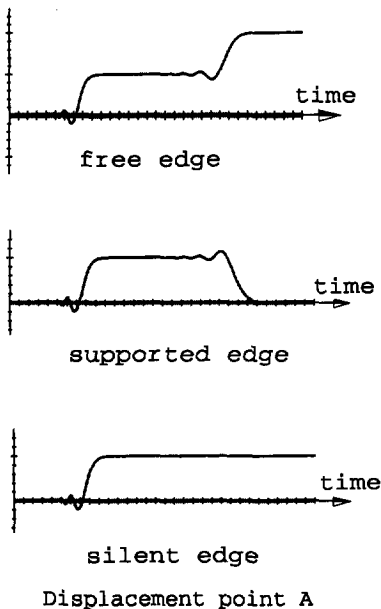


Figure 5.24 - Three end conditions of the bar

The following data are used:

$$EA = 10^6, \quad \rho A = 1, \quad P = 1.00, \quad L = 1.00, \quad \Delta t = 0.000025$$

The structure is subdivided into 40 elements of the length $\Delta x = 0.025$. To obtain a maximum accuracy with respect to time we apply $\gamma = 2$ to the linear model with. The time step Δt is chosen in such a way that numerical stability is guaranteed.



In order to smooth out some discretisation errors, we introduce some internal damping by the addition of a damping matrix $C = 10^{-6} K$, which corresponds with 0.05% of the critical damping. The silent boundary is modelled by a viscous damper with damping factor $c = 1000$. In fig. 5.25 the results of the displacement are shown at the centre of the bar.

Figure 5.25 - Response dependent on boundary conditions

These results show that the silent boundary is perfectly modelled by the viscous damper at the bar end.

Example 3 : The FWD test

One of the most widely used nondestructive test procedures for pavements is the so-called Falling Weight Deflectometer test in combination with a stress analysis program. During the test an impact loading is applied to the structure.

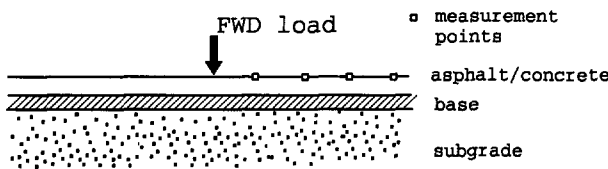


Figure 5.26 - Pavement subjected to a FWD test

In a series of measurement points deflectometers collect the envelope of the extreme displacements. By means of some calculation model the E -modulus of the structure layers are analyzed back from the test data. Usually this back-analysis is based on a static analysis of peak load F_0 of the impact load.

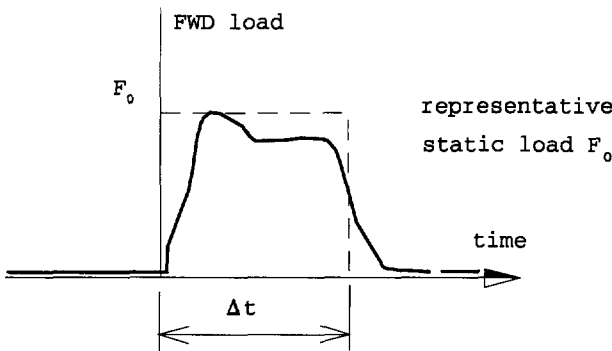


Figure 5.27 - The FWD test load

In this approach the dynamic effects are ignored. We simulate such a test in which we take into account the dynamic effects. The direct integration process (linear model) is applied using $\gamma = 0$. Since much physical damping is modelled, we do not need any artificial damping, thus $\gamma = 0$ suffices.

Two different structures are considered. First we analyze a concrete pavement structure with finite dimensions and subsequently an asphalt pavement with infinite dimensions. The subgrade consists of sand. Both beams are subjected to a FWD load.

These structures are modelled by Pasternak foundations. For such a model we need to know the parameters of the shear contribution. We only consider the contribution of the subgrade and drop the contribution of the base. Although the base contribution is much larger than the subgrade contribution, consideration of the subgrade only appears to be notable.

The following parameters are used as the starting point:

$$\begin{aligned} E_{\text{asphalt}} &= 6 \cdot 10^6 \text{ kN/m}^2 \\ E_{\text{concrete}} &= 3 \cdot 10^7 \text{ kN/m}^2 \\ E_{\text{sand}} &= 125\,000 \text{ kN/m}^2 \\ \rho_{\text{sand}} &= 2000 \text{ kg/m}^3 \end{aligned}$$

The peak load that we apply equals to $F = 20 \text{ kN}$. The thickness of the layer is 0.20 m . To get the shear parameter we perform a static 2D f.e.m. analysis on structures of which the properties reflect a real half-plane problem, a Winkler model and a Pasternak model respectively.

The half-plane model is taken as reference model, see figure 5.28.

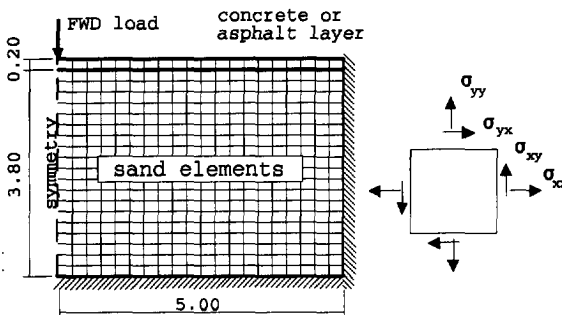


Figure 5.28 - 2D plane strain model

To model the Winkler model we assume the sand elements to be orthotropic following the constitutive equations

$$\begin{aligned} \sigma_{xx} &= 0 \\ \sigma_{yy} &= E \epsilon_{yy} \\ \sigma_{xy} &= 0 \end{aligned} \tag{5.15}$$

For this model one layer of sand elements is sufficient. The dimensions are chosen in such a way that the Young's modulus E corresponds with Winkler's subgrade modulus $k = 60000 \text{ kN/m}^3$.

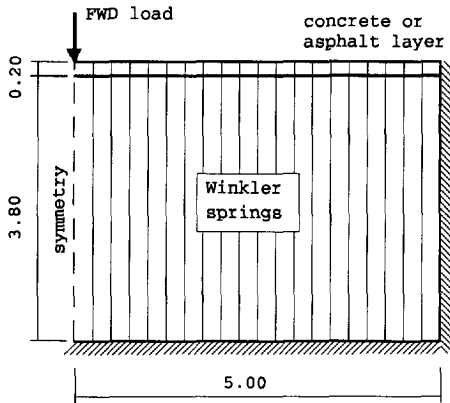


Figure 5.29 - Winkler model

To model the Pasternak model we added a layer of sand elements which takes into account some shear deformation following

$$\begin{aligned} \sigma_{xx} &= 0 \\ \sigma_{yy} &= E \epsilon_{yy} \\ \sigma_{xy} &= G \gamma_{xy} \end{aligned} \tag{5.16}$$

where $G = 0.5 E$.

The thickness H of the shear layer is taken variable.

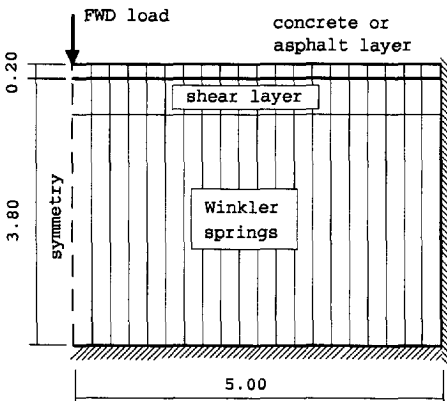


Figure 5.30 - Pasternak model

For both the concrete beam and the asphalt beam the results of the displacements of the surface are compared. The results are shown in the figures 5.31 and 5.32. Independent from the beam it turns out that the Pasternak model with a shear layer of $H = \pm 0.50 \text{ m}$ is very close to the half-plane solution.

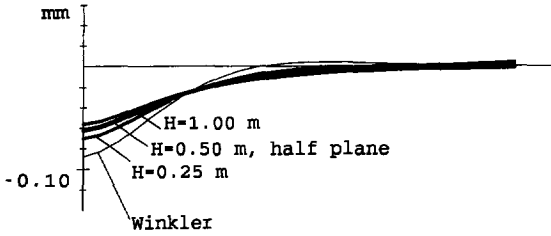


Figure 5.31 - Displacement concrete beam

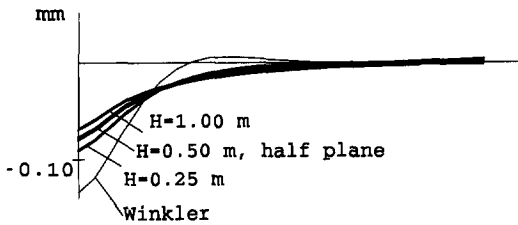


Figure 5.32 - Displacement asphalt beam

To simulate the FWD test we apply a time dependent sine load with amplitude $F = 20 \text{ kN}$, see figure 5.33.

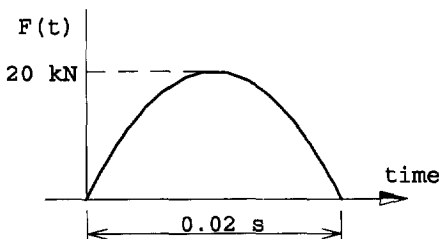


Figure 5.33 - Sine load representing the FWD load

The parameters of the concrete beam are taken from the first example. For the foundation we substitute

$$\begin{aligned}
 k &= 60000 \text{ kN/m}^3 \\
 GA^* &= 31250 \text{ kN} \quad (H = 0.40 \text{ m}) \\
 \rho &= 2000 \text{ kg/m}^3
 \end{aligned}$$

To model the dynamic properties we have to consider the damping properties (the silent bed) and mass properties (the co-moving mass). Because of the finite size of the concrete pavement structure we do not apply silent boundaries; the edges are free.

The first test only models the mass properties of the beam and the stiffness properties of the beam and the sand, see figure 5.34.

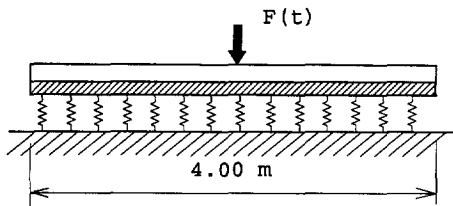


Figure 5.34 - Model of concrete pavement with Winkler springs only

The envelope of the displacements of this analysis is compared with the static solution, see figures 5.35 and 5.36.

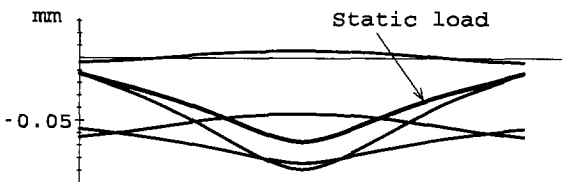


Figure 5.35 - Displacements static load and FWD load at different time points

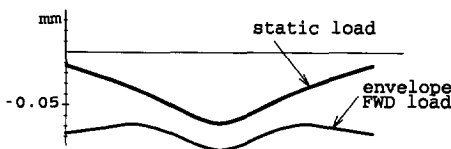


Figure 5.36 - Displacements static load and envelope FWD load

The results show very little correspondence between the static and the dynamic analysis. Evidently the model is insufficient.

The second test also models the silent bed, see figure 5.37. The "damping" properties of the bed are given by

$$c = \sqrt{E \rho} = 500 \text{ kN s/m}^2$$

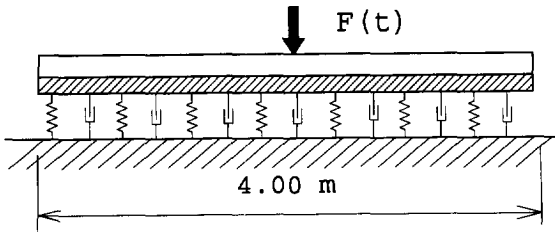


Figure 5.37 - Model of concrete pavement with Winkler springs and silent bed

The results of this model, subjected to the FWD load, are again compared with the static solution, see figures 5.38 and 5.39.

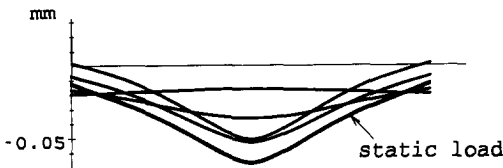


Figure 5.38 - Displacements static load and FWD load at different time points

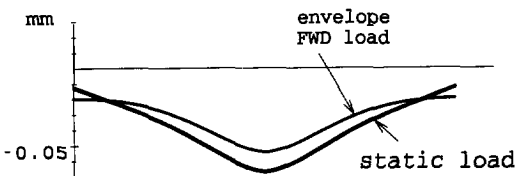


Figure 5.39 - Displacements static load and envelope FWD load

Now the correspondence between the static and the dynamic analysis is much better. The boundary effects, however, are very disturbing for a correct interpretation of the results following the static analysis.

In both tests we do not model the inertia properties of the sand. In the third test we consider the added mass of a sand layer with thickness 0.00 m, 2.00 m and 4.00 m respectively. The results of the dynamic analysis are shown in figure 5.40.

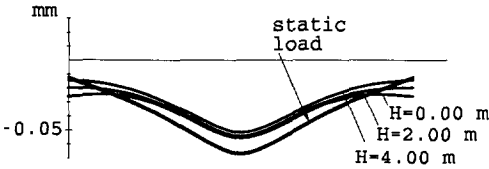


Figure 5.40 - Envelopes displacements concrete beam with different masses of subgrade

The results show that the contribution of the inertia forces of the sand are almost negligible. For a dynamic analysis of the FWD load there is no need to model the mass properties of the sand.

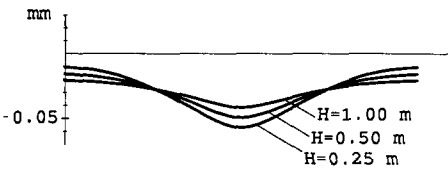


Figure 5.41 - Envelopes displacements concrete beam with different sizes of shear layer

The last test shows the effects of the shear layer thickness. We consider thicknesses of $H = 0.25\text{ m}$, 0.50 m and 1.00 m . The results again show the importance of the modelling of a shear layer. Following the static analysis we found an optimal thickness of $0.40 - 0.50\text{ m}$ in which it should be noted that this number only models the contribution of the sand only; the contribution of the base is not yet taken into account! One more test is performed on the asphalt beam.

For the asphalt beam we substitute

$$E = 6 \cdot 10^6 \text{ kN/m}^2$$

$$\rho = 2000 \text{ kg/m}^3$$

The sand is modelled as mentioned above. The dimensions of the concrete beam and the asphalt beam are the same. The asphalt beam, however, is not limited; the beam is assumed infinite. Our model is limited to 4.00 m , the surrounding is modelled by silent boundaries. No lumped springs are applied.

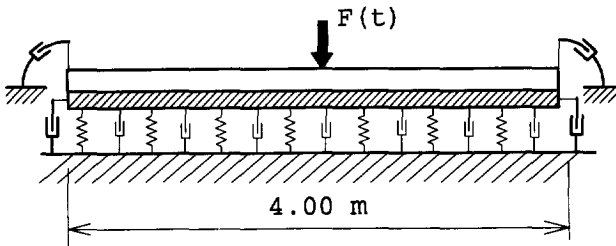


Figure 5.42 - Model of an asphalt beam with a silent bed and silent boundaries

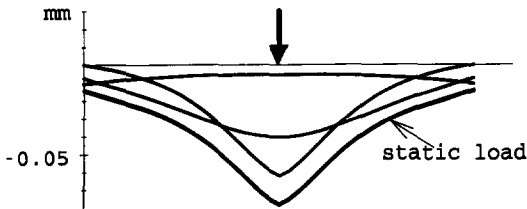


Figure 5.43 - Displacements static load and FWD load at different time points

The results show very little disturbance of the boundaries. The shape of the envelope of the response is almost identical, except a multiplication factor close to 1.00, see figure 5.44.

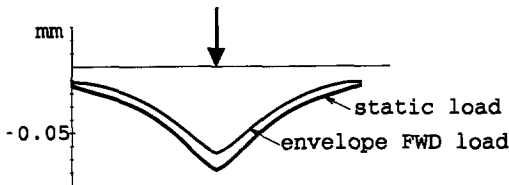


Figure 5.44 - Displacements static load and envelope FWD load

Conclusions

- The analysis of plates and beams on an elastic foundation under static and dynamic loads can be considerably improved by modelling a shear layer in addition to the Winkler springs.
- The analysis of plates and beams on an elastic foundation under dynamic loads requires modelling with silent beds and, if necessary, silent boundaries. The modelling of inertia properties, however, does not affect the results very much.

- The assumptions of the static back-analysis of the FWD test on asphalt beams seems to be justified. The interpretation of the measurements of the FWD test on concrete beams will be cumbersome because of edge disturbances.

It has to be noted that the subgrade in our examples is very stiff; it is not self-evident that these conclusions can be extrapolated to beams on a much weaker subgrade.

Example 4 : Moving load across a joint.

Some old concrete pavements have been constructed without dowels. Those structures are known to have developed longitudinal unevenness around the joints, which definitely does not contribute to the driver's comfort. The question is to what extent dynamic effects contribute to the development of these unequalities. To simulate the problem we apply a moving load of 20 kN with a speed of 25 m/s. The beam properties are taken from example 1.

The foundation is modelled by a shear layer (the base) and a combined elastic bed and silent bed. To model the joint we apply a dry friction element. Both the base and the dry friction element satisfy the ideal elasto-plastic material model for shear forces, see (5.4) .

We use the following parameters:

- k = 20 000 kN/m² subgrade modulus
- GA^* = 100 000 kN shear stiffness base
- c = 500 kN/m damping factor subgrade
- F_0 = 5 kN limit shear force in base

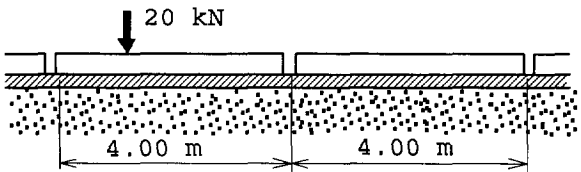


Figure 5.45 - Moving load on a concrete pavement

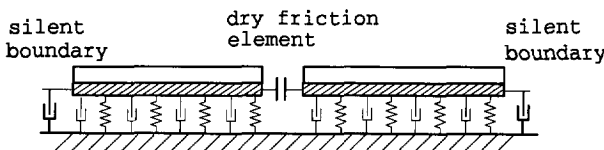


Figure 5.46 - Model of a concrete pavement with Winkler springs and a silent bed

Figure 5.46 shows the structure model. The direct integration process (linear model) is applied using $\gamma = -0.3$. Because we expect disturbances because of the nonlinear character of the problem we apply some artificial damping (together with the choice of a negative γ we apply the optimal θ value following (4.32)).

To remove disturbances from the boundaries we add silent boundaries.

Because of the possibility of gap forming between beam and base and because of the elasto-plastic material model the analysis is basically nonlinear.

The two beams are subdivided into 40 elements each. The integration process is carried out in such a way that with the moving load close to the joint the integration steps are taken smaller and smaller.

The load application is terminated at the point that the moving load arrives at the right hand side of the structure (at $t = 0.32$); the integration process continues in an unloaded situation until $t = 0.70$. Overall we use 204 integration steps.

The figures 5.47, 5.48 and 5.49 show the results of the displacements and the shear forces in the beam and the foundation after passage of the moving load (at $t = 0.70$).

Figure 5.50 shows the displacements in the foundation around the joint during the passage of the moving load.

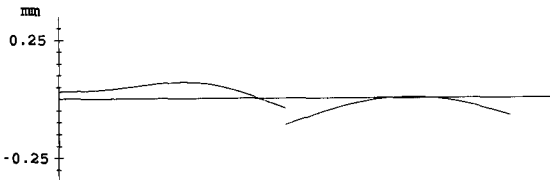


Figure 5.47 - Displacements undoweled joint after passage of a moving load ($t = 0.70$) with respect to the start deformation

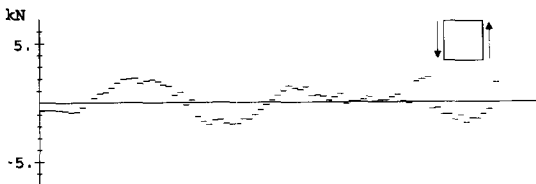


Figure 5.48 - Shear forces beam after passage of a moving load



Figure 5.49 - Shear forces base after passage of a moving load

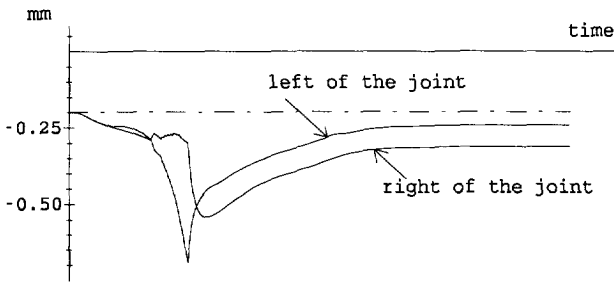


Figure 5.50 - Displacements of the joint

From figure 5.47 we can easily read that the crossing of a joint by a moving load results into a permanent deformation of the right hand side as compared to the left hand side. This observation corresponds perfectly well with the experience of undoweled, old concrete pavements. From figure 5.48 we read that some residual forces are accumulated in beam and base. The values, however, are too small to cause any damage.

In modern concrete pavements dowels are applied quite often in the transverse joints. Taking into account a dowel, following figure 5.18, with dowel stiffness $k_d = 200000 \text{ kN/m}$, we obtain the results of the figures 5.51 until 5.54. To avoid permanent deformations the application of dowels is quite effective.

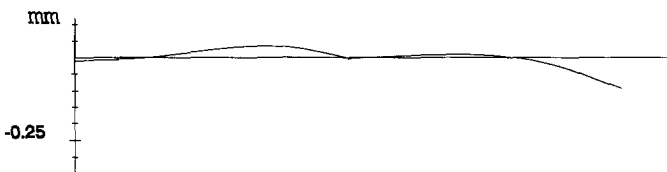


Figure 5.51 - Displacements in a doweled joint after passage of a moving load ($t = 0.70$) with respect to the start deformation



Figure 5.52 - Shear forces in the beam after passage of a moving load

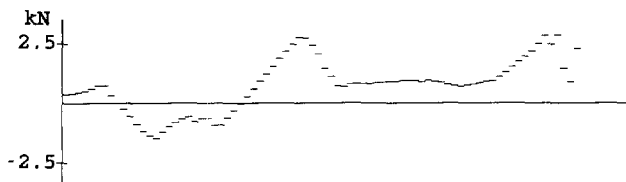


Figure 5.53 - Shear forces in the base after passage of a moving load

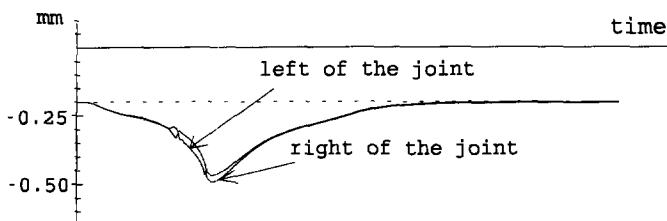


Figure 5.54 - Displacements of the joint

5.4 Circular plates

In the preceding sections a pavement structure was modelled by a beam on an elastic foundation. The starting point for this model was a two-dimensional description of the structure, consisting of one horizontal direction and the depth. In many cases this starting point is too limited for an acceptable approximation of the real behaviour.

A model based on circular plates may in some cases satisfy the required three-dimensional observations of the structure. Our objective here is to analyze the FWD test of section 5.3 with circular plate elements. This section pays also attention to the effects of temperature loads and gap development in combination with the FWD load.

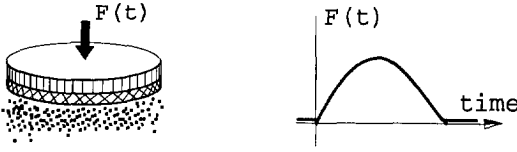


Fig. 5.55 - Circular plate on an elastic foundation, subjected to a FWD load

To describe the stresses we introduce radial moment M_r , tangential moment M_θ , shear force V and load p_z , see fig. 5.56. The deformations are given by displacement w , rotation ϕ , curvatures κ_r and κ_θ and shear deformation ψ . First we formulate the static case with the help of equilibrium conditions, kinematic conditions and constitutive equations.

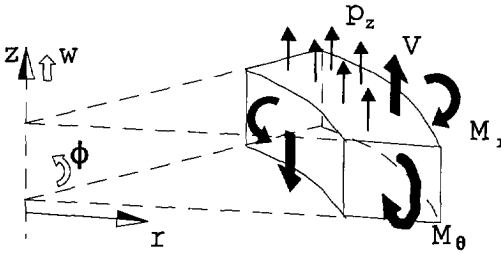


Figure 5.56 - Axisymmetric forces and moments

Equilibrium

The plate forces of a circular plate have to satisfy

$$\begin{aligned}
 M_{r,r} + \frac{1}{r} M_r - \frac{1}{r} M_\theta - V &= 0 \\
 V_{,r} + \frac{1}{r} V + p_z &= 0
 \end{aligned}
 \tag{5.17}$$

Kinematic conditions

The kinematic conditions are given by

$$\begin{aligned}
 \kappa_r &= \phi_{,r} \\
 \kappa_\theta &= -\frac{1}{r} \phi \\
 \psi &= w_{,r} - \phi
 \end{aligned}
 \tag{5.18}$$

Constitutive equations

The constitutive deformations are given by

$$\begin{aligned} \kappa_r &= \frac{1}{D} (M_r - \nu M_\theta) \\ \kappa_\theta &= \frac{1}{D} (M_\theta - \nu M_r) \\ \psi &= \frac{1.2}{Gh} V \end{aligned} \quad (5.19)$$

with

$$D = \frac{Eh^3}{12(1-\nu^2)}$$

Boundary conditions

At the boundaries $r = r_1$ and $r = r_2$ we have to satisfy the equilibrium conditions following

$$\begin{aligned} r = r_1 : \quad V &= -F_1 & \text{and} & \quad M_r = T_1 \\ r = r_2 : \quad V &= F_2 & \text{and} & \quad M_r = -T_2 \end{aligned} \quad (5.20)$$

with distributed edge forces F and torques T .

Usually the f.e.m. approach does not satisfy all conditions. With the analysis of the Reissner type of plates, as given above, we have to face the problem of shear locking. In many cases shear locking is held responsible for a poor convergence of results to an exact solution. In the next section we will propose a hybrid stress approach [44] by which problems such as shear locking are avoided and sometimes even exact results are generated.

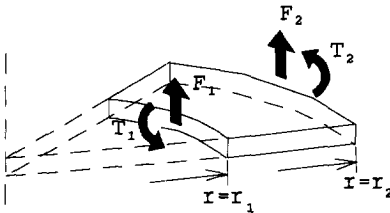


Figure 5.57 - Edge forces

A hybrid stress element

The hybrid stress method ignores the kinematic conditions of (5.18) and the equilibrium conditions at the boundaries (5.20). Instead the approximation has to satisfy the condition:

$$\begin{aligned}
 R = & -2\pi \int_{r_1}^{r_2} [\delta M_r \kappa_r + \delta M_\theta \kappa_\theta + \delta V w] r dr + \\
 & +2\pi [(-\delta\phi M_r - \delta M_r \phi + \delta w V + \delta V w) r]_{r=r_1}^{r=r_2} + \\
 & -2\pi [(\delta\phi T + \delta w F) r]_{r=r_1, r=r_2} = 0
 \end{aligned} \tag{5.21}$$

for every admissible variation δM_r , δM_θ and δV at $[r_1, r_2]$ and δw , $\delta\phi$ at the boundaries. The equilibrium conditions (5.17) and constitutive equations (5.19) and the kinematic boundary conditions have to hold for every variation.

We take the following approximation of the plate forces:

$$\begin{aligned}
 M_r &= \beta_1 \ln r - \beta_1 + \frac{\beta_2}{r^2} - \beta_3 + 2\beta_4 + \frac{3}{16} p_0 r^2 \\
 M_\theta &= \beta_1 \ln r - \frac{\beta_2}{r^2} - \beta_3 + \frac{1}{16} p_0 r^2 \\
 V &= 2 \frac{\beta_4}{r} + \frac{1}{2} p_0 r
 \end{aligned} \tag{5.22}$$

with four stress parameters β and uniformly distributed load p_0 .

Elaboration following the hybrid stress method results into a stiffness matrix K^e , which is free of shear locking and which even generates, under certain conditions, exact solutions.

A special case is the central element with $r_1 = 0$. If we ignore the (nonexisting) point load F_j we may assume that $\beta_1 = \beta_2 = \beta_4 = 0$.

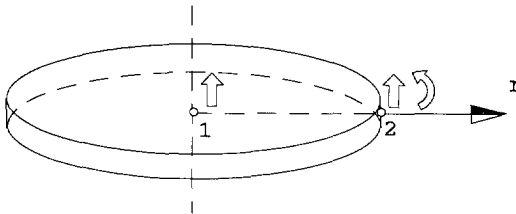


Figure 5.58 - Central element

The stiffness matrix is now given by

$$\mathbf{K}^e = 2\pi \begin{bmatrix} 0 & 0 & 0 & 0 \\ 0 & 0 & 0 & 0 \\ 0 & 0 & 0 & 0 \\ 0 & 0 & 0 & (1+\nu)D \end{bmatrix} \quad (5.23)$$

which shows that displacement w at $r = 0$ is not considered. In fact only rotation $\phi = \phi_2$ contributes. Displacement w_1 has to be chosen completely dependent of w_2 .

To evaluate the consistent mass matrix and the stiffness of the foundation we need an approximation of displacement $w(r)$ and rotation $\phi(r)$ at $[r_1, r_2]$. For these purposes we use the approximations:

$$\begin{aligned} w(r) &= \frac{1}{\Delta r} \left[(r_2 - r) w_1 + (r - r_1) w_2 + \frac{1}{2} (r - r_1)(r - r_2)(\phi_2 - \phi_1) \right] \\ \phi(r) &= \frac{1}{\Delta} r \left[(r_2 - r) \phi_1 + (r - r_1) \phi_2 \right] \end{aligned} \quad (5.24)$$

with $\Delta r = r_2 - r_1$ and assuming that

$$\Psi_{,r} = w_{,rr} - \frac{\phi_2 - \phi_1}{\Delta r} = 0$$

The elastic foundation contributes to the strain energy by

$$\delta E_f = 2\pi \int_{r_1}^{r_2} \left[\delta w k w + \delta w_{,r} k^* w_{,r} \right] r dr \quad (5.25)$$

with Winkler's subgrade modulus k and Pasternak's shear stiffness k^* .

The kinematic energy yields the mass matrix where we take into account translational inertia forces and rotational inertia moments following

$$\delta E_k = 2\pi \int_{r_1}^{r_2} \left[\delta \dot{w} \rho h \dot{w} + \delta \dot{\phi} \rho I \dot{\phi} \right] r dr$$

with

$$I = \frac{1}{12} h^3$$

The FWD test on a circular plate

The FWD test of chapter 5.3 has been re-analyzed with the use of circular plate elements.

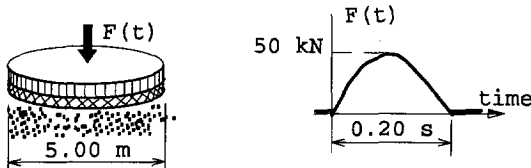


Figure 5.59 - Concrete plate and FWD load

We consider a finite concrete plate with a diameter of 5.00 m and an infinite asphalt plate.

At the centre of the plate a FWD load of 50 kN is applied during 0.02 seconds. The load is applied at a circular surface with a diameter of 0.50 m. The static loads are dead weight and a temperature gradient ΔT . Gapping is possible. The following structure data are used:

E	$= 3 \cdot 10^7 \text{ kN/m}^2$	Young's modulus concrete
E	$= 6 \cdot 10^6 \text{ kN/m}^2$	Young's modulus asphalt
ν	$= 0$	Poisson's ratio
ρ	$= 2000 \text{ kg/m}^3$	density
cte	$= 10^{-5}$	coefficient thermal expansion
h	$= 0.20 \text{ m}$	thickness plate
k	$= 60\,000 \text{ kN/m}^3$	Winkler's subgrade modulus
k^*	$= 31\,250 \text{ kN/m}$	shear stiffness of the base
c	$= 500 \text{ kN s/m}^3$	damping factor silent bed

Artificial damping is introduced by taking $\gamma = -0.3$ (and the optimal θ). The structure is subdivided into 50 equal elements.

The following time integration steps are chosen

0.000	(0.00010)	0.002
0.002	(0.00025)	0.007
0.007	(0.00050)	0.020
0.020	(0.00100)	0.050
0.050	(0.00250)	0.100

The concrete slab is subjected to a FWD load in combination with different temperature conditions. Because of the limited size of the slab, and the high values of Young's modulus and subgrade modulus, the slab releases easily from the base. With $\Delta T = 5^\circ$ the concrete slab touches the base only at the edge: everywhere else the slab is released from the base.

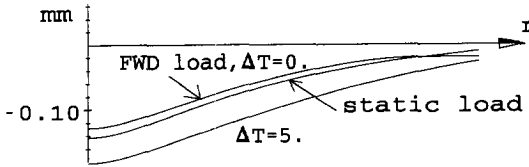


Figure 5.60 - Envelope displacements concrete slab

Figure 5.60 shows that for $\Delta T = 0$ the correspondence between the static solution and the envelope of the FWD load is very good. However, as soon as gapping develops because of temperature loads the results rapidly begin to differ.

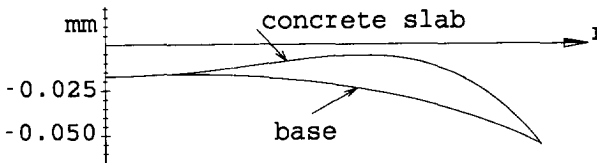


Figure 5.61 - Concrete slab under dead weight and temperature load $\Delta T = 4$

The analysis of the asphalt slab with silent boundaries shows an even better correspondence between static load and envelope of the FWD load, see fig. 5.62. In this case temperature loads do not play a role because the slab size is much larger than 5.00 m while the Young's modulus is smaller. Gapping is not expected to occur with asphalt slabs.

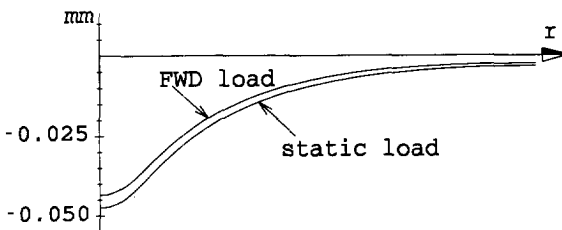


Figure 5.62 - Envelope displacements asphalt slab

In our analyses sofar we applied a very stiff subgrade. The analysis of a SDOF system, based on the used parameters and subjected to a FWD load, shows a strong dependency on the stiffness and damping properties. We have, therefore, re-analyzed the concrete slab supported by a much weaker subgrade, namely $k = 6000 \text{ kN/m}^3$ and $c = 158 \text{ kNs/m}^3$. Now the results deviate far more from the static solution.

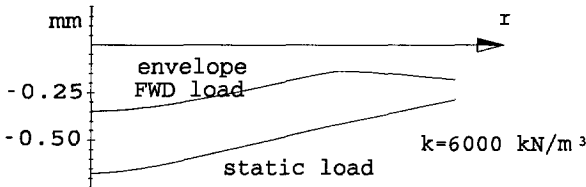


Figure 5.63 - Envelope displacements concrete slab on a weak subgrade

Conclusions

- The modelling of beams and plates on an elastic foundation can be improved considerably by taking into account the shear properties of the foundation. Even with plates that are directly supported by the subgrade, the contribution is already notable.
- Temperature loads applied to concrete plates easily cause gapping between the foundation and the plate. Differences between the expected, nongapping, static solution and the dynamic response diverge rapidly.
- For plates subjected to an FWD load it is mainly the damping - the silent bed - that contributes to the time dependent phenomena. Mass hardly contributes. The dynamic response of concrete and asphalt plates on a stiff subgrade corresponds very well with the static solution; the dynamic response of a concrete plate on a weak subgrade considerably deviates from the static solution.

5.5 Numerical guidelines

In order to test the role of artificial damping we analyze the response of the asphalt beam to a pulse load. We investigate the asphalt beam of section 5.3, which we modelled by a Timoshenko beam (40 elements), a Pasternak foundation, a silent bed and silent boundaries, see figure 5.64. The pulse load is given by $P = 0.4 \text{ kN s}$.

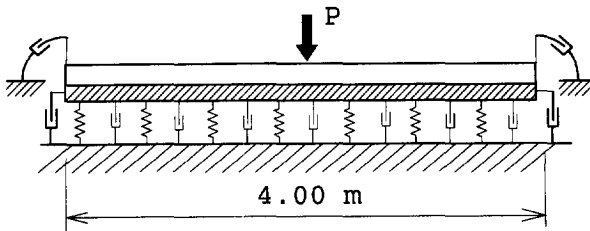


Figure 5.64 - Model of the asphalt beam

The first analysis is carried out with 500 time steps

$t = 0$	(0.00001)	0.0010
$t = 0.0010$	(0.00002)	0.0040
$t = 0.0040$	(0.00005)	0.0100
$t = 0.0100$	(0.00020)	0.0360

No physical damping of the beam is taken into account. By taking $\gamma = 0$ (and an optimal value of $\theta = 0$) no artificial damping is introduced. As reference are taken the displacements of the application point of the pulse load and the shear forces, immediately at the right side of this point. Figure 5.65 shows the results.

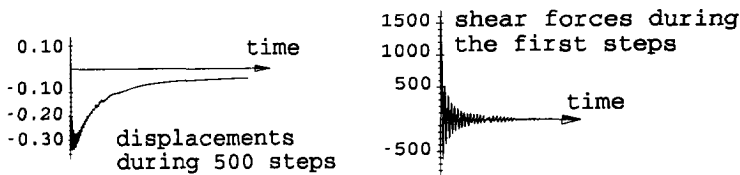


Figure 5.65 - Integration with 500 steps and no damping in the beam

Both the displacements and the shear forces show "overshooting". Although the disturbances are damped (by the silent bed and the silent boundaries) the results are not acceptable.

The problem can be completely solved by introducing some physical damping; we introduce:

$$C_{beam} = 0.000025 K_{beam}$$

which corresponds with the damping of a few promilles of the lowest frequency.

The results in figure 5.66 show a much better performance; we call them "exact".

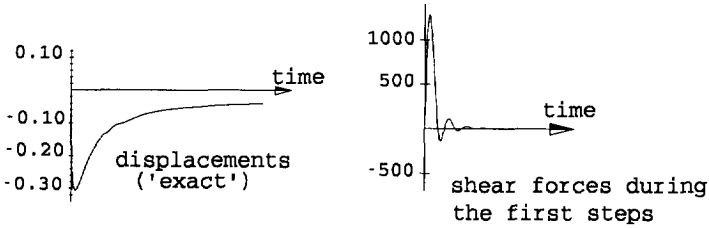


Figure 5.66 - Integration with 500 steps and some physical damping in the beam

For the next test we used 60 equal time steps, $\Delta t = 0.0006$, and some physical damping. Again the results are disappointing, see figure 5.67.

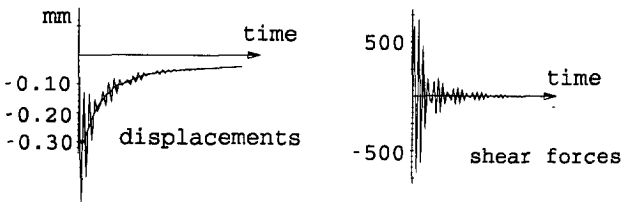


Figure 5.67 - Integration with 60 equal steps and no artificial damping

To improve these results we need to introduce artificial damping, see section 4.5. Taking $\gamma = -0.3$ (and $\theta^2 = 0.1$) we obtain the results as shown in figure 5.68.

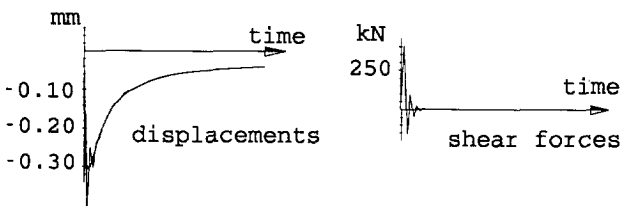


Figure 5.68 - Integration with 60 equal steps and some artificial damping

These results show the effectiveness of artificial damping with large integration steps. In fact, this method is very "robust" because no special attention is paid to the choice of time step or the damping factor.

Another approach is to take variable integration steps as used in the first two tests. This time we used 50 time steps, taken ten times larger than the time steps of the first test and no artificial damping.

The results, see figure 5.69, are certainly as good as the preceding test. The choice of the time steps is very essential to the result, and thus this approach is less "robust".

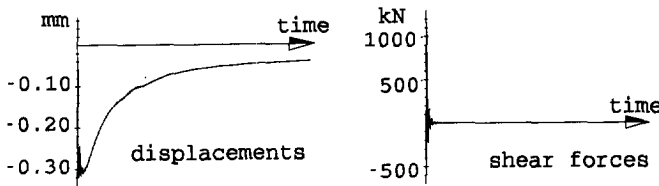


Figure 5.69 - Integration with 50 variable steps with no artificial damping

We test the quadratic models in the same way. Because numerical stability is only guaranteed for $\gamma = 0$ we have only one choice. No artificial damping is applied. These tests are carried out with 60 equal time steps. The results, see figure 5.70, show strong numerical disturbances.

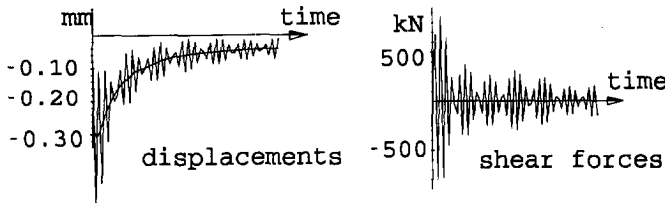


Figure 5.70 - Quadratic model using 60 equal steps

The results can be considerably improved by application of suitable variable integration steps (we took 50 time steps, ten times larger than the steps of the first test with 500 steps). The results of figure 5.71 are almost identical to the "exact" results.

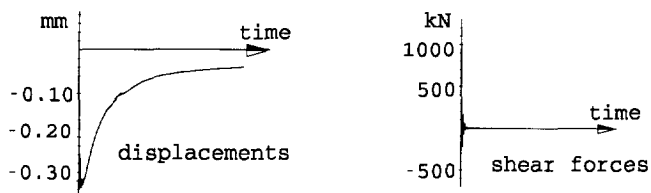


Figure 5.71 - Quadratic model using 50 variable steps

Again we may conclude that we can obtain very accurate results with the quadratic model. The model, however, is not very "robust" since we have to choose the integration steps very carefully.

6. EARTHQUAKE LOADS AT ADOBE STRUCTURES

6.1 Introduction

A most important subject of time dependent sollicitation at structures is the application of earthquake loads. In many parts of the world seismic activities have to be very seriously considered in the design of structures. In highly developed countries, such as Japan and California, much attention is paid to the development of analysis methods and structural design of earthquake resistant buildings. Quite often these structures are made of concrete and steel and therefore expensive.

In many developing countries low-cost houses are built of a very cheap material called adobe, which is a mixture of dried mud and natural fibres. Unfortunately, these structures are not very earthquake resistant, which means that in seismically active areas, such as the Andes countries in South America, earthquakes cause many casualties.

Programs for improvement of design methods for better structures are being developed. Most of the research is carried out in field experiments, very little attention is paid to the application of numerical simulation techniques. Because experimental research is very expensive and difficult to realize, it is very worthwhile to apply more numerical simulations to these research projects.

Our approach is to numerically apply a real earthquake load (the so-called El Centro earthquake) to a representative structure and to study the calculated response.

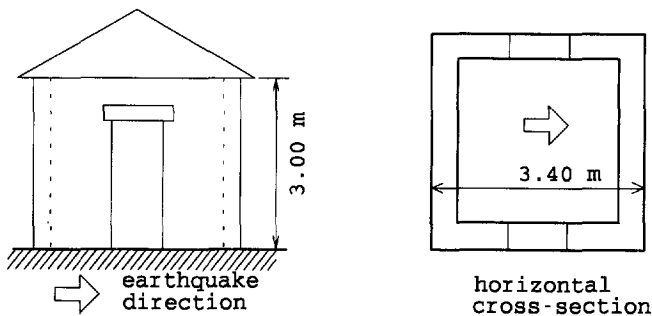


Figure 6.1 - A very simple adobe house under earthquake load

In the analysis critical phenomena such as cracking of the adobe and bond stress release of bamboo reinforcements are taken into account. In a previous study [47] the bending loads at the closed wall of the structure have been studied. Here we analyze the in-plane loads at the front wall of the structure.

These analyses are carried out on 486 PCs, with which one simulation requires a few hours of computation time. In this way many structural variants can be studied at low costs and within reasonable time.

6.2 Constitutive equations of adobe

To analyze adobe structures we have to formulate the material properties of adobe. The most important phenomenon is the initiation of cracks and the behaviour of these cracks (after initiation). Per element more than one crack may be initialized. In our analyses we apply the fixed smeared crack model. During the considered load time these cracks may close and open; slipping is also considered. To be able to apply the smeared crack model we introduce *elastic* strains, which are directly related to the stresses, and *nonelastic* strains, which represent the smeared cracks. Therefore the *total* strains are

$$\boldsymbol{\varepsilon} = \boldsymbol{\varepsilon}^{el} + \boldsymbol{\varepsilon}^{non}$$

The nonelastic strains of the smeared cracks represent the crack width of one discrete crack. These strains are used to control the closure of cracks during the dynamic analysis; the stresses are used to control the opening of cracks during the analysis.

The constitutive equations of intact adobe are given by linear plane stress/strain relations in which

$$\begin{aligned}\sigma_{xx} &= \frac{E}{1-\nu^2} \varepsilon_{xx}^{el} + \frac{\nu E}{1-\nu^2} \varepsilon_{yy}^{el} \\ \sigma_{yy} &= \frac{\nu E}{1-\nu^2} \varepsilon_{xx}^{el} + \frac{E}{1-\nu^2} \varepsilon_{yy}^{el}\end{aligned}\quad (6.1)$$

$$\sigma_{xy} = G \gamma_{xy}^{el}$$

and inversely

$$\begin{aligned}\varepsilon_{xx}^{el} &= \frac{1}{E} \sigma_{xx} - \frac{\nu}{E} \sigma_{yy} \\ \varepsilon_{yy}^{el} &= -\frac{\nu}{E} \sigma_{xx} + \frac{1}{E} \sigma_{yy} \\ \gamma_{xy}^{el} &= \frac{1}{G} \sigma_{xy}\end{aligned}\quad (6.2)$$

Also after crack initiation these relations are still valid.

It is assumed that cracks are initiated by a violation of the Drucker-Prager failure criterion. Unlike the usual assumption for concrete, referring to the Rankine criterion, we apply the *Drucker-Prager* criterion in the tension/tension and the tension/compression stress state. On the other hand we do not pay attention to the compression/compression stress state because the criterion for that state is far beyond the expected stresses. This criterion requires

$$\alpha I_1 + \sqrt{|I_2|} \leq k \quad (6.3)$$

with the stress invariants

$$I_1 = \frac{1}{3}(\sigma_1 + \sigma_2 + \sigma_3)$$

$$I_2 = \frac{1}{6}(\sigma_1 - \sigma_2)^2 + \frac{1}{6}(\sigma_2 - \sigma_3)^2 + \frac{1}{6}(\sigma_3 - \sigma_1)^2$$

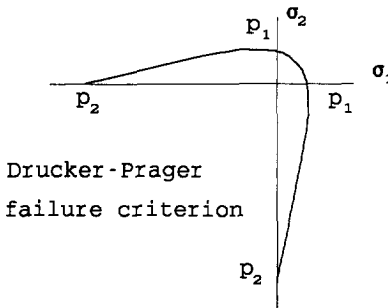


Figure 6.2 - Drucker-Prager criterion

Introducing the limit uniaxial tension stress p_1 and the limit uniaxial compression stress p_2 and substituting $\sigma_3 = 0$ we may replace α and k by

$$\alpha = \sqrt{3} \frac{p_1 - p_2}{p_1 + p_2} \quad (6.4)$$

$$k = \frac{2}{3} \sqrt{3} \frac{p_1 p_2}{p_1 + p_2}$$

For adobe we use the parameters $p_1 = 0.04 \text{ MPa}$ (tension) and $p_2 = 1.2 \text{ MPa}$ (compression).

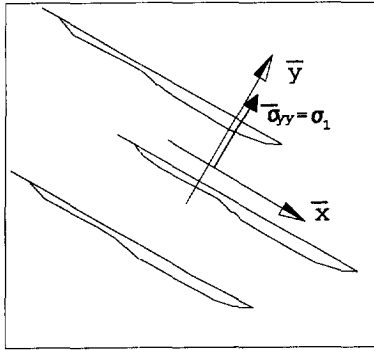


Figure 6.3 - Local axes defined by a new crack

Usually it is assumed that direction \bar{x} of the crack is perpendicular to direction \bar{y} of the maximum stress (see figure 6.3). The local \bar{x} -axis corresponds with the direction of the crack, the local \bar{y} -axis is defined by the maximum stress σ_1 at the time of cracking. After cracking the local stresses and strains are referred to by $\bar{\sigma}$ and $\bar{\epsilon}$.

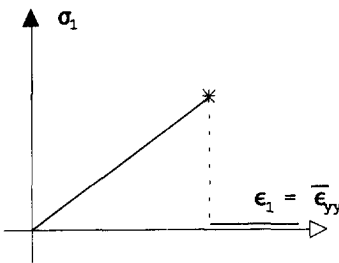


Figure 6.4 - Brittle crack

Because the material is very brittle the maximum stress σ_1 drops down to zero immediately after violation of the crack criterion. No softening is considered, because no material data on softening of adobe are existing

The drop of stress σ_1 from its maximum value to zero implies the introduction of a discontinuity of the stress $\bar{\sigma}_{yy}$, and consequently a discontinuity of the elastic strain $\bar{\epsilon}_{yy}$.

Because we do not accept a discontinuity of the total strains we have to introduce a sudden rise to the nonelastic strain $\bar{\epsilon}_{yy}^{non}$, given by

$$\bar{\epsilon}_{yy}^{non} = \frac{1 - \nu^2}{E} \sigma_1 \quad (6.5)$$

This strain represents the initial crack width of new cracks.

6.3 Constitutions of adobe with one crack

After initiation a crack will be open. Dependent on the load history a crack may close and slip. For each of these conditions the constitutive equations have to be formulated. We distinguish different constitutions for open cracks, closed cracks and slipping cracks. All these conditions are formulated with respect to the local $\bar{x}-\bar{y}$ reference frame as defined by the direction of the cracks.

Open crack

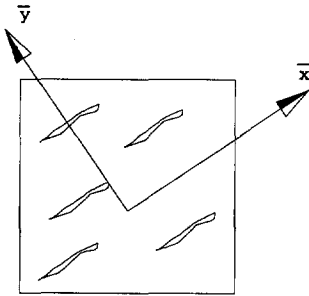


Figure 6.5 - Open cracks

An open crack requires that

$$\begin{aligned} \bar{\sigma}_{yy} &= 0 \\ \bar{\sigma}_{xy} &= 0 \end{aligned}$$

and

$$\bar{\epsilon}_{yy}^{non} > 0$$

Based on these conditions we get the incremental constitutive equations

$$\begin{aligned} \Delta \bar{\sigma}_{xx} &= E \Delta \bar{\epsilon}_{xx} \\ \Delta \bar{\sigma}_{yy} &= 0 \\ \Delta \bar{\sigma}_{xy} &= 0 \end{aligned} \quad (6.6)$$

in which $\Delta \bar{\epsilon}_{xx}$, $\Delta \bar{\epsilon}_{yy}$ and $\Delta \bar{\gamma}_{xy}$ are the total strain increments.

The increments of the nonelastic strains are given by

$$\begin{aligned}\Delta \bar{\epsilon}_{xx}^{non} &= 0 \\ \Delta \bar{\epsilon}_{yy}^{non} &= \nu \Delta \bar{\epsilon}_{xx} \\ \Delta \bar{\gamma}_{xy}^{non} &= \Delta \bar{\gamma}_{xy}\end{aligned}\tag{6.7}$$

The cracks close if $\bar{\epsilon}_{yy}^{non} + \Delta \bar{\epsilon}_{yy}^{non} < 0$

Closed and slipping crack

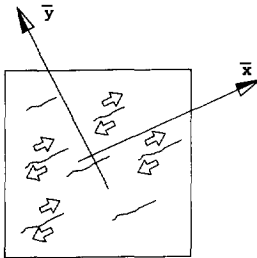


Figure 6.6 - Slipping cracks

A slipping crack requires that

$$\begin{aligned}\bar{\sigma}_{yy} &< 0 \\ |\bar{\sigma}_{xy}| &= -\eta \bar{\sigma}_{yy}\end{aligned}$$

in which η = the internal friction coefficient.

For adobe we take $\eta = 1$.

Coefficient η defines the friction angle α given by

$$\text{tg } \alpha = \eta$$

In the following sections we will sometimes use angle α instead of friction coefficient η .

Based on these conditions we get the incremental constitutive equations

$$\begin{aligned}\Delta \bar{\sigma}_{xx} &= \frac{E}{1-\nu^2} \Delta \bar{\epsilon}_{xx} + \frac{\nu E}{1-\nu^2} \Delta \bar{\epsilon}_{yy} \\ \Delta \bar{\sigma}_{yy} &= \frac{\nu E}{1-\nu^2} \Delta \bar{\epsilon}_{xx} + \frac{E}{1-\nu^2} \Delta \bar{\epsilon}_{yy} \\ \Delta \bar{\sigma}_{xy} &= \pm \eta \left(\frac{\nu E}{1-\nu^2} \Delta \bar{\epsilon}_{xx} + \frac{E}{1-\nu^2} \Delta \bar{\epsilon}_{yy} \right)\end{aligned}\tag{6.8}$$

and the nonelastic strain increments

$$\begin{aligned}\Delta \bar{\epsilon}_{xx}^{non} &= 0 \\ \Delta \bar{\epsilon}_{yy}^{non} &= 0 \\ \Delta \bar{\gamma}_{xy}^{non} &= \Delta \bar{\gamma}_{xy} \mp \frac{2\eta}{1-\nu} (\nu \Delta \bar{\epsilon}_{xx} + \Delta \bar{\epsilon}_{yy})\end{aligned}\quad (6.9)$$

A slipping crack opens if

$$\bar{\sigma}_{yy} + \Delta \bar{\sigma}_{yy} > 0$$

and stops slipping if

$$|\bar{\sigma}_{xy} + G \Delta \bar{\gamma}_{yx}| < -\eta (\bar{\sigma}_{yy} + \Delta \bar{\sigma}_{yy})$$

Closed, nonslipping crack

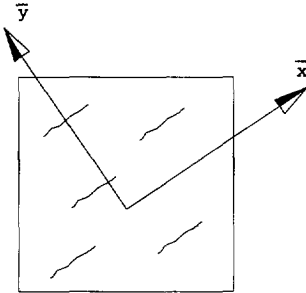


Figure 6.7 Closed cracks

A closed, nonslipping crack requires that

$$\begin{aligned}\bar{\sigma}_{yy} &< 0 \\ |\bar{\sigma}_{xy}| &< -\eta \bar{\sigma}_{yy}\end{aligned}$$

With a closed, nonslipping crack we satisfy the linear elastic isotropic conditions following

$$\begin{aligned}\Delta \bar{\sigma}_{xx} &= \frac{E}{1-\nu^2} \Delta \bar{\epsilon}_{xx} + \frac{\nu E}{1-\nu^2} \Delta \bar{\epsilon}_{yy} \\ \Delta \bar{\sigma}_{yy} &= \frac{\nu E}{1-\nu^2} \Delta \bar{\epsilon}_{xx} + \frac{E}{1-\nu^2} \Delta \bar{\epsilon}_{yy} \\ \Delta \bar{\sigma}_{xy} &= G \Delta \bar{\gamma}_{xy}\end{aligned}\quad (6.10)$$

and the nonelastic strain increments are zero.

$$\begin{aligned}\Delta \bar{\epsilon}_{xx}^{non} &= 0 \\ \Delta \bar{\epsilon}_{yy}^{non} &= 0 \\ \Delta \bar{\gamma}_{xy} &= 0\end{aligned}\tag{6.11}$$

A crack begins to slip if

$$|\bar{\sigma}_{xy} + \Delta \bar{\sigma}_{xy}| > -\eta(\bar{\sigma}_{yy} + \Delta \bar{\sigma}_{yy})$$

Note that a direct change from a closed crack to an open crack is almost impossible.

For small values of $\bar{\sigma}_{yy}$ we always meet the condition that slipping has to be initiated first.

6.4 Constitutions of adobe with two cracks

Because the direction and the magnitude of stresses change quickly it is possible that more than one crack develops at one point. We have carefully to examine this possibility.

Each of the cracks satisfies one of the constitutions as defined in the previous section. The combination, however, introduces several complications.

We distinguish the following combinations:

- two cracks closed
- two cracks open
- one crack closed, one crack slips
- one crack open, one crack closed
- one crack open, one crack slips
- two cracks slip

Each of these combinations has to be examined.

Two cracks closed

The incremental constitutive equations are isotropic following (6.1). This combination does not require any special attention.

Two cracks open

With two open cracks all stiffness disappears. The rigidity matrix is zero. All strain increments are increments of the nonelastic strains.

One crack closed, one crack slips

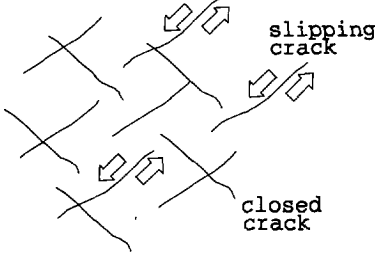
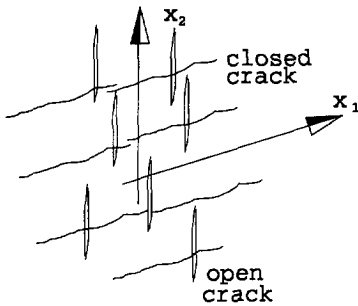


Figure 6.8 - One crack closed, one crack slips

The constitutive equations are those of one slipping crack only, see (6.8) and (6.9).

One crack open, one crack closed



With one crack open only a uniaxial stress state is possible. If the slip condition of the closed crack is not violated the closed cracks can transfer these stresses. This condition is satisfied if

$$|ctg(x_1, x_2)| < \eta \tag{6.12}$$

The constitutive equations are those of one open crack only.

Figure 6.9 - One crack closed, one crack open

One crack open, one crack slips

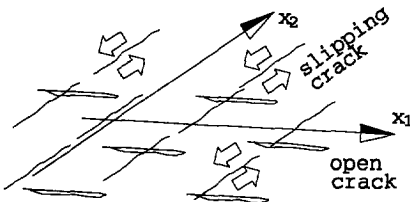


Figure 6.10 - One crack slips, one crack open

If condition (6.11) is not satisfied the crack will slip. Thus the combination of an open crack and a slipping crack occurs if

$$|ctg(x_1, x_2)| > \eta$$

Under these conditions all stiffness disappears. The constitutive equations are those of two open cracks.

Two cracks slip

The most complicated constitution is two slipping cracks.

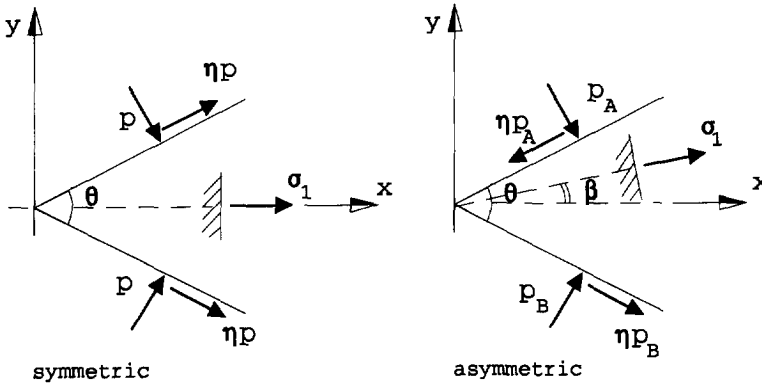


Figure 6.11 - Two slipping cracks

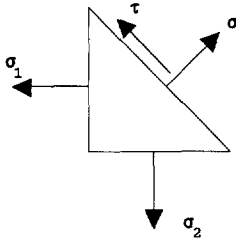
Basically we have two different cases, namely the symmetric condition and the asymmetric condition, see figure 6.11. Between the two crack directions we define the angle θ , while the principal stress direction of σ_1 defines the angle β with respect to the bisectrix between the two crack directions.

In the symmetric case $\beta = 0$, in the asymmetric case β has a nonzero value. In the crack we have compression stresses p_A and p_B and the corresponding friction stresses; in the symmetric case $p = p_A = p_B$.

To formulate the constitutive equations we introduce the mean stress σ and the deviator stress τ following

$$\begin{aligned}\sigma &= \frac{1}{2}(\sigma_1 + \sigma_2) \\ \tau &= \frac{1}{2}(\sigma_2 - \sigma_1)\end{aligned}\tag{6.13}$$

in which σ_1 is the minimum and σ_2 the maximum stress.

Figure 6.12 - Mean stress σ and deviatoric stress τ

Dependent on the symmetric or the asymmetric case we get a direct relation between τ and σ following

$$\tau = \chi \sigma$$

with the auxiliary quantity

$$\chi = -\frac{\sin\alpha}{\sin(\alpha + \theta)} \quad \text{symmetric case} \quad (6.14)$$

$$\chi = -\frac{\sin\alpha}{\cos\theta} \quad \text{asymmetric case}$$

in which friction angle α is related to friction coefficient η (see section 6.3).

For β we obtain

$$\beta = 0 \quad \text{symmetric case}$$

$$\beta = \frac{\pi}{4} - \frac{1}{2}\alpha \quad \text{asymmetric case}$$

Introducing volume strain $e = \varepsilon_1 + \varepsilon_2$ we may substitute that $\Delta e^{non} = 0$, thus

$$\Delta\sigma = \frac{1+\nu}{1-\nu} G \Delta e = G^* \Delta e \quad (6.15)$$

$$\Delta\tau = \chi G^* \Delta e$$

The incremental constitutive equations are now given by

$$\Delta\sigma_{xx} = \Delta\sigma - \Delta\tau \cos 2\beta = (1 - \chi \cos 2\beta) G^* \Delta e$$

$$\Delta\sigma_{yy} = \Delta\sigma + \Delta\tau \cos 2\beta = (1 + \chi \cos 2\beta) G^* \Delta e \quad (6.16)$$

$$\Delta\sigma_{xy} = \Delta\tau \sin 2\beta = \chi G^* \Delta e$$

Although these conditions are rare, they have to be considered to complete the procedures.

6.5 Bamboo properties

In order to reinforce a structure an annular beam has to be added to the top of the walls. Horizontal bamboo strips between the layers of adobe bricks contribute in the same way.

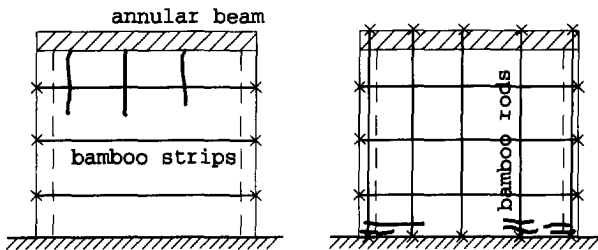


Figure 6.13 - Expected cracks and reinforcements

To fix the annular beam to the wall and to avoid the development of horizontal cracks vertical bamboo rods are added.

The most important properties of bamboo are breaking, debonding and slipping. Breaking occurs if the limit axial stress is exceeded, slipping occurs if the limit shear stress between adobe and bamboo is exceeded. These phenomena need some explication.

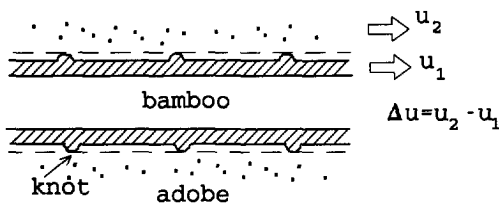


Figure 6.14 - Bamboo rod in adobe

To understand the debonding and slip properties we have to realize that bamboo is very smooth with sparsely distributed knots. The zone beyond a knot yields by exceeding the limit bond stress τ_{bond} . This we call debonding.

Usually the shear stress immediately drops to a lower level, $\tau_{\text{slip}} = \mu \tau_{\text{bond}}$, after debonding and slipping is introduced. If the shear stresses decrease because of load variations, the slipping stops.

The parameter μ is called the friction coefficient and ranges between 0.5 and 1.

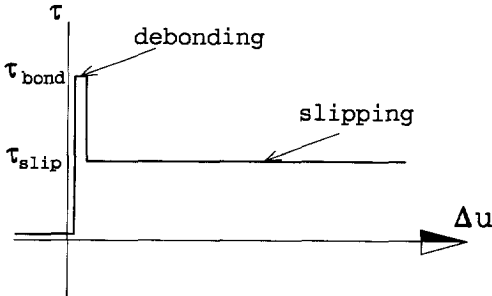


Figure 6.15 - Bond stress limits between bamboo and adobe

We model the slip behaviour after release of the bond stress to τ_{slip} , by the introduction of dry friction elements between adobe and bamboo.

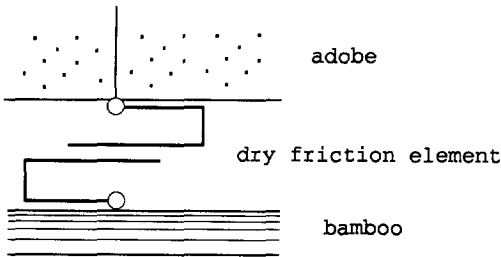


Figure 6.16 - Model of bamboo-adobe interface

The dry friction element begins to slip if the slip stress is exceeded, the dry friction element stops slipping if the displacement between adobe and bamboo moves against the direction of the slip force - see fig. 6.17 -.

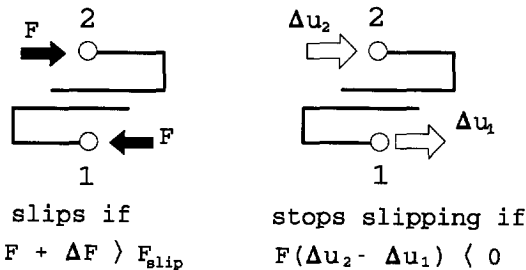


Figure 6.17 - Dry friction element

Breaking occurs if the limit tension or compression stress is exceeded. We assume brittle breaks, thus the axial stress drops to zero immediately after initiation of the break, see figure 6.19.

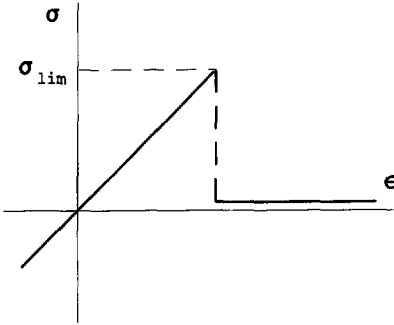


Figure 6.18 - Brittle breaking of bamboo

6.6 Essential problems

To implement features as discussed in the previous sections, we developed a computer program called ADOBE. During the development of ADOBE we met some problems that had to be solved before the requested features could actually be implemented.

Nonconverging processes

In section 3.7 we noticed that a strong variation in stiffness properties may cause nonconverging processes. The opening and closing of the smeared cracks is such a process in which the stiffness properties vary suddenly and strongly. The nature of the problem can easily be demonstrated by a simple static example with a gap element. The following spring model, including a gap element, is subjected to a static load, see figure 6.19. The initial gap is $\Delta u_0 = F/k$.

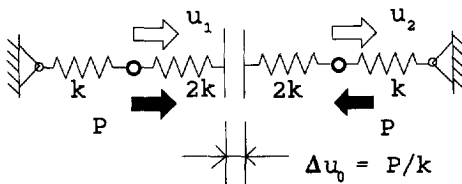


Figure 6.19 - A simple spring model with a gap element

We apply load steps F at the nodes 1 and 2 and we assume a constant stiffness during the application of the load steps. Starting with an open gap we obtain a gap Δu , given by

$$\Delta u = \Delta u_o - 2 \frac{F}{k} = -\frac{F}{k}$$

Our conclusion is that the gap has to be closed.

Starting with a closed gap we solve the equations

$$\begin{aligned} 2k u_1 - k u_2 &= F \\ -k u_1 + 2k u_2 &= -F \end{aligned} \quad (6.18)$$

with the solution $u_1 = \frac{1}{3} \frac{F}{k}$, $u_2 = -\frac{1}{3} \frac{F}{k}$ and a gap Δu , given by

$$\Delta u = \Delta u_o - \frac{2}{3} \frac{F}{k} = \frac{1}{3} \frac{F}{k}$$

Based upon this analysis we conclude that the gap has to be open.

For our integration procedure we have to apply either a closed or an open gap that does not change during the integration step Δt . Since an open gap predicts a closed gap and a closed gap predicts an open gap, we enter a nonconverging process.

In our time-dependent processes with smeared cracks we have overcome this problem by adjustment of the time step Δt^* in such a way that the crack closes at $t = \Delta t^*$. About Δt^* we process the integration procedure with an open crack and at $\Delta t = \Delta t^*$ we continue with a closed crack. ADOBE includes an automatic selection of time step Δt^* .

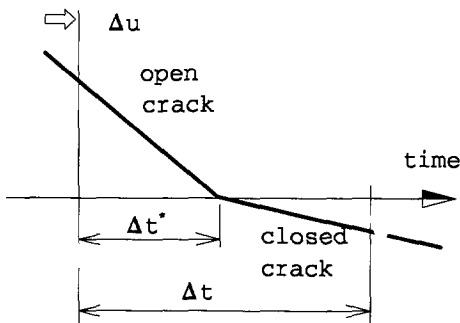


Figure 6.20 - Refinement of time step with closure of an open crack

Local vibrations

One of the phenomena we considered is the release of bamboo from adobe by violation of the bond stress and the subsequent slip and fixation of the two materials. During a dynamic analysis the slipping part of the bamboo elements quite often shows a quickly varying response. This behaviour, which is called local vibration, can be explained by the high stiffness of bamboo as compared to adobe, which implies very high frequencies for the slipping bamboo. We solved this problem by including some artificial damping.

6.7 The numerical model

In the preceding sections we described the properties of bamboo and adobe and considered some numerical aspects. Given the structural shape, the choice of four-node rectangular elements is most natural. We choose constant shear elements because these elements are also applicable for the modelling of the bending behaviour of the annular beam and the lintels of doors and windows.

The bamboo stiffeners are modelled by two-node rod elements. No mass or damping is taken into account. After release of the bond stresses dry friction elements are introduced to model the interface between bamboo and adobe.

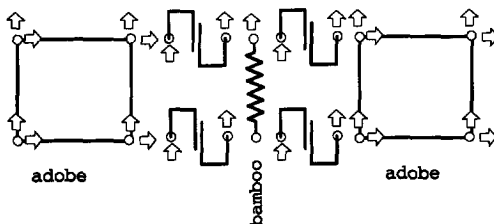


Figure 6.21 - Elements for modelling bamboo and adobe

The limit friction stress - the slip stress - is related to the bond stress by a user supplied parameter μ where $\tau_{\text{slip}} = \mu \tau_{\text{bond}}$. The adobe cracking parameters are given by a maximum tension stress, a maximum compression stress and a friction coefficient to model the slipping of cracks.

The smeared cracks are examined at the centre of the elements. This implies three nonelastic strain parameters and five elastic strain parameters. By this choice the material properties are assumed to be homogeneous within the element.

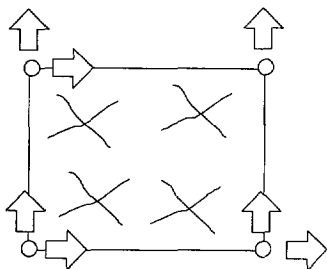


Figure 6.22 - Homogeneous properties within the elements

The element stiffness matrix is evaluated by application of the 2 x 2 Gauss point integration rule.

Some attention has to be paid to the implementation of a time step reduction. In the current version of ADOBE the time step will, if necessary, be reduced automatically.

In this procedure no iterations are processed.

Following our model in chapter 3 we solve

$$H_{01} \Delta u = p_0$$

and subsequently we compute the initial pulses for the next time interval by

$$p_1 = H_{11} \Delta u$$

After solution of Δu the criteria are checked and we may decide, by introducing a reduction factor λ , to use a reduced time step $\Delta t^* = \lambda \Delta t$ instead of Δt . The problem is to correctly compute the pulse loads to be applied at the beginning of the next integration step.

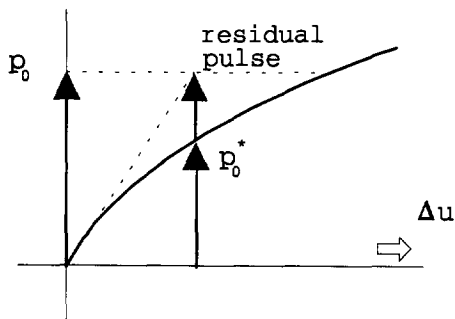


Figure 6.23 - Residual lumped pulses at the beginning of a time step

Because the initial pulse includes contributions that are dependent on the time interval Δt - e.g. the load contributions - we get different contributions with a different time interval Δt^* , thus

$$H_{01}^* \Delta u^* = p_0^* \neq p_0 \quad (6.19)$$

in which

$$H_{01}^* = \left(\frac{1}{4} - \frac{1}{12} \gamma \right) \Delta t^* K + \frac{1}{2} C + \frac{1}{\Delta t^*} M$$

$$\Delta u^* = \mu \Delta u$$

The difference is added to the initial pulses p_1^* of the next integration step. This contribution is added by application of the modified calculation

$$p_1^* = \left(\lambda - \frac{1}{2} \right) \Delta t f - H_{11}^* \Delta u \quad (6.20)$$

in which

$$H_{11}^* = \left(\frac{1}{2} \lambda^2 - \frac{1}{4} + \frac{1}{12} \gamma \right) \Delta t K + \left(\lambda - \frac{1}{2} \right) C - \frac{1}{\Delta t} M$$

In this way we do not lose pulse contributions.

6.8 Two adobe houses

We apply an in-plane earthquake load to the walls of two different houses. Both houses are built of adobe bricks. The first one is a one-storey house. For this house we assume a timber lintel over the door opening. Reinforcement of these houses is obtained by the application of bamboo rods and strips and timber annular beams.

We apply the load to the front wall of the one-storey building. For this structure we analyze both the unreinforced and the reinforced variant, see figure 6.24 .

The second house is a two-storey building, which is reinforced by bamboo rods and strips and two annular timber beams just above the door and the windows. We analyze on the front wall and one of the side walls of this structure.

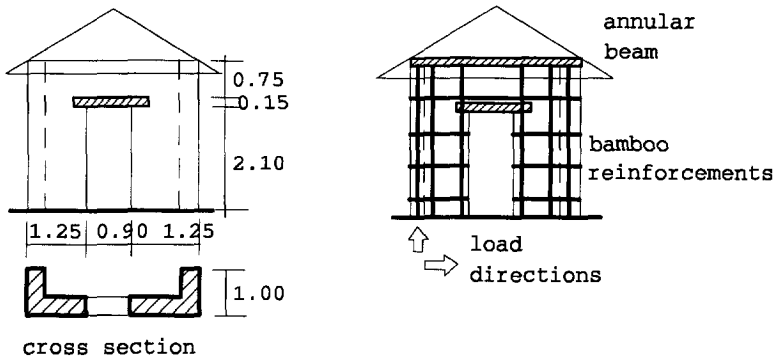


Figure 6.24 - Front wall of a one-storey house (measures in mm)

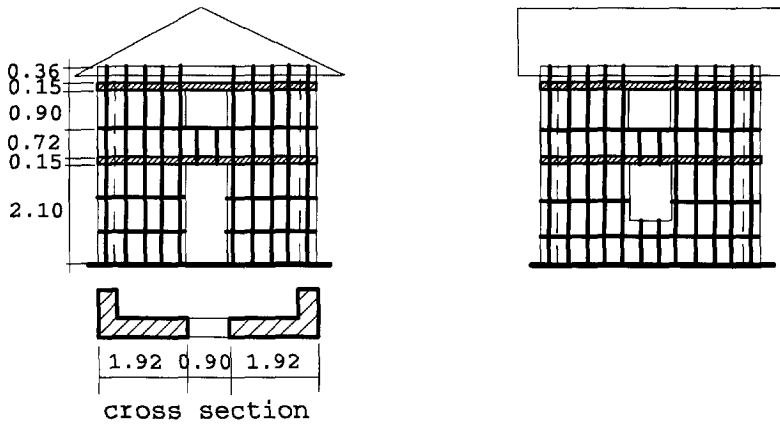


Figure 6.25 - Front wall and side wall of a two-storey house (measures in mm)

To these structures we apply the 'El Centro' earthquake load, see fig. 6.26. The horizontal load factor is 1.00 and the vertical load factor is 0.20.

The analyses are carried out using $\gamma = -0.3$ and $\theta^2 = 0.1$. We expect many disturbances caused by the nonlinear problem, so we certainly need some artificial damping.

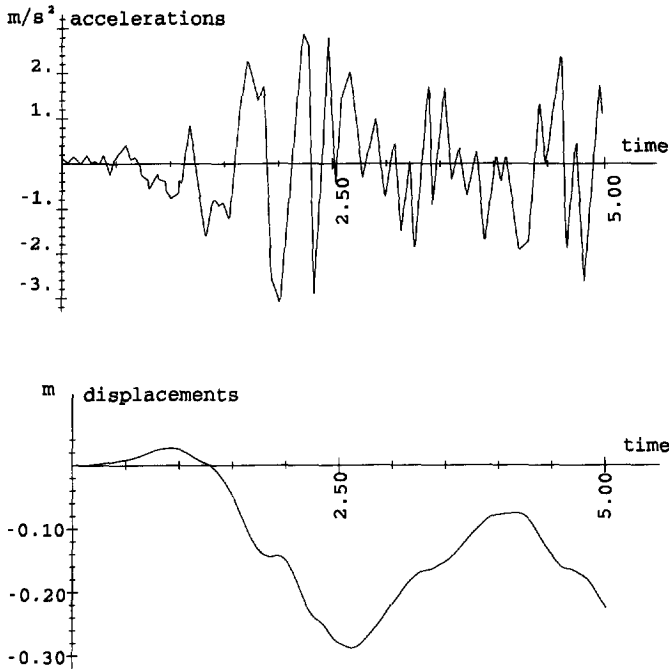


Figure 6.26 - Five seconds of the El Centro earthquake

The following material properties are used:

Adobe

E	$= 170 \text{ N/mm}^2$	Young's modulus
ν	$= 0.30$	Poisson's ratio
ρ	$= 1670 \text{ kg/m}^3$	density
p_1	$= 0.04 \text{ N/mm}^2$	maximum tension stress
p_2	$= 1.2 \text{ N/mm}^2$	maximum compression stress
μ	$= 1.00$	friction coefficient

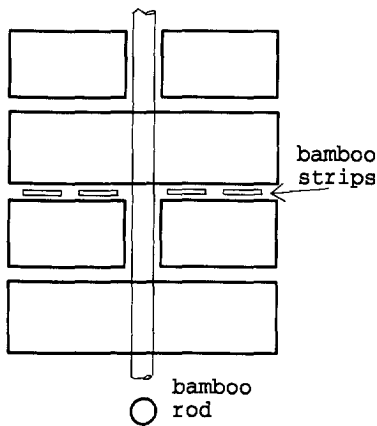
Timber

E	$= 2000 \text{ N/mm}^2$
ν	$= 0.20$
ρ	$= 800 \text{ kg/m}^3$

Nonlinear properties are not considered.

Bamboo

- $E = 17000 \text{ N/mm}^2$
- $\rho = 0.$
- $p_1 = 100 \text{ N/mm}^2$ maximum tension stress
- $p_2 = 100 \text{ N/mm}^2$ maximum compression stress
- $\tau = 0.03 \text{ N/mm}^2$ maximum bond stress
- $\mu = 0.50$ ratio maximum slip stress vs bond stress



Vertically the reinforcement is applied by intact bamboo rods, horizontally the reinforcement is applied by bamboo strips. At the corners and at the door opening the bamboo strips are tied to vertical rods. At the top and at the bottom the rods are fixed to the annular beam and the foundation.

Figure 6.27 - Bamboo reinforcement

The bamboo dimensions are given by cross section A and perimeter S in which

$$A = 120 \text{ mm}^2, S = 59 \text{ mm} \text{ vertical rods (per rod)}$$

$$A = 120 \text{ mm}^2, S = 118 \text{ mm} \text{ horizontal strips (per strip)}$$

Floor loads and roof loads are carried by the side walls only. Assuming a roof load of 2 kN/m^2 and a floor load of 2 kN/m^2 we get line loads of $p = -4.74 \text{ kN/m}$ at the first floor annular beam and at the top annular beam.

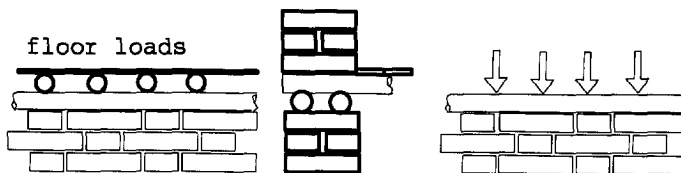


Figure 6.28 - Application of floor and roof loads

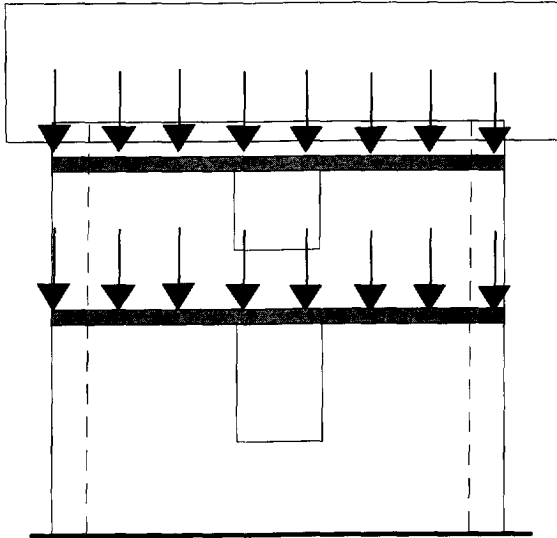


Figure 6.29 - Side wall loaded by roof and floor

Because the most violent accelerations occur in the beginning we only calculate the response during the first three seconds. Taking a time step $\Delta t=0.0025$ we need 1200 integration steps. Because many cracks and bond releases are initiated and each crack opens and closes many times the total number of integration steps will increase drastically. The first analysis is the application of the earthquake load to the front wall of the unreinforced one-storey house. Finite element mesh and crack patterns are shown in figure 6.30.

The response of the structure shows rapid collapse after application of the first heavy accelerations. Cracks are initiated under the supports of the door lintel and propagate to the top and the bottom. Since the structure is not ductile due to the absence of a bamboo skeleton it cracks very soon from the top downwards.

It is striking that the crack band concentrates in one row of elements. This is a consequence of the neglect of any softening in adobe after cracking and of the adopted crack-closing mechanism.

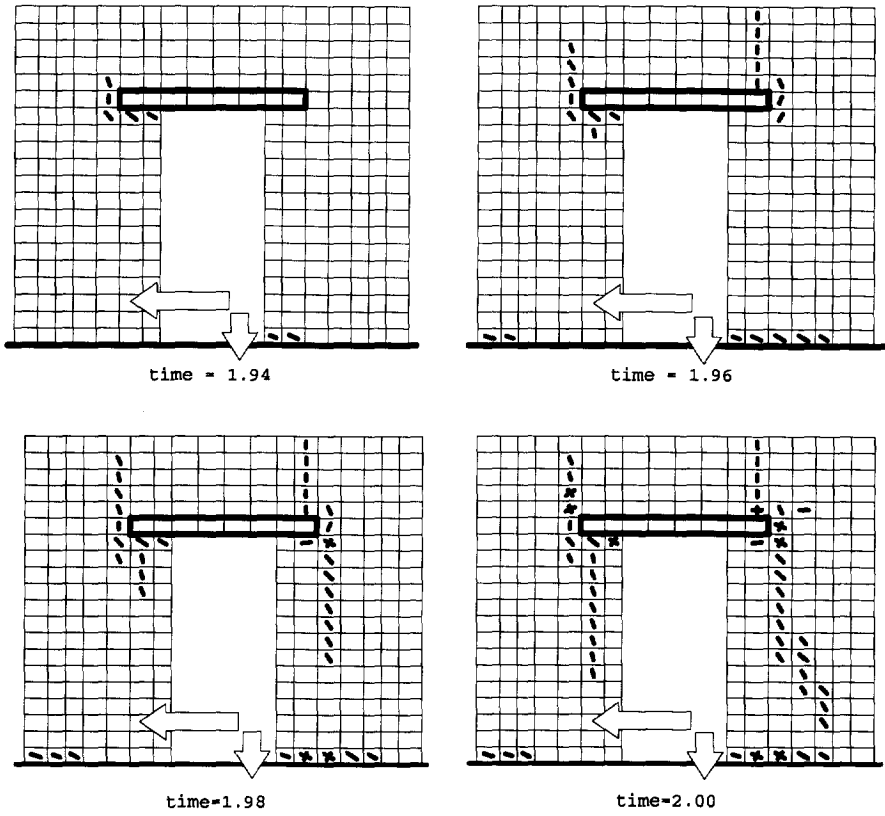


Figure 6.30 - Crack pattern of an unreinforced one-storey house

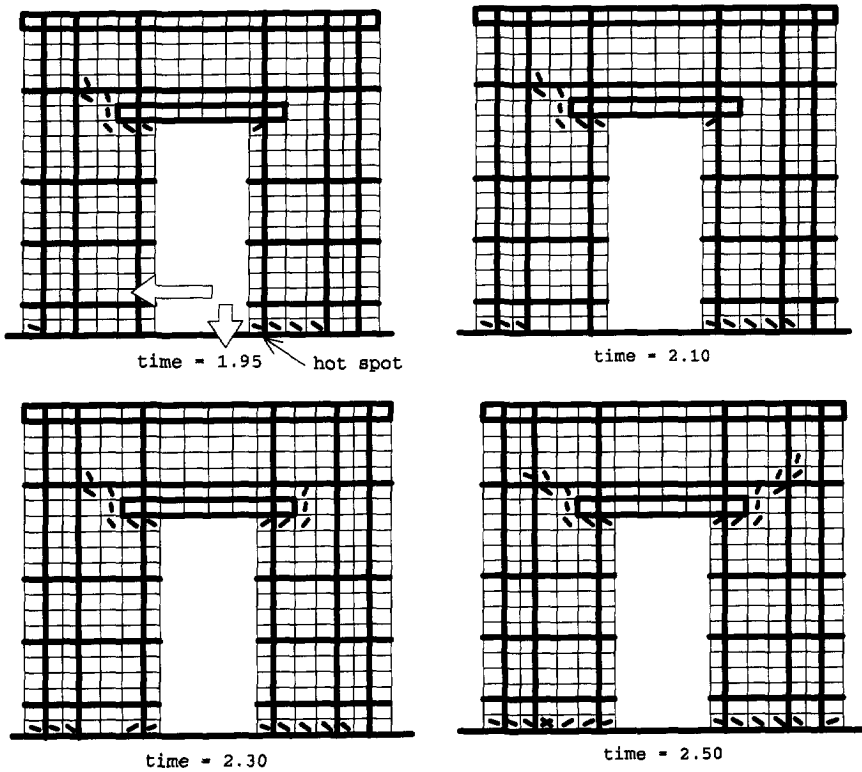


Figure 6.31 - Crack pattern of a reinforced one-storey house

In the second analysis the earthquake load is applied to the front wall of a bamboo reinforced one-storey house. The same mesh as in the first analysis is applied.

Figure 6.31 shows the crack pattern just after its initiation at $t = 1.90$ and at time points that more or less correspond with the knots of the acceleration record at $t = 2.10$, $t = 2.30$ and $t = 2.50$.

Figure 6.35 shows the debonded parts of the bamboo reinforcement and the principal stresses at $t = 2.60$. From these pictures we can obtain and verify a lot of interesting information. The bamboo reinforcement shows the development of a crack pattern at $\pm 45^\circ$; no vertical cracks have arisen.

Figure 6.35 shows that especially the bamboo rods next to the door opening are subjected to much slipping. Most of the slipping occurs around the lintel.

Inspection of the cracks at the right hand side of the lintel shows that most of the mass is located left of this crack pattern. Because the accelerations are active into the right hand side direction these cracks are now open. The inertia forces are directed via the left hand side to the supports. The resultant of the inertial forces is in the left hand side direction. This results in a diagonal compressive adobe strut over the wall and tensile stresses in large parts of the annular beams.

Evidently this structure is much stronger than the unreinforced one. The cracks are again initiated under the supports of the door lintel. Now the cracks propagate, much slower, to the top corners of the wall. Although the adobe bricks are cracked, the structure does not collapse. Because the bamboo stresses are far from the limit values, see figure 6.32, the structure still obtains much ductility from the bamboo skeleton.

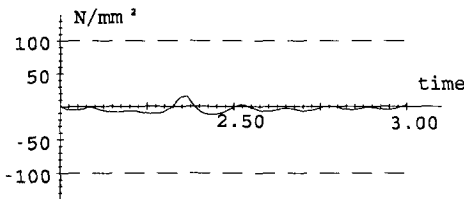


Figure 6.32 - Bamboo stresses at hot spot (see fig. 6.31) between $t = 2.00$ and $t = 3.00$

Although it is recognized that one-storey houses are much safer than two-storey houses a lot of these two-storey houses are built in the Peruvian altiplanos. We will separately analyze the front wall and the side wall of such a structure, see figure 6.25. Both the front wall and the side wall are reinforced by bamboo rods and strips and annular beams at the first floor and the top.

The analysis of the two-storey house shows much damage to the adobe wall at the supports and just above the annular beam crossing the door opening, see figures 6.33, 6.34 and 6.36. The pictures in fig. 6.36 are shown at $t = 2.60$, immediately after a strong acceleration in the right hand side direction. Because of the large inertia moment of the entire structure with respect to the supports, all cracks under 45° are still open, and whereas many bamboo rods are still slipping. The annular beams, which try to reduce horizontal accelerations in the right hand side direction, show considerable tension stresses. Although much more reinforcement has been applied than to the one-storey house, all bamboo rods at the first floor have started to slip.

The trajectories picture of figure 6.36 shows that much load is transferred via the adobe wall between door and window. Recalling the alternating character of the load this part of the structure is damaged most severely. After 2.5 seconds the front wall is seriously damaged but still behaves well. Without reinforcements the structure would collapse definitely.

The analysis of the side wall shows a similar behaviour. It is notable that the floor loads contribute to a better resistance of the wall against cracking of the adobe bricks and debonding of the bamboo reinforcements. The bamboo stresses in the side walls are much smaller than the bamboo stresses in the front wall. Substantial less cracking occurs along the annular beam and along the foundation.

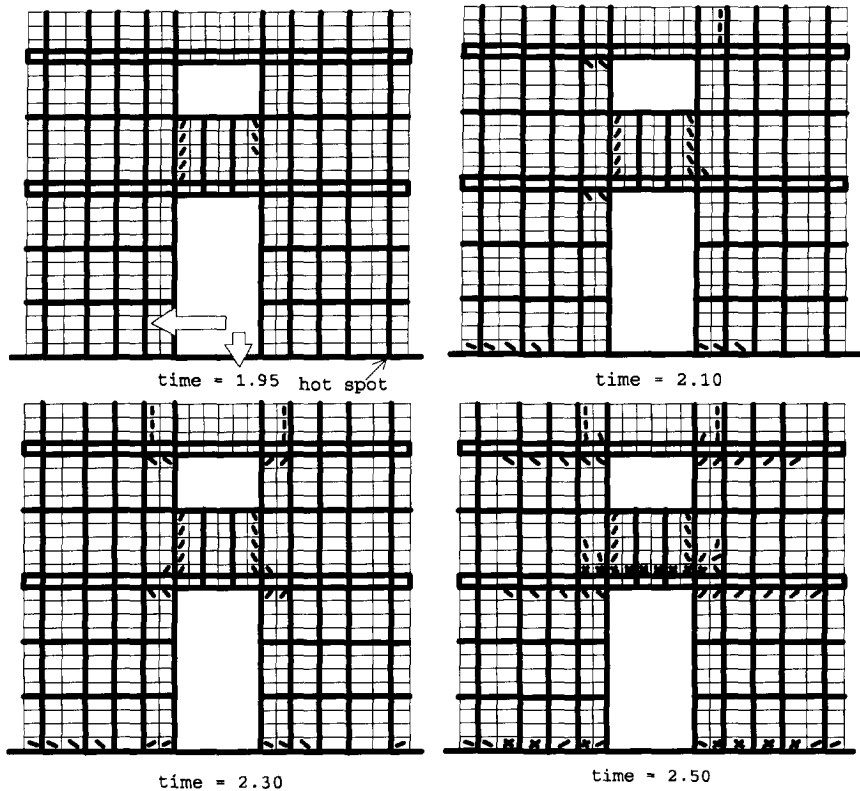


Figure 6.33 - Crack patterns in the front wall of a two-storey house

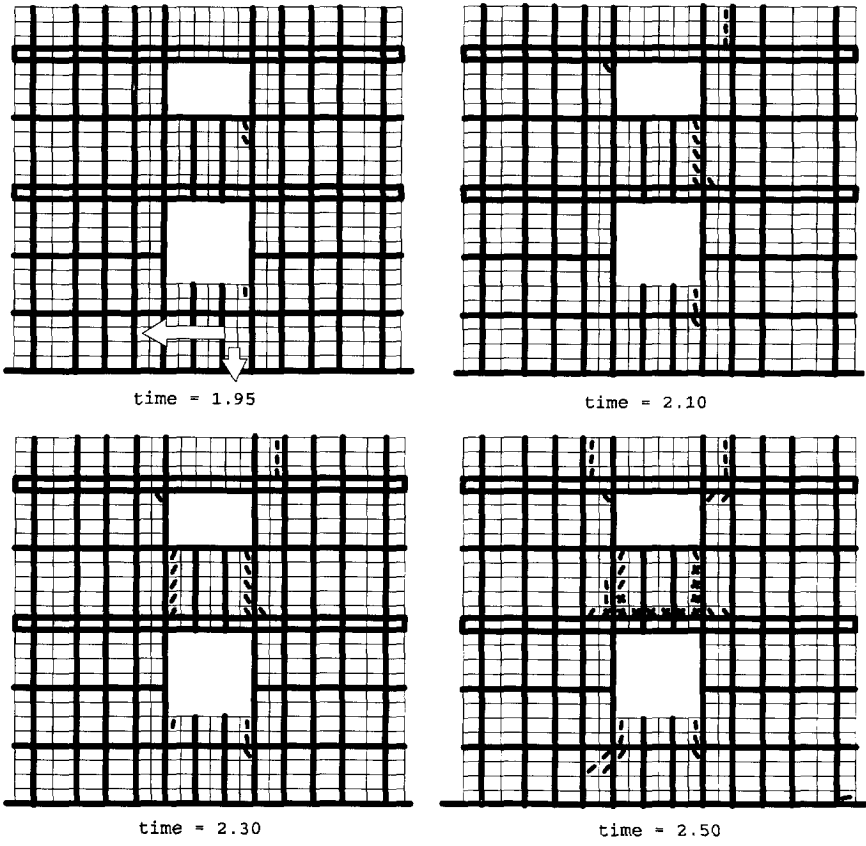
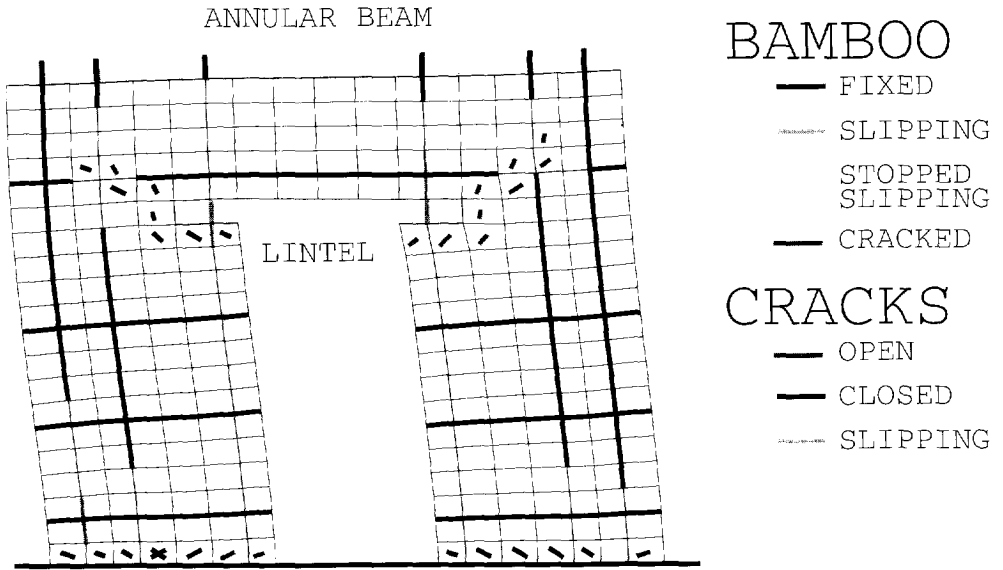
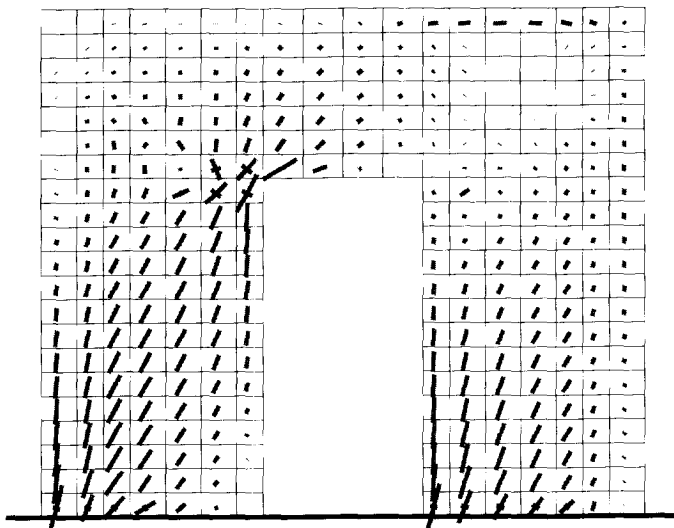


Figure 6.34 - Crack patterns in the side wall of a two-storey house

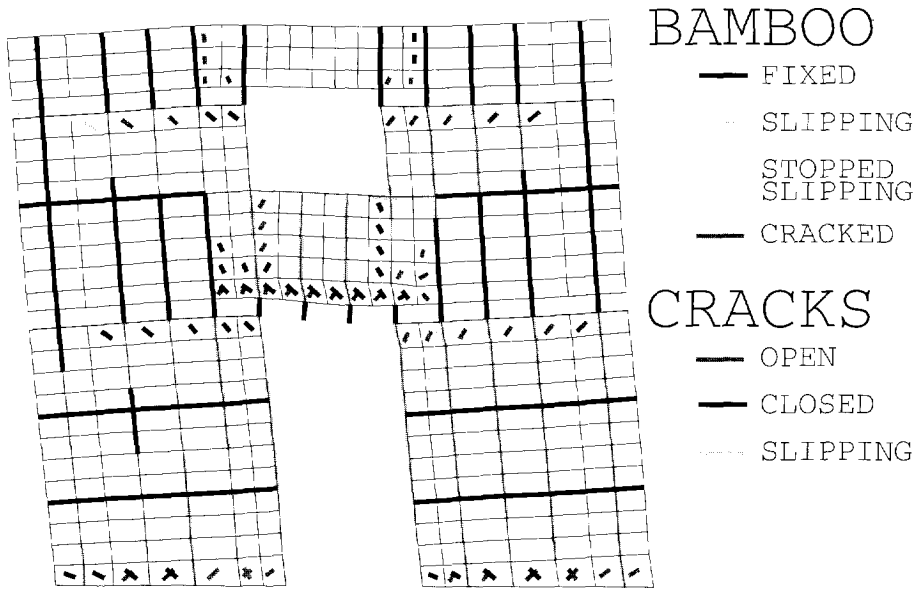


DEFORMATIONS AT T=2.60

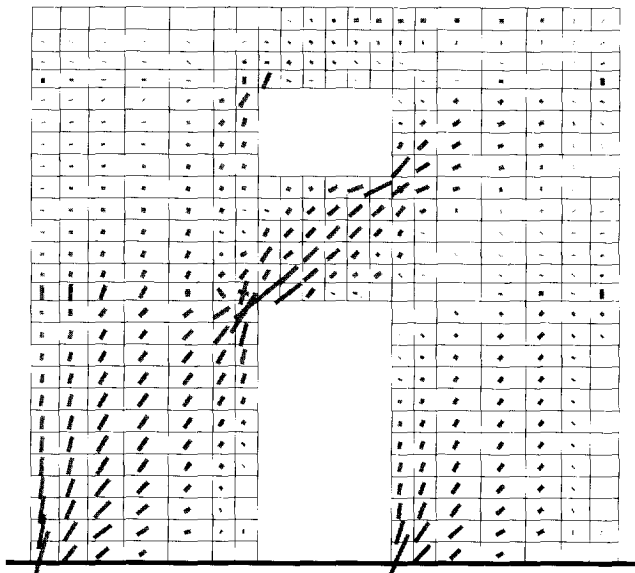


PRINCIPAL STRESSES AT T=2.60

Figure 6.35



DEFORMATIONS AT T=2.50



PRINCIPAL STRESSES AT T=2.50

Figure 6.36

The reduced stiffness, associated with the crack pattern in figure 6.36, can be shown by the displacements of the top with respect to the foundation. This crack pattern has mainly developed between $t = 2.30$ and $t = 2.50$. The large, relative horizontal displacements of the top, see figure 6.37, after $t = 2.30$ can be explained by the reduced stiffness of the structure.

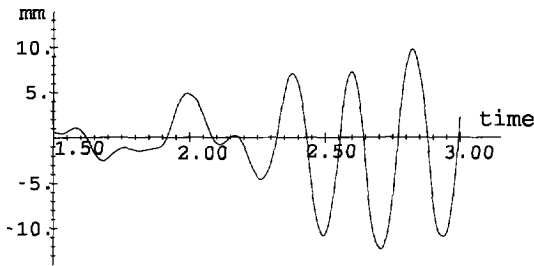


Fig. 6.37 - Horizontal displacements of the top of the front wall

The structure obtains much of its ductility from the bamboo skeleton. Nevertheless, both analyses show bamboo stresses that are much smaller than the limit stresses. Figure 6.38 shows the bamboo stresses at the 'hot spot' of the front wall.

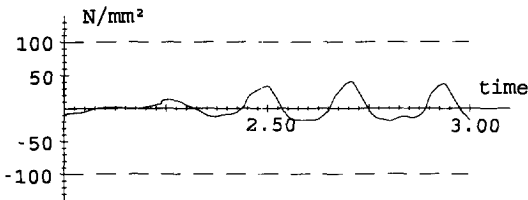


Figure 6.38 - Bamboo stresses at hot spot (see fig. 6.34) between $t = 2.00$ and $t = 3.00$

Conclusions

The application of annular beams and reinforcement in the form of bamboo rods and strips very much contribute to the better safety of adobe houses. Reinforcements do not prevent the cracking of adobe walls; the safety is obtained from the bamboo skeleton. With a medium size earthquake such as the El Centro earthquake, an unreinforced structure collapses and a reinforced structure survives.

Some limitations of our analyses have to be mentioned. Much of the ductility of the structure depends on the properties of the bamboo reinforcements. In our analyses we modelled the bamboo behaviour by its static properties only, assuming zero mass and damping. In reality it is to be expected that fast moving, short waves travel along the debonded, slipping rods. Especially the bond stresses are difficult to predict. A more detailed analysis requires more information on the debonding process; probably softening has to be considered. It is very likely that the limit slip τ_{slip} - see section 6.5 - will reduce after several slip periods; on the other hand large compression stresses at the bamboo rod will increase the limit slip stress.

Other limiting factors are the limit bond stress of the fixation points of the bamboo strips and rods, the knots will probably contribute to the additional stiffness, etc. Since very little information is available such an analysis was not anticipated.

7. CONCLUSIONS AND RECOMMENDATIONS

The analysis of time dependent structural mechanics problems has been complicated by the mixture of a pure mathematical approach for the numerical modelling with respect to time and the mechanical approach to model the structure. Because of this mixture insight in these methods was limited to a very selective group of users. Much more transparency has been obtained by reformulation of the time-space problem from a pure mechanical point of view.

A consequent application of the Galerkin variational method with respect to time and geometry we get numerical relations between lumped pulses and discrete displacements. These relations for dynamics correspond perfectly well with the classic finite element models for statics, with relations between lumped forces and discrete displacements. The application of quadratic shape functions with respect to time has yielded a completely new series of very accurate integration models. A review of numerical stability and artificial damping has yielded interesting interpretations and some new results. All these results together show that a pure mechanical approach of the basic problem yields more transparent models than the classic mixed models.

These models have been applied to real problems in pavement engineering and seismic structural problems. The analysis of these problems quite often depends on an appropriate description of nonlinear material properties, called the constitutive equations. By a simultaneous discretisation to time and geometry these properties have been taken into account in a very natural way.

From the pavement engineer's point of view the investigation shows the important role of damping and shear deformation of the base and the subgrade for the modelling of these problems. Application of the Winkler spring model and a static analysis often implies oversimplification of the real problem.

The analysis of the adobe houses under seismic loading show that one-storey and two-storey houses, reinforced by bamboo and annular beams, are sufficiently strong to survive a medium-size earthquake. Cracking of the adobe walls cannot be prevented; collapse, however, does not occur.

Summarizing :

It has been shown that a purely mechanical approach of the geometry and time discretisation results into more transparent tools to model all kinds of linear and nonlinear structural analysis problems.

Some recommendations:

At many points we met the limits of our knowledge by lack of relevant data, or simply by lack of time. One subject is the need for a robust higher-order model with respect to time. We developed an unconditional numerically stable model with sufficient artificial damping to guarantee the robustness. Elaboration of some applications still has to prove the expectations of this model.

The study of the pavement structures showed the need to add some more parameters to the usual structure idealisation, that is the static analysis of a plate on a Winkler foundation. To get more insight it is very tempting to start a full 3D time dependent nonlinear analysis and to verify these numerical data by experimental data. One of the main problems is the big gap between the pavement engineering discipline and the sophisticated finite element software to solve these problems. Our approach may help to reduce this gap. The final goal must be to design simple transparent models the parameters of which are justified by insight obtained from the full depth analysis.

The investigation of the seismic loaded adobe houses revealed many problems that are similar to reinforced concrete. Several problems, especially those related to the bamboo-adobe interface, have not yet been tackled. No data are available about the bond stress limits of the fixation points and the anchorage. Softening of the bond stress release as well as softening during crack initiation is ignored, etc. The insight can be improved considerably by a profound numerical and experimental investigation of the bond stress release of one single bamboo rod.

The analysis also showed numerical shortcomings. Despite the numerical stability and the artificial damping, the sharp changes in stiffness by the crack opening and closing of cracks in the adobe wall and the slipping/nonslipping of the bamboo/adobe interface we were forced to reduce the time steps to, sometimes, very small values. Our approach has not yet given us a solution for this problem. A real break-through requires algorithms that can overcome this problem.

SUMMARY

The analysis of time-dependent structural mechanics problems can be carried out by the use of direct integration methods. In the past the analysis of time-dependent problems mainly emphasized the mathematical 'modelling' of these methods, whereas the discretisation with respect to the geometry by means of the f.e.m. techniques, mainly emphasized the mechanical modelling of the structure. Because discretisation to time and geometry was realized from very different points of view, the insight in these methods was limited to a very small group of users. More transparency of these methods can be obtained by reformulation of these processes both to time and geometry from a pure mechanical point of view.

Chapter 1 contains a general discussion of existing solution techniques, chapter 2 shows the mathematical presentation of the most widely used direct integration methods. Based upon this inventory conditions are formulated for optimal integration techniques.

In chapter 3 we start to formulate the dynamics problem with respect to time and geometry. Boundary conditions are also formulated with respect to time and geometry. The application of the Galerkin variational condition with respect to a finite time and geometry domain yields finite element models that relate discrete pulses to discrete displacements. The method includes a free parameter γ that can be applied for optimisation from different points of view. Existing models such as the Newmark- β method, can be interpreted in this way. New higher-order models are presented. Incremental techniques for the solution of nonlinear static problems, based on residual forces and displacements, are similar to incremental techniques for the solution of the nonlinear dynamics problems, based upon residual pulses and displacements. Applications for the solution of some SDOF systems are shown.

In chapter 4 we investigate issues such as numerical stability, accuracy and artificial damping. Based on the investigation of the numerical stability a higher-order model with unconditional numerical stability is proposed. The investigation of numerical stability of higher order models shows that numerical instability may be considered as a failing process to step between two tops of a single vibration mode. Artificial damping, necessary to guarantee robustness, is investigated; optimal values are found dependent on the free model parameter of the linear model. Stress damping ensures robustness of the linear model, pulse damping ensures the robustness of the quadratic model.

The chapters 1 until 4 emphasize the development of a series of generic models for the solution of dynamic problems. The chapters 5 and 6 show the application of the developed models. Chapter 5 discusses a pavement engineering problem and in chapter 6 a house-building problem in seismic active areas is discussed. Both cases demonstrate

very well the applicability of these integration algorithms for the analysis of nonlinear structural behaviour.

Chapter 5 shows the application of the models for beams and plates on an elastic foundation. For these structures, subjected to a Falling Weight Deflectometer load, we investigated the role of damping, inertia and shear transfer of base and subgrade. It turned out that even for pavements without a base the introduction of a shear layer (Pasternak model, Vlassow theory) lead to significant differences. The dynamic response of a stiff pavement (concrete) on a weak subgrade appears to be very dependent on the damping properties of the subgrade, the dynamic response of softer pavements (asphalt) on a stiff subgrade hardly differed from the static solution. Special attention was paid to the use of gap elements - to model the release of concrete plates from the base by temperature loads - and a limited yielding of the base under the joint of two concrete slabs. It was shown that the constitutive relations can be formulated very well by relations between discrete pulses and displacements. The application of the new higher-order model showed the performance of this model. Nevertheless these models are not elaborated fully because of their complexity.

Chapter 6 analyzes the structural response of one-storey and two-storey houses to an earthquake load. Nonlinear properties of adobe bricks and bamboo reinforcement are taken into account. During the first three seconds of the applied earthquake load the most violent accelerations are applied to the structures. The analyses show that these structures would collapse without reinforcement. Assuming a good anchorage and fixation of the added bamboo reinforcements, these structures survive a medium size earthquake load.

Chapter 7 summarizes the development of finite element models based on lumped pulses and discrete displacements. It is shown how this procedure improves the transparency of these models from a mechanical point of view. Application to pavement engineering problems shows that better and easy-to-use models are available. It is, however, necessary to obtain more accurate data for the extra parameters by additional numerical and experimental research. The application to adobe houses shows the applicability of numerical simulations to predict the response to earthquake loads. As soon as more information is obtained about the softening properties of these materials even better numerical simulations can be developed.

SAMENVATTING

De berekeningen van dynamica-problemen uit de toegepaste mechanica worden vaak uitgevoerd met behulp van directe integratiemethoden. In het verleden werd de aandacht voor de tijdsafhankelijke berekening vooral gericht op de wiskundige 'modellering' van deze problemen, terwijl de modellering naar de geometrie door middel van de eindige-elementenmethode de aandacht vooral op de mechanica richtte. Doordat de discretisering van geometrie en de discretisering naar de tijd vanuit verschillende disciplines werd uitgevoerd bleef het inzicht in deze methoden beperkt tot een zeer kleine groep gebruikers. Het inzicht in deze methoden kan aanzienlijk worden verbeterd door deze processen zowel naar geometrie als naar tijd vanuit een pure mechanica-benadering opnieuw te formuleren.

In hoofdstuk 1 wordt een globale bespreking van de bestaande methoden gegeven. In hoofdstuk 2 wordt de wiskundige presentatie gegeven van de meest gebruikte directe integratiemethoden. Op grond van dit overzicht worden de voorwaarden voor een optimale directe integratiemethode geformuleerd.

In hoofdstuk 3 wordt eerst het dynamicaprobleem geformuleerd met betrekking tot geometrie en tijd. Ook de randvoorwaarden worden met betrekking tot geometrie en tijd geformuleerd. De toepassing van de Galerkin variatie-eis over een eindig geometrie- en tijdsgebied resulteert in relaties tussen discrete pulsen en verplaatsingen. De methode kent een vrije parameter γ waarmee naar diverse gezichtspunten kan worden geoptimaliseerd. Bestaande modellen zoals de Newmark- β methode kunnen op deze manier worden afgeleid. Nieuwe hogere orde modellen met nauwkeurigheid $O(\Delta t^2)$ worden voorgesteld. Nauwe overeenkomst wordt gesignaleerd tussen rekenmethoden voor de oplossing van nietlineaire staticaproblemen, gebaseerd op residuele krachten en verplaatsingen, en rekenmethoden voor de oplossing van nietlineaire dynamica-problemen, te baseren op residuele pulsen en verplaatsingen. Enige toepassingen aan de hand van SDOF systemen demonstreren het gebruik.

In hoofdstuk 4 worden onderwerpen onderzocht zoals numerieke stabiliteit, nauwkeurigheid en kunstmatige demping. Op grond van het numerieke stabiliteitsonderzoek wordt een hogere-orde model met onbeperkte numerieke stabiliteit voorgesteld. Het onderzoek toont ook aan dat numerieke instabiliteit kan worden opgevat als een ontsprekend proces om van de ene golftop naar de andere te stappen. Kunstmatige demping is nodig om de 'robuustheid' van de rekenmodellen te kunnen garanderen. Een optimale dempingsfactor kan worden gekoppeld aan de in hoofdstuk 3 aangegeven vrije parameter γ voor het lineaire model. Voor het kwadratische model is kunstmatige demping met succes te introduceren door middel van demping van de impulsen.

In de eerste vier hoofdstukken heeft het accent gelegen op het ontwikkelen van generieke modellen om dynamicaproblemen op te lossen. In de hoofdstukken 5 en 6 behandelen we toepassingen van de ontwikkelde modellen. In hoofdstuk 5 is een probleem uit de wegbouwkunde gekozen en in hoofdstuk 6 een woningbouwprobleem in een aardbeefgevoelig gebied. Beide voorbeelden demonstreren goed hoe de integratie-algorithmen zich laten combineren met nietlineair gedrag.

Hoofdstuk 5 toont de toepassing van de modellen voor liggers en platen op een elastische bedding. Voor deze constructies, die worden belast door de Falling Weight Deflectometer testbelasting, onderzoeken we het belang van de bijdragen van demping, traagheid en afschuifvervorming van de ondergrond. Het blijkt dat zelfs voor een plaat zonder fundering de bijdrage van een afschuiflaag (Pasternak, Vlassow) reeds merkbare invloed heeft. De dynamische respons van een stijve toplaag (beton) op een zachte ondergrond blijkt in hoge mate afhankelijk te zijn van de demping; de dynamische respons van een zachtere toplaag (asfalt) op een stijve ondergrond verschilt nauwelijks van de statische oplossing. Aparte aandacht is gegeven aan de zogenaamde 'gap'-elementen, bedoeld om het loslaten te modelleren van betonnen platen van de fundering als gevolg van een temperatuurbelasting, en aan 'dry friction'-elementen voor de modellering van een beperkt bezwijkgedrag onder de overgang tussen twee betonplaten. Het blijkt dat de gewenste constitutieve eigenschappen zeer goed zijn te modelleren door relaties tussen discrete pulsen en verplaatsingen. Enkele berekeningen met het nieuwe hogere-orde model tonen aan dat dit model goed kan worden toegepast. Dit model is echter niet verder uitgewerkt vanwege de grotere complexiteit.

In hoofdstuk 6 voeren we een dynamische sterkteberekening uit voor één en twee verdiepingen huizen, gemaakt van adobe en bamboe, die worden belast door een aardbeving. Nietlineaire eigenschappen van adobe en bamboe worden in rekening gebracht. Bij de gesimuleerde aardbeving worden de zwaarste belastingen uitgeoefend gedurende de eerste drie seconden. De berekening laat zien dat huisjes zonder versteviging van bamboe en ringbalk spoedig bezwijken. Uitgaande van stevige verbindingen en verankering van de bamboe kunnen deze constructies een middelmatig zware aardbeving doorstaan.

In hoofdstuk 7 wordt samengevat hoe een eindige-elementenmodel, gebaseerd op discrete verplaatsingen en geconcentreerde pulsen wordt opgebouwd. Aangegeven wordt op welke punten deze aanpak verhelderend werkt op het mechanica-inzicht bij beoordeling en gebruik van deze modellen.

Uit de toepassing op wegbouwkundige problemen blijkt dat betere en eenvoudiger hanteerbare modellen bereikbaar zijn. Het is dan wel nodig dat waarden voor de extra parameters in voldoende mate numeriek en experimenteel worden onderbouwd.

Uit de toepassing op de adobe huizen blijkt de bruikbaarheid van een numerieke simulatie voor het voorspellen van de respons op een aardbeving. De simulatie zou nog aanzienlijk kunnen worden verbeterd als er meer gegevens over de softening van het materiaalgedrag ter beschikking zouden komen.

REFERENCES

- [1] N.M. Newmark, 'A method of computation for structural dynamics', J. Engng Div., ASCE 85, p. 67-94, 1959
- [2] J.C. Houbolt, 'A recurrence matrix solution for the dynamic response of elastic aircraft', J. Aeronautical Sciences 17, p. 540-550, 1950
- [3] E.L. Wilson, I. Farhoomand, K.J. Bathe, 'Nonlinear dynamic analysis of complex structures', Earthquake Eng. and Struct. Dyn, 1, p. 241-252, 1973.
- [4] H.M. Hilber, Th.J.R. Hughes, R.L. Taylor, 'Improved numerical dissipation for time integration algorithms in structural dynamics', Earthquake Eng. and Struct. Dyn., 5, p. 283-292, 1977
- [5] R.D. Krieg, 'Unconditional stability in numerical time integration methods', J. Appl. Mech, 40 p. 417-421, 1973
- [6] W.L. Wood, M. Bossak, O.C. Zienkiewicz, 'An alpha modification of Newmark's method', Int. J. Num. Meth. Eng., 15, p. 1562-1566, 1980
- [7] G. Bazzi, E. Anderheggen, 'The ρ -family of algorithms for time-step integration with improved numerical dissipation', Earthquake Eng. and Struct. Dyn., 10, p. 765-771, 1982.
- [8] K.J. Bathe, E.L. Wilson, 'Numerical methods in finite element analysis', Prentice Hall, Englewood Cliffs, N.J., 1976.
- [9] Th.J.R. Hughes, 'The finite element method', Prentice Hall, Englewood Cliffs, N.J., 1987
- [10] M. Abramowitz, I.A. Stegun, 'Handbook of mathematical functions', Dover Publ., N.J., 1964
- [11] M. Gerardin, M. Hogge, S. Idelsohn, 'Implicit finite element methods', in 'Computational methods for transient analysis.' p. 417-471, Elseviers, Amst., 1983
- [12] R. Glowinski, E.Y. Rodin, O.C. Zienkiewicz, 'Energy methods in finite element analysis', John Wiley Sons, N.Y., 1979
- [13] M.A. Dokainish, K. Subbraraj, 'A survey of direct time-integration methods in computational structural dynamics, I. Explicit methods', Comp. & Struct, 32, p. 1371-1386, 1989
- [14] M.A. Dokainish, K. Subbraraj, 'A survey of direct time-integration methods in computational structural dynamics, II. Explicit methods', Comp. & Struct, 32, p. 1387-1401, 1989
- [15] Th.J.R. Hughes, 'Transient algorithms and stability', in 'Computational methods for transient analysis', p. 67-155, Elseviers, Amst., 1983

- [16] C.W. Gear, *Numerical initial value problems in ordinary differential equations*, Prentice Hall, N.J., 1971
- [17] K.C. Park, *Evaluating time integration methods for nonlinear dynamic analysis*, in *Finite element analysis of transient nonlinear behaviour*, p. 35-38, AMD 14, N.Y., ASME, 1975
- [18] J.H. Argyris, P.C. Dunne, T. Angelopoulos, *Nonlinear oscillations using the finite element technique*, *Comp. Meth. in Appl. Mech. and Engng.*, 2, p. 203-250, 1973
- [19] G.L. Goudreau, R.L. Taylor, *Evaluation of numerical methods in elastodynamics*, *Comp. Meth. in Appl. Mech. and Engng.*, 2, p. 69-97, 1973
- [20] O.C. Zienkiewicz, W.L. Wood, N., W. Hine, R.L. Taylor, *A unified set of single step algorithms, Part 1: General formulation and applications*, *Int. J. Num. Meth. in Engng*, 20, p. 1529-1552, 1984
- [21] J. Blaauwendraad, A. W.M. Kok, *Elementenmethode voor constructeurs*, Agon Elseviers, Amst. 1973.
- [22] J.S. Przemieniecki, *Theory of matrix structural analysis*, Mc. Graw Hill, N.Y., 1968
- [23] A.W.M. Kok, *A theoretical manual for STRUDL*, JRC Euratom, Ispra, 1981
- [24] C. Runge, *Über die numerische auflösung von differential gleichungen*, *Math. Annln* 46, p. 167-175, 1895
- [25] W. Kutta, *Beitrag zur näherungsweise integration totaler differentialgleichungen*, *Z. Math. Phys.*, 46, p. 435-453, 1901
- [26] H.B. Hilber, Th.J.R. Hughes, *Collocation, dissipation and "overshoot" for time integration schemes in structural dynamics*, *Earthquake Eng. and Struct. Dyn.*, 6, p. 99-117, 1978
- [27] A.W.M. Kok, *Pulses in finite elements*, *Proc. First. Conf. on Comp. in Civ. Engng.*, N.Y., 1981
- [28] J. Blaauwendraad, A.W.M. Kok, *Handicraft in finite elements*, *Proc. Int. Conf. Num. Meth. Engng*, Swansea, NUEMETA 87, 1987
- [29] A.W.M. Kok, *Nonlinear dynamics: An iteration procedure*, *Proc. Seminar Investigations of Materials and Civil Engineering Structures*, p. 32-45, Wroclaw, 1988
- [30] J.T. Oden, *A general theory of finite elements - I: Topological considerations*, *Int. J. Num. Meth. Engng*, 1, 1969
- [31] J.T. Oden, *A general theory of finite elements - II: Applications*, *Int. J. Num. Meth. Engng*, 1, 1969

- [32] T. Belytschko, R.L. Chiapetta, H.D. Bartel, '*Efficient large scale nonlinear transient analysis by finite elements*', Int. J. Num. Meth. Engng, 10, p. 579-596, 1976
- [33] S.P. Chan, H.L. Cox, W.A. Benfield, '*Transient analysis of forced vibrations of complex structural mechanics systems*', J.R. Aeronautical Soc., 66, p. 457-460, 1962
- [34] I. Fried, '*Finite element analysis on time dependent phenomena*', AIAA Jnl 7, p. 1170-1173, 1973
- [35] O.C. Zienkiewicz, R.W. Lewis, '*An analysis of various time-stepping schemes for initial value problems*', Earthq. Engng. Struct. Dyn., 1, p. 407-408, 1973
- [36] S. Klein, D.M. Trujillo, '*An unconditionally stable finite element analysis for nonlinear structures*', Comp. & Struct., 16, p. 187-197, 1983
- [37] O.C. Zienkiewicz, '*A new look at the Newmark, Houbolt and other time stepping formulae: a weighted residual approach*', Earthq. Engng. Struct. Dyn., 5, p. 413-418, 1977
- [38] L. Khazanovich, A.M. Ionides, '*Finite element analysis of slabs-on-grade using higher order subgrade soil models*', ASCE Specialty Conf., Vickburg, MS, Sept. 1993
- [39] A.C. Pronk, '*The Pasternak foundation: an attractive alternative for the Winkler foundation*', 5-th Int. Conf on Concrete Pavement Design and Rehabilitation, Purdue Univ., April 1993
- [40] L.J. M. Houben, '*Two-dimensional finite element analysis of unreinforced concrete pavements*', 2-nd Int. Workshop on Theoretical Design of Concrete Pavements, 1990, Siguenza, Spain
- [41] S. Zaghoul, Th White, '*Nonlinear dynamic analysis of concrete pavements*', 5-th Int. Conf. on Concrete Pavement Design and Rehabilitation, Purdue Univ., April 1993
- [42] M. Cohen, P.C. Jennings, '*Silent boundary methods for transient analysis*', Computational methods for transient analysis (in Comp. Meth. in mechanics, ed. T. Belytschko, T. Hughes), Amst. 1983
- [43] A.A.A. Molenaar, '*Ongewapende betonverhardingen*', Course notes e54, TU Delft, 1974
- [44] T.H.H. Pian, '*Basis of finite elements for solid continue*', Int. J. Num. Meth. in Engin., 1969, vol. 1, p. 1
- [45] A. Podhorecki, '*The viscoelastic space-time element*', Comp. & Struct., 23, p. 535, 1986
- [46] C.I. Bajer, '*Triangular and tetrahedral space-time finite elements in vibration analysis*', Int. J. Num. Meth. in Engin., 23, 1986, p. 2031

- [47] G. Sovero, C. Malpartida, A.W.M. Kok, '*Modelling of reinforced adobe walls in bending with discrete elements*', Report DUT, dept Civ. Eng., Febr. 1993
- [48] A.W.M. Kok, '*Dynamic analysis of beams on a Pasternak foundation*', Proc. 5-th Int. Conf. Comp. in Civil and Building Engin., p. 553-560, Anaheim, Calif., June 1993
- [49] L.J. Sluis, '*Wave propagation, localisation and dispersion of softening solids*', Dissertation Delft University of Technology, Delft, 1992
- [50] G.T.H. Sweere, '*Unbound granular bases for roads*', Dissertation Delft University of Technology, Delft, 1990
- [51] A.P. Allaart, '*Design principles for flexible pavements*', Dissertation Delft University of Technology, Delft, 1992
- [52] J. Blaauwendraad, '*TILLY User's Manual 3.3*', Delft, November 1994
- [53] J.G. Rots, '*Computational Modeling of Concrete Fracture*', Dissertation Delft University of Technology, Delft, 1988

CURRICULUM VITAE

26 juni 1940 Geboren te 's-Gravenhage

sept. 1952-juni 1958

St. Aloysius College te 's-Gravenhage, afgesloten met HBS-b diploma

sept. 1958-febr. 1966

Propadeuse Civiele Techniek, diploma Wiskundig ingenieur

dec. 1965-heden

Werkzaam in onderwijs en onderzoek bij de Faculteit der Civiele Techniek, Technische Universiteit Delft.

Start ontwikkeling eindige elementenmethode. Mede-auteur boek elementenmethode [21] (1973). Verzorgt college elementenmethode aan de Faculteit der Civiele Techniek. Verzorgt mede cursussen elementenmethode bij de Betonvereniging.

Introduceert het ICES programma-systeem aan de TU Delft en maakt dit toegankelijk voor onderwijs en onderzoek aan de faculteiten (1974). Organiseert wereldwijde ICES conferentie (1977). President ICES Users Group 1983-1987.

Schrijft op uitnodiging van Euratom een 'Theoretical Manual for STRUDL' [23], (1981). Doceert in vele PATO-cursussen.

Verzorgt inleidende cursussen elementenmethode aan universiteiten in ontwikkelingslanden (Ghana, Peru). Begeleidt onderzoeksproject voor aardbevingsbestandig bouwen in de Andes.